A Study on Regional Drought Analysis using Teleconnections and Suitable Global Climate Models for Telangana State

Submitted in partial fulfilment of the requirements
for the award of the degree of

DOCTOR OF PHILOSOPHY
in
CIVIL ENGINEERING

by
Koppala Sreelatha
(Roll No: 716002)

Supervisor
Prof. P. Anand Raj

DEPARTMENT OF CIVIL ENGINEERING
NATIONAL INSTITUTE OF TECHNOLOGY
WARANGAL- 506 004 (T.S.) INDIA
JANUARY 2024

DEDICATION

This dissertation is dedicated to The Almighty, the eternal source of wisdom and guidance, whose divine presence has illuminated the path of this academic pursuit. In fond remembrance, I pay tribute to the late K Subbarayudu, my revered father, whose enduring wisdom and perseverance continue to inspire my scholarly endeavors. Gratitude extends to my beloved mother, K Lakshmi Devi, whose unwavering love and encouragement have been the bedrock of my academic journey.

Professor P Anand Raj, my esteemed project guide, whose mentorship has been invaluable in shaping the scholarly contributions within this thesis. Additionally, this work is dedicated to V Ravi Kumar, my husband and confidant, whose unwavering support has added depth to this academic endeavor, creating a collaborative pursuit of knowledge and shared aspirations.

Educational gurus who guided me from school to college, imparting invaluable knowledge and nurturing a lasting passion for learning.

DECLARATION

This is to certify that the work presented in the thesis entitled **"A STUDY ON REGIONAL DROUGHT ANALYSIS USING TELECONNECTIONS AND SUITABLE GLOBAL CLIMATE MODELS FOR TELANGANA STATE"** is a bonafide work done by me under the supervision of **Prof. P. Anand Raj** and was not submitted elsewhere for the award of any degree. I declare that this written submission represents my ideas in my own words and where others' ideas or words have been included, I have adequately cited and referenced the original sources. I also declare that I have adhered to all principles of academic honesty and integrity and have not misrepresented or fabricated or falsified any idea / data / fact /source in my submission. I understand that any violation of the above will be a cause for disciplinary action by the Institute and can also evoke penal action from the sources which have thus not been properly cited or from whom proper permission has not been taken when needed.

(KOPPALA SREELATHA)

(Roll No: **716002**)

Date: 5-1-2024

NATIONAL INSTITUTE OF TECHNOLOGY
WARANGAL

CERTIFICATE

This is to certify that the thesis entitled "**A STUDY ON REGIONAL DROUGHT ANALYSIS USING TELECONNECTIONS AND SUITABLE GLOBAL CLIMATE MODELS FOR TELANGANA STATE"** that is being submitted by **Ms. Koppala Sreelatha** for the award of the degree of **DOCTOR OF PHILOSOPHY** in the Department of Civil Engineering, National Institute of Technology, Warangal, is a record of bonafide research work carried out by her under my supervision and it has not been submitted elsewhere for award of any degree.

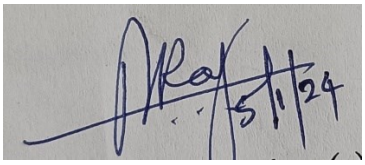

Prof. P. ANAND RAJ
Thesis Supervisor
Department of Civil Engineering
National Institute of Technology
Warangal-506004 (T.S.) – INDIA

ABSTRACT

Drought is a multifaceted natural climatic hazard that significantly affects both ecosystem and society. In comparison to other natural hazards, such as floods, storms, hurricanes, the spatial extent of droughts is usually much larger. Climate variability precipitates a heightened occurrence and severity of droughts on a global scale. Notably, India stands as one of the most drought-prone regions worldwide, experiencing drought events approximately every three years across distinct geographic areas, with a particularly profound impact observed in semi-arid regions. As a result, it is important to investigate drought at regional and local scale with climatic conditions and its variations. Global Climate Models (GCMs) are the only models available for projecting climate systems at any timescale. Occurrence and distribution of drought characteristics can be analysed by using GCMs datasets. Understanding the dynamics of drought and its impacts in the context of climate change on a regional scale is therefore a vital area of research, so in this study the regional frequency analysis of droughts using suitable GCMs for Telangana state is carried out in view of recent catastrophic events.

In the first section, selection of suitable GCMs of Precipitation (P), Maximum Temperature (T_{max}), Average Temperature (T_{avg}) and Minimum Temperature (T_{min}) entails the application of Standard Statistical Performance Metrics (SSPMetrics) over the period 1975-2005 in Telangana State, India. Skill Score (SS), Normalized Root Mean Square Deviation (NRMSD) and Correlation Coefficient (CC) SSPMetrics are utilized to evaluate 36 Coupled Model Intercomparison Project 5 (CMIP5) dataset models against observed data. Weights assigned to SSPMetrics are determined from entropy and sensitivity analysis. Compromise Programming (CP) is subsequently employed to rank the GCMs for each variable at individual grid point using distance measure method. The Group Decision-Making Approach (GDMA) is then applied to derive a combined ranking at each grid point. The ensemble climate models deemed suitable for each variable are identified as follows: for P, FGOALS-g2, CMCC-CMS and INMCM4.0; for T_{max}, BCC-CSM1.1(m), CanESM2 and MIROC5; for T_{avg}, MIROC5, CNRM-CM5 and BCC-CSM1.1(m); for T_{min}, CanESM2, BCC-CSM1-1(m) and ACCESS 1.0 from historical simulations of CMIP5 GCMs. The computed net strength of each GCMs aligns with the ensemble model results. The determined ensemble GCMs are suitable for utilization in subsequent climate impact assessment studies that focus on precipitation, temperature or both such as studies on drought, flood, temperature extremes and other regional scale climatic phenomena.

In the second section of the study, regionalization of the study area and evaluating of drought indices, namely Standardized Precipitation Index (SPI), Standardized Precipitation Evapotranspiration Index (SPEI), Self-Calibrated Palmer Drought Severity Index (SC_PDSI) and their properties(Severity and Duration) are assessed. Regionalization process involved the analysis of hydro-meteorological data to discern homogeneous regions with akin characteristics. Application of Fuzzy-C-Means - Unsupervised classification is used for clustering and optimum number of clusters are identified as three for Telangana state. Subsequently, Drought indices are computed over a 12-month time scale for three identified homogenous regions from the year 1975 to 2017. The findings reveal that, in the context of the SPI, Region 1 exhibited severe drought period during August 2011 to September 2013, registering with -34.9 severity. The lengthiest drought episode in this region spanned from September 1984 to September 1987, encompassing a duration of 37 months. In the case of Region 2, exhibited severe and prolonged drought between June 2001 and August 2005, recording -44.43 severity and 51 months of duration. Region 3 experienced severe drought from August 1984 to August 1986, with a severity of -38.5, while the lengthiest drought event spanned from July 2014 to September 2016, encompassing 27 months of duration. SPEI, Region 1 exhibited severe and protracted drought event from August 2006 to September 2013, manifesting a severity of -81.07 and persisting for a duration of 86 months. For Region 2, experienced severe and extended drought spans during August 2006 to June 2013, registering -75.1 of severity and persisting for 83 months. Region 3 witnessed its most severe drought event during the period from March 2014 to December 2017, characterized by a severity of -68.02, while the lengthiest drought event occurred from March 2007 to May 2011, encompassing a duration of 51 months. For SC_PDSI, region 1, most severe and longest drought event occurred during September 2000 to June 2003 with severity -79.77 and duration 33 months; Region 2 exhibits its most severe and extended drought event, spanning from February 1984 to September 1985, characterized by -38.92 of severity and lasting for 19 months of duration. Conversely, Region 3 confronted an exceptionally severe drought event extending from May 1979 to June 1988, registering -227.75 of severity and persisting for 110 months of duration. Overall, these valuable insights of severity and duration of SPI, SPEI and SC_PDSI prove effective for analysing and assessing regional drought conditions.

In the third section, the investigation delves into unravelling the impact of teleconnection on the relationship between drought indices (SPI, SPEI, SC_PDSI) and four prominent climatic indices: Southern Oscillation Index (SOI), Dipole Mode Index (DMI), Multivariate ENSO

Index (MEI) and NINO3.4 are analysed for 1975-2017. Furthermore, interconnection between drought indices and climate indices is examined using Wavelet Coherence method. The results indicate that, drought pattern of DMI with SPI, SPEI and SC_PDSI is observed during 1984, 1985 and 1992. MEI and NINO 3.4 with SPI, SPEI and SC_PDSI during 1984 - 1986; SOI matched well during the year 1992 and 1993 with all the drought indices. Inter annual variability coherence for SPI with MEI is observed at 16 - 40 months (1982-1994 and 1995-2017 and SOI inter annual coherence is evident between 1975-1990 and 1995-2017; whereas Nino 3.4 intermittency is noticed at 1978-1992 and 2002-2015. Coherence is demoted with all the climate indices in the case of SPEI only SOI exhibited a highly significant influence at 14 to 40 months between 2002- 2014. Whereas significant coherence is smaller for SC_PDSI with DMI, MEI and NINO 3.4. SOI and MEI has significant coherence with SPI followed by SPEI and SC_PDSI compared to other climate indices. This reliable and robust quantitively results helps to understand relation between the climate and drought indices and new insights for further drought investigation.

In section four, multivariate frequency analysis of Severity-Duration-Frequency (SDF) and Severity-Area-Frequency (SAF) curves are developed with SPI and SPEI at 12- month time scale at a threshold of -0.8. for three regions for time span of 1975-2017 (observed), 1975-2005, 2006-2035, 2036-2065, and 2066-2095 (projected datasets) using drought characteristics. The temporal evolution of drought entails a comprehensive examination of drought attributes through the analysis of SPI and SPEI within three homogeneous regions. This scrutiny encompasses both observed data and four distinct projected datasets. The objective is to discern the nuanced characteristics of drought over time, thereby contributing valuable insights to the understanding of drought dynamics. Increase of number of droughts are noticed in all regions for future periods compared to observed period of IMD. Mean interarrival time between droughts of SPI and SPEI is found to be maximum for Region 1 and Region 3 in historic period latter it is decreased further in projected periods. Maximum severity is showing increasing trend in all regions during 2036-3065 and 2066-2095 future periods. The incidence of moderate drought events exhibits an elevated frequency during both historical and anticipated future periods across all delineated regions i.e., nearly 30% of the droughts are moderate droughts for all the regions. The best fit copula for three regions is: for SPI – Clayton(region1), Gumbel((region2) and Frank(region3). SPEI, Gumbel(region1), Frank(region2), and Frank(region3). In later part of twenty-first century mean interarrival time is observed to be reducing and number of droughts are observed to be increasing for both SPI

and SPEI. A possibility of high number of droughts with less mean arrival time is expected with high severity and duration in the future at Region 1 followed by Region 3 and Region 2 respectively. Projected drought SDF curves represent highest severity as noticed for Region 1 and duration for Region 3 for SPI whereas for SPEI highest severity and duration is noticed for Region 1. All the curves rise convex upwards for region 1 & 2 and concave upwards for Region 3 which represents increase in severity with increase in duration for SPI and SPEI.

Projected SAF curves depict drought severity and its spatial extent in relation to the drought return period, elucidating the spatial and recurrent patterns inherent in drought occurrences. These curves prove instrumental in examining the anticipated annual severity of droughts in the future, encompassing the associated percentage coverage of the affected area. Moreover, SAF curves facilitate the comparative analysis of historical droughts against those projected from future climate scenarios derived from GCMs outputs. The temporal evolution reveals a discernible escalation in drought severity associated with varying durations over time. Projections indicate that drought hazard is poised to reach its zenith during the periods of 2036-2065 and 2066-2095, surpassing levels observed in other analysed epochs. Leveraging information gleaned from SDF and SAF curves concerning drought severity, duration, percentage coverage of the area and return period, allows for the precise calculation of drought severity within designated regions. This information proves valuable for addressing agricultural demand and formulating optimal crop management strategies.

The results and findings based on the application of statistical techniques in this study gives insight to use suitable GCMs for drought related climate impact studies and this study offers a view on potential drought condition in Telangana state, India.

Keywords: Global Climate Models, SSPMetrics, CP, Drought indices, SPI, SPEI, SC_PDSI, Severity, Duration, Teleconnections, Drought Frequency Analysis

ACKNOWLEDGEMENTS

Primarily, my gratitude is extended to the Almighty for the bestowed grace, wisdom, and knowledge that guided my exploration, facilitated overcoming challenges encountered, and instilled the determination necessary for the successful pursuit and completion of my research.

At this significant juncture, I extend my sincere appreciation and deepest gratitude to the individuals whose unwavering support has been instrumental in making this study possible. Their invaluable contributions, in various capacities, have played a pivotal role in the realization and success of my research endeavor.

With a profound sense of gratification and esteemed privilege, I extend my heartfelt gratitude to my research supervisor, Prof. P. Anand Raj of the Department of Civil Engineering. His consistent support, invaluable suggestions, and empathetic guidance have been instrumental throughout this academic endeavor. I consider myself exceptionally fortunate to have had a supervisor who granted me the autonomy to independently explore research findings and present this work with a touch of artistry. My gratitude for the generosity of his guidance is immeasurable. Additionally, I extend my thanks to Alpha aunty for her positive support during challenging situations.

I am pleased to express my profound gratitude to Prof. T D Gunneswara Rao, Professor in the Department of Civil Engineering and Chairman of the Doctoral Scrutiny Committee. His enlightening guidance and substantial assistance have been invaluable contributors to the successful completion of this work.

I extend my gratitude to Prof. Dr. K Venkata Reddy, Professor in the Department of Civil Engineering, Dr. P Hari Prasad Reddy, Associate Professor in the Department of Civil Engineering, and Prof. K N S Kasi Viswanadham, Professor in the Department of Mathematics, all esteemed members of the Doctoral Scrutiny Committee. Their guidance and assistance during the investigation phase were invaluable to the progress and completion of this research.

I express my gratitude to Prof. Deva Pratap, Sri V N Kameswara Rao, Prof. N V Umamahesh, Prof. K V Jayakumar, the late Prof. E Venkata Rathnam, Prof. P Rathish Kumar, Prof. M Chandrasekhar, Prof C S R K Prasad, Dr. P Venkateswara Rao, Dr. T P Tezeswi, Dr. G Kalyan Kumar, and Dr. B Umesh—esteemed faculty members of the Department of Civil Engineering at NITW. Their moral support throughout the period of my research work has been instrumental and is sincerely appreciated.

I am also thankful to Prof Dr. Avinash D. Vasudeo, Department of Civil Engineering, VNIT Nagpur, Prof. Dr. Yashwant Bhaskar Katpatal, Department of Civil Engineering, VNIT Nagpur, Dr. Sreekanth Sampath, Scientist, CWPRS, Pune, Jotsana G Ambedkar, Scientist, CWPRS, Pune, Dr. Kaluvai Yella Reddy, OSD at Govt of Andhra Pradesh, Prof. Dr B Jayarami Reddy, Department of Civil Engineering, YV University Kadapa whose wisdom and expertise have significantly influenced my academic and professional trajectory. I am profoundly grateful for the privilege of learning from their experiences and contributions, which have left an enduring impact on my career.

I take great pleasure in expressing my gratitude to individuals such as M. Sri Ram Chand, Swamy Giri, Jewdas, Prasad, Uday Kumar, N Venkatesh, Oggu Praveen, K Satish Kumar, B Sagar, Y Subbarao, S Ashok, G Venkat, B Eswar, S Mounika, Kiran Teeparthi, Rakesh K, Mr. Kausalendra Verma (IITB) and Soumya (VNIT Nagpur). Their unwavering patience in offering essential technical suggestions, support, and understanding has been invaluable to me.

I extend my appreciation to my fellow research scholars: Koteswar Rao, G. Mallikarjuna Rao, M. Venu Yadav, Sukesh, Hanuma, Chaitanya, Nitesh, Srikanth, Raja Rajeshwari, M Sudhakar, Seenu, Soumya, Radhika, Kavin, Suchit, Guru, Murali, Sirisha, Sowjanya, Aneesha, Vani, Kumar, Shiva Shankar, Ramakanth, Bharat, Atul, Nagi Reddy, Manikanta, Jithendra, Karan, Priyanka, Sruthi, Hari Priya, Sagarika, Praful, Suram Anil and Pranay. I express my gratitude for their valuable direct or indirect suggestions throughout the duration of my research work.

I express my gratitude to Sri P. Ashok Kumar, Sri R. Hussain, Sri P. Rajendra Prasad, Sri. Naresh, Sri Md. Hussain, Bala Raju, and the entire administrative staff for their gracious assistance and cooperation throughout the research period. I extend a special heartfelt appreciation to the security staff of NITW for their dedicated support.

An immense debt of profound gratitude is extended to my parents, Smt. K Lakshmi Devi, and Late K Subbarayudu, for their unwavering sacrifices, tireless efforts, and continuous encouragement. They have stood beside me during every phase of this journey, providing steadfast support. Additionally, I express my gratitude to my sister, Swathi, and brother, Raghu. Special thanks are offered to my nephew, VIYAN VIRAT, and my daughter, EVA NAOMI, whose presence brought unlimited happiness and solace during the challenging times that marked the conclusion of my research work and dissertation.

I extend my heartfelt appreciation to my extended family friends, Suresh, E Lalitha, Late Shilpa, Mrinmayee Ganage, Sagar, Rohini, Ram Bhupal, Taif, Sudhakar, Sravan, Y Subbarao and Family (Sandhya akka, Tulasi Ram, and Pooja Sri), Mr. & Mrs. John's family, Mr. & Mrs. Shyam's family, Mr. & Mrs. Bijo's family and Bhavin. Their steadfast encouragement and unwavering support have been a source of great strength.

My heartfelt gratitude goes to my husband, Mr. Ravi Kumar, whose unwavering support, enduring affection, and constant encouragement became my guiding light throughout the entire research period. In moments of challenge, his steadfast commitment provided a comforting foundation, and I am profoundly thankful for his integral role in the heartfelt completion of this academic journey.

Finally, I thank everyone who contributed either directly or indirectly, in successful completion of this work.

- ***Sreelatha***

CONTENTS

List of symbols

$E[\ ]$	Expectation of a random variable
$F_Z(z)$	Cumulative distribution function of random variable Z
$f_Z(z)$	Probability density function of random variable Z
$P\{\}$	Probability of an event
H	Energy efficiency
P_{tx}	Transmitted signal power
E	Energy consumption
H	Depth of the water
Q	Root mean square acoustic pressure
T	Temperature
W	Wind speed
F	Signal frequency
R_b	Data rate
M	Modulation level
K	Channel estimation error factor
σ^2	Variance
Ξ	SIC inefficiency
G	Goodput

List of abbreviations

A-D	Anderson- Darling test
AIC	Akaike Information Criterion
ANN	Artificial Neural Network
CC	Correlation Coefficient
CDF	Cumulative Distribution Function
CDO	Climate Data Operator
C-M	Cramer-von Mises test
CMIP5	Coupled Model Intercomparison Project Phase 5
CP	Compromise Programming
Fpi	Fuzziness partition index
GCMs	Global Climate Models
GDMA	Group Decision-Making Approach
hur	humidity
IMD	India Meteorological Department
IOD	Indian Ocean Dipole
K-S	Kolmogorov Smirnov test
L-L	Log Likelihood
MEI	Multivariate ENSO Index
MLR	Multi Linear Regression
NCEP	National Centers for Environmental Prediction
NRMSD	Normalized Root Mean Square Deviation
P	Precipitation
Pe	Partition entropy
psl	mean sea level pressure
RCP	Representative Concentration Pathways
RMSE	Root Mean Square Error
SAF	Severity-Area-Frequency
SC_PDSI	Self-Calibrated Palmer Drought Severity Index
SDF	Severity-Duration-Frequency
Si	Separation index

SOI	Southern Oscillation Index
SPEI	Standardized Precipitation Evapotranspiration Index
SPI	Standardized Precipitation Index
SS	Skill Score
SSPMetrics	Standard Statistical Performance Metrics
SVM	Support Vector Machine
ta air	temperature
tasmax	maximum temperature
tasmin	minimum temperature
T_{avg}	Average Temperature
T_{max}	Maximum Temperature
T_{min}	Minimum Temperature
ua	u-wind
va	v-wind
zg	geopotential height

LIST OF TABLES

LIST OF FIGURES

CHAPTER 1

INTRODUCTION

1.1 Global Climate Models

1.1.1. Overview of GCMs and Climate Change

Global Climate Models (GCMs) serve as indispensable numerical tools in comprehending the complex physical processes of the land surface, ocean and atmosphere, particularly in the context of simulating impacts for regional and hydroclimatological studies. The evaluation of climate change, particularly its potential influences on hydrometeorological variables, is of paramount importance and GCMs have proven instrumental in projecting future scenarios (Jiang et al., 2003). The ramifications of alterations in precipitation and temperature patterns exert profound effects on diverse societal dimensions, impacting the accessibility of water, reservoir operations, irrigation practices, in addition to the incidence of extreme events such as floods and droughts. Acknowledging the gravity of these consequences, GCMs have been customized to indicate the existing climate conditions with their implications on hydrological variables within interconnected networks (Pitman et al., 2012) (Smith and Chiew, 2010).

Despite their global applicability, GCMs exhibit limitations when applied at local or regional grid scales. External forcings are implicitly described at the global scale, but the models often fall short of indicating the effects of global climate changes at more localized levels (Reichler & Kim, 2008). The precision of GCMs diminishes gradually when applied at finer scales, introducing uncertainties related to variability in simulations and challenges in downscaling to local or regional levels (Xu, 1999). Therefore, identifying and selection of GCMs has become necessary for climate impact assessment.

1.1.2 Selection of Global Climate Models and their Applications

The evaluation of GCMs at regional or local hydrological scales is riddled with uncertainties, attributed to factors such as random internal climate variability, anthropogenic activities and the physical responses embedded in the model equations (Hawkins & Sutton, 2011; Mujumdar & Nagesh Kumar, 2012). Given these uncertainties, it becomes imperative to

thoroughly evaluate GCMs before employing them in climate change studies. The evaluation of GCMs extends beyond mere scrutiny, encompassing the selection of suitable models that demonstrate optimal performance (Smith & Chiew, 2010). This evaluation is crucial for simulating hydroclimatic variables and conducting hydrological modeling studies (Pitman et al., 2012).

A plethora of studies worldwide has been dedicated to simulating GCMs for the validation of climatic parameters, utilizing statistical performance metrics to gauge their efficacy (Errasti et al., 2011; ; Sperber et al., 2013; Perkins et al., 2007; Salman et al., 2019). The methodologies for evaluating GCMs have evolved, incorporating various statistical performance metrics, including SS, CC, Normalised Root Mean Square Error, Root Mean Square Error and other innovative approaches (Fordham et al., 2011; Gleckler et al., 2008; Johnson & Sharma, 2009; Pitman et al., 2012; Tebaldi & Knutti, 2007). Recent studies explore the strength of individual models and there is a growing emphasis on the selection of suitable ensembles to enhance consistency in simulations (Johnson et al., 2011; Tebaldi & Knutti, 2007). The utilization of CP, known for its ability to identify optimal solutions in multi-criteria decision-making, emerges as a promising avenue for the selection of an ensemble of GCMs, demonstrating its efficacy in diverse contexts (Salman et al., 2018; Raju et al., 2016; Maxino et al., 2008). Recent literature reflects a burgeoning body of research dedicated to assessing model performance at both regional and basin levels, emphasizing the evolving nature of this critical field.

1.2 Drought Monitoring

Drought, as a complex natural hazard, intricately influences ecosystems, society and the economy. Precise quantification of drought at the regional scale is imperative for a comprehensive understanding of its multifaceted impacts (Mishra & Singh, 2010). Despite the interrelated nature of various drought definitions, distinct types exhibit variations in duration and resource impact. Meteorological drought, denoted by periods of exceptionally low or absent precipitation, forms the climatic basis. The repercussions of precipitation on reservoirs, streamflow and groundwater collectively constitute hydrological drought. Agricultural drought focuses on crop responses to heightened heat stress and insufficient soil moisture. Additionally, socioeconomic drought is intricately connected to economic factors such as water supply and demand for agricultural products, with substantial impacts stemming from hydrological, meteorological and agricultural

droughts. Consequently, the imperative to monitor drought emerges as a fundamental requirement for in-depth investigation across these sectors (Tallaksen and Van Lanen, 2004).

In recent decades, the global surge in drought-related incidents has been a focal point of concern (Allen et al., 2011; Kang & Sridhar, 2017, 2018). The escalating frequency of drought occurrences in India, akin to numerous other nations, has been pronounced since 1965 (Bisht et al., 2018b; Shewale & Shravan Kumar, 2005). Projections suggest a progressive increase in both the average duration and intensity of drought events in India spanning the temporal domain from 2010 to 2099, as contrasted with the reference historical epoch spanning 1979 to 2005. This trend underscores a pronounced regional challenge of considerable significance. (Bisht et al., 2019). The dynamics of drought in this context are primarily influenced by variations in the monsoon and the demand for water vapor in precipitation, culminating in the manifestation of extreme events (Loon et al., 2013). Drought complexities are exacerbated by the surging demand for water, driven by population growth, irrigated agriculture and industrialization. The escalated demand for water resources engenders the unsustainable exploitation of both surface and subsurface reservoirs, thereby instigating conflicts among stakeholders during drought events. Consequently, the necessity to systematically monitor drought occurrences at a regional scale becomes imperative for precise water resource assessment, efficacious management and the formulation of robust mitigation strategies.

Drought, a recurrent phenomenon within varied climatic regimes, is intricately governed by multifaceted factors such as precipitation patterns, temporal distribution, intensity, duration, temperature variations, humidity levels and wind speed. The cumulative impact of these variables manifests gradually over extended periods, spanning months to years. The gradual and insidious nature of drought necessitates sophisticated management strategies, given the inherent uncertainty associated with precisely ascertaining its initiation and cessation. In addressing this challenge, drought indices emerge as invaluable tools for monitoring, quantifying and evaluating droughts. These indices simplify the intricate nature of drought into a singular numerical value, facilitating a more comprehensive understanding (Vicente-Serrano et al., 2010). Over the course of temporal evolution, these metrics have assumed a pivotal role in the delineation and assessment of drought, significantly contributing to the domains of drought monitoring and the formulation of early warning systems. Notwithstanding the abundance of diverse drought indices, an ongoing scholarly

dialogue endures regarding the efficacy with suitability of each respective index. The persisting discussion underscores the intricate nature of drought assessment, necessitating a thorough exploration of the strengths and limitations of various indices for robust and context-specific drought monitoring in the pursuit of effective resource management.

In recent decades, the Palmer Drought Severity Index (PDSI), SPI and SPEI drought indices have emerged as widely adopted globally (Hayes et al., 2011). Despite their wide utility across diverse water-related sectors, each index presents inherent limitations. The SPI, in its application, exhibits a pronounced dependence on precipitation data, thereby overlooking other salient variables that could significantly impact the comprehensive characterization of drought event. In contrast, the PDSI derives its computation from duration and weighting factors based on datasets exclusively observed within the geographical confines of the United States, thus limiting to diverse climate zones with its generalizability (Palmer, 1965; Zhang et al., 2018). Furthermore, the PDSI lacks the inherent multi-time scale features intrinsic to SPI, introducing challenges in its comparability with metrics associated with runoff and reservoir storage. Recognizing these limitations, Wells et al., (2004) introduced the Self-Calibrated PDSI (SC_PDSI), a novel drought index designed to accommodate local variations and applicable to diverse regions. Several comprehensive studies (Dai, 2011; Kang & Sridhar, 2019; Mishra & Singh, 2010; Zhang et al., 2015a) have extensively examined the strengths and weaknesses of SPI, SPEI and PDSI. From this thorough analysis, it becomes evident that employing multiple drought indices is imperative for an intricate analysis and evaluation of drought at regional scales. This multifaceted approach ensures a more robust and comprehensive understanding of the complex dynamics inherent in drought assessments.

For global socio-economic security, monitoring and understanding the droughts, along with their temporal and spatial evolution. The evaluation of drought indices allows for identifying their precision of drought events. Different indices may capture droughts with varying degrees of sensitivity and specificity. Precision in identification ensures that drought assessments are reliable indicators of actual conditions on the ground (Mckee et al., 1993). Evaluating the drought indices and their properties is crucial for ensuring their reliability and accuracy in representing drought conditions. Assessing the ability of drought indices to integrate multiple climatic variables is essential for capturing the complexity of drought conditions. Vicente- Serrano et al., 2011

emphasized the need to assess indices that consider both meteorological and hydrological variables. The significance of assessing the statistical robustness and precision of indices helps to enhance their reliability in characterizing drought events. Evaluating the properties and characteristics of indices ensures that the information generated is actionable and aligns with real-world scenarios.

1.3 Drought Indices and Link with Teleconnections

Droughts, as prolonged and severe climatic events, pose significant challenges to ecosystems, agriculture and water resources globally. The accurate assessment and prediction of drought conditions necessitate a comprehensive understanding of the complex interplay between meteorological variables and large-scale climate patterns. Drought indices such as the SPI, SPEI and SC_PDSI have emerged as vital tools for quantifying and characterizing drought severity. Concurrently, teleconnections, which signify long-range atmospheric and oceanic interactions, play a pivotal role in influencing regional climate patterns (Ashok et al., 2003; Kug et al., 2009; Torrence & Compo, 1998).

The global nature of drought necessitates a holistic exploration of its dynamics by considering both regional and large-scale climatic influences. For India, a country with diverse climatic zones, understanding the linkage between drought indices and teleconnections becomes particularly crucial. Prominent teleconnections such as the Southern Oscillation Index (SOI), Multivariate ENSO Index (MEI), Dipole Mode Index (DMI) and Niño 3.4 index significantly impact India's climate (Kripalani & Kulkarni, 2001; Kripalani & Singh, 1993). Investigating how these teleconnections influence the performance of widely used drought indices in this unique regional context is essential for advancing our knowledge of drought patterns and improving predictive models.

Many studies aimed to contribute to the understanding of global and regional drought patterns by assessing the intricate relationships between drought indices and teleconnections using wavelet coherence approach (Grinsted et al., 2004). By examining data from various climatic zones worldwide and focusing on India's diverse regions, the study seeks to identify patterns, correlations and potential variations in the performance of drought indices under the influence of teleconnections. Insights gained from this investigation are expected to have implications for

drought monitoring, prediction and adaptation strategies on both a global scale and within the specific regional context of India.

1.4 Drought Frequency Analysis

Drought, regarded as a natural hazard, manifests when there is a sustained deficiency in precipitation over prolonged durations. It signifies a transient departure from typical meteorological conditions and can occur as various climatic patterns. In contrast, aridity is a permanent climatic condition determined by long-term weather patterns in a specific region (Araghi et al., 2018; Karamouz et al., 2012). Therefore, the impact of climate change is anticipated to elevate both aridity and drought, posing significant challenges to agriculture, ecosystem and economy (Dai, 2013; Lobell et al., 2008). To execute effective water resource planning and management understanding the characteristics of dry conditions is crucial (Shiau J. T., 2006). Drought, being a complex natural disaster encompasses various factors like severity, intensity and duration (Kang & Sridhar, 2019; Mishra & Singh, 2010). Unlike other natural disasters, drought exerts their influence over large area extent (Kang & Sridhar, 2017; Sehgal et al., 2017; Wilhite et al., 2014). Consequently, analyzing drought conditions requires consideration of multivariate complexities and spatial variations.

India experiences drought events approximately once every three years across different geographical regions. In recent decades, the nation has confronted extended and severe drought conditions, marked by an escalating frequency in diverse areas (Bisht et al., 2019). Notably, a substantial proportion (approximately 70-90%) of the annual rainfall in India transpires during the Southwest monsoon from June to September (Bisht et al., 2018a, 2018b). Since most of the country rely on monsoonal precipitation, the failure of the monsoon can engender drought conditions (Kumar et al., 2013). In several aspects the distribution of drought in India is studied (Das et al., 2016; Gupta et al., 2020; Janga Reddy & Ganguli, 2012) and climate change exacerbates the vulnerability of India's water supplies to drought. Therefore, an imperative lies in conducting a regional investigation that centers on elucidating the imminent spatial and temporal attributes of drought. This endeavor is crucial for providing decision-makers and planners with essential insights, facilitating the formulation of efficacious policies aimed at mitigating the adverse effects associated with drought hazards.

Numerous investigations have systematically examined the intricate of monsoon rainfall at spatial and temporal nuances. Selected researchers documented an escalation in mean precipitation levels during the monsoon season, concurrently noting discernible variabilities at inter annual time spans (Chaturvedi et al., 2012; Fan et al., 2012). At the global level, regional inquiries have been undertaken to scrutinize the distinctive features of spatial and temporal drought phenomena. Multivariate models, exemplified by Spatial Duration Function (SDF) and Standardized Anomaly Function (SAF) curves, offer valuable tools for the comprehensive assessment of regional drought risk (Mishra & Singh, 2010). Drought curves are meticulously computed across diverse return periods, facilitating the establishment of mathematical relationships elucidating the interplay among severity, duration, interarrival time, area coverage and intensity. Providing a quantitative representation of various drought characteristics, these curves are crucial tools for a comprehensive understanding of droughts (Kang & Sridhar, 2021; Rajsekhar et al., 2015a).

1.5 Motivation of the Study

The selection of an appropriate GCMs not only help in understanding the physical aspects of drought but also in assessing the potential impacts on agriculture, water resources, ecosystems, and human populations. It also facilitates more accurate analysis of drought conditions by integrating climate variability, including the impacts of large-scale teleconnections. This holistic approach enhances our understanding of the complex interactions shaping drought dynamics and supports informed decision-making for sustainable development and climate resilience efforts. the increasing frequency of drought in recent years in India, using advanced GCMs can provide valuable insights into how drought risks may evolve in the future under different climate change scenarios. This information is vital for policymakers, planners, and stakeholders to make informed decisions regarding water management, agriculture practices, and disaster preparedness

1.6 Objectives of The Study

The primary objective of this study is to conduct a comprehensive regional analysis of drought by incorporating teleconnections and selecting suitable Global Climate Models over Telangana state, India.

To enhance clarity, the primary objective is subdivided into four sub-objectives outlined below.

1. Identifying and selecting suitable GCMs for Precipitation, Maximum, Minimum and Average Temperature.

2. Regionalization and evaluation of major drought events their properties using SPI, SPEI and SC_PDSI

3. Assessing the relationship between drought indices and teleconnections

4. Investigating multivariate frequency analysis: SDF and SAF using Copula

1.7 Outline of the Thesis

The study carried out in this investigation is organized in the following chapters. The thesis comprises of eight chapters: introduction, literature review, study area and data collection, four chapters for each sub objectives and finally conclusions in chapter 8.

Chapter 1 provides Introduction of comprehensive overview of the Global Climate Models and their role in understanding with climate change. Then analysis based on drought indices and its characteristics and overview of Teleconnections and drought frequency analysis.

Chapter 2 deals with the literature review covering each of the problems studied by earlier researchers. The summary of each of these studies are critically reviewed.

Chapter 3 deals with exploration of study area and data collection. Subsequent to this chapter, four additional chapters are presented, addressing each specific sub objective under consideration.

Chapter 4 deals with Selection of suitable GCMs for study area.

Chapter 5 deals with Regionalization and evaluation of drought characteristics (severity and duration)

Chapter 6 deals with the intricate relationship between drought indices and teleconnections.

Chapter 7 deals with the drought frequency analysis and development of Severity-Duration-Frequency and Severity-Area-Frequency curves.

Chapter 8 deals with summary, Conclusions and provides a glimpse into the Future outlook of the undertaken work.

CHAPTER 2

LITERARTURE REVIEW

In this section, a comprehensive examination of the studies conducted by previous investigators regarding the selection of GCMs, drought indices, their characteristics and their interconnections with teleconnection factors is presented.

2.1 Global Climate Models

A significant advancement were achieved in the development of GCMs to simulate the prevailing climate and forecast forthcoming climatic changes by *Xu, (1999)*. Demonstrating commendable proficiency at continental and hemispheric spatial scales, these models successfully captured a substantial portion of the complexity inherent in the global system. However, a fundamental limitation emerged in their incapacity to represent local sub grid-scale features and dynamics. This study provided a critical examination of the existing disparity between the capabilities of GCMs and the requisites of hydrological modelers. It delved into methodologies aimed at mitigating the gap, evaluating both advantages and shortcomings in various approaches. The discourse culminated in the identification of challenges that had to be addressed in comprehending the impacts of climate change in future studies.

An essential endeavor to examine coupled GCMs, as utilized in the Fourth Assessment Report (AR4) of the Intergovernmental Panel on Climate Change (IPCC), was investigated by Perkins et al. (2007). This scrutiny is specifically targeted at 12 distinct regions within Australia, with a particular emphasis on the meticulous examination of the daily simulation outputs for P, T_{max} and T_{min}. A robust assessment methodology is introduced centering on Probability Density Functions (PDFs) and a quantitative metric devised to assess the accuracy of each climate model in replicating observed PDFs for every variable within each designated region. Surprisingly, the coupled climate persisted. Averaging over Australia, a subset of climate models demonstrates commendable performance, capturing more than 80% of observed PDFs for P and T_{min} simulation is generally satisfactory, with a majority of GCMs capturing over 80% of observed PDFs. T_{max} simulation is also reasonable, with a significant portion of climate models exhibiting fidelity in capturing over 80% of observed PDFs. This study presented an overarching ranking of GCMs,

emphasizing their performance in P, T_{max} and T_{min} and an aggregate over these variables. This assessment identified skillful climate models for Australia, offering valuable guidance for their application in impacts assessments reliant on precipitation or temperature. It is essential to note that these results pertain specifically to the Australian context and the methodology can serve as a potent tool for selecting climate models in impacts assessments.

Involvement in the execution of numerous climate models across shared experiments, have yielded extensive datasets containing projections of future climate under various scenarios as studied by *Tebaldi & Knutti, (2007)*. These multi-model ensembles systematically capture uncertainties arising from initial conditions, parameters and structural aspects of model design. Consequently, diverse methodologies had emerged to probabilistically quantify uncertainty in future climate. This paper elucidated the rationale behind employing multi-model ensembles, conducted a comprehensive review of existing methodologies and performed a comparative analysis of their outcomes, focusing on regional temperature projections. The intricacies associated with interpreting multi-model results are thoroughly examined, addressing challenges stemming from the absence of climate projection verification, model dependence, bias, tuning issues and the complexities inherent in comprehending an ensemble of opportunity.

The performance evaluation of GCMs featured AR4 of IPCC concerning their ability to simulate P, T_{max} and T_{min} across the Murray-Darling Basin in Australia was studied by *Maxino et al., (2008)*. Utilizing daily data from the AR4, this study computed the mean and PDFs for each variable. The assessment focused on the skill of GCMs in reproducing the observed PDFs, serving as a basis for identifying GCMs with significant proficiency over the basin. Notably, the models from the Commonwealth Scientific and Industrial Research Organization (CSIRO), Institute Pierre Simon Laplace (IPSL) and MIROC-m demonstrated commendable fidelity in capturing the observed PDFs for P, T_{max} and T_{min}. While other models exhibited competence in one or two variables, this study manifested limitations or unassessed for the third variable. Thus, this study recommended CSIRO, IPSL and MIROC-m for users requiring model results in this basin, emphasizing the contextual specificity of this recommendation. The outlined methodology offers a quantitatively based and straightforward approach to model selection for impact assessment in regions with abundant data. Importantly, the approach emphasizes the simulation of daily derived PDFs, which

proves more challenging and robust than merely simulating the mean, providing a stronger basis for its application in impacts assessment.

Leveraging findings from the AR4 of the IPCC, this study employed extreme value theory to discern alterations in the 20-year return levels for daily T_{max} and T_{min} in Australia by *Perkins et al., (2009)*. The evaluation GCMs encompasses three key aspects: (a) mean performance (b) adeptness in replicating the observed PDFs and (c) proficiency in capturing the tails of the PDFs. Each ensemble of weak-skilled models indicated more substantial increases in both T_{max} and T_{min} return levels compared to their strong-skilled counterparts. Statistical analysis revealed a significant disparity between weak and strong skilled ensembles in T_{max}. Consequently, weak-skilled models projected statistically larger increments in warming for both T_{max} and T_{min} across Australia, regardless of the criterion used to assess skill. This study underscored the significance of model skill in influencing the magnitude of projected temperature changes, shedding light on the nuanced implications of model performance for temperature-related assessments.

The unprecedented availability of 6-hourly data from multi-model GCMs was examined by *McSweeney et al., (2015)*. This advancement prompted an examination of the feasibility of dynamically downscaling multiple GCMs. The proposed approach facilitates the generation of high-resolution climate projections, thereby enabling a nuanced evaluation of climate vulnerability and impacts. While the comprehensive dynamic downscaling of the entire CMIP5 ensemble necessitated substantial technical and human resources, such an extensive undertaking becomes was deemed superfluous. This study delineated a methodological framework for selecting a subset of 8–10 GCMs from the available CMIP5 models, to represent suitable GCMs of individual regions, such as Southeast Asia, Europe and Africa. The process aimed to exclude models deemed least realistic for each region, while concurrently capturing the maximum conceivable range of variations in surface temperature and precipitation across the specified continental-scale regions. Within the subset of CMIP5 GCMs featuring 6-hourly fields, three models (MIROC-ESM, MIROC-ESM-CHEM and IPSL-CM5B-LR) were identified as inadequately simulating key regional climate aspects, earning them the classification of 'implausible.' Subsequently, the remaining models underwent a selection methodology aimed at precluding the inclusion of the least performant models unless their exclusion would substantially diminish the range of sampled

projections. This meticulous process culminated in the identification of a refined set of models well-suited for generating downscaled climate change information, thereby facilitating a coherent and comprehensive multi-regional assessment of climate change impacts and adaptation strategies.

The ensemble of Earth system models accessible in the repository of the fifth phase of the CMIP5 was regarded as a representation of uncertainty in the trajectory of future climate conditions is proposed by *Sanderson et al., (2015a)*. However, the existence of shared code, forcing and validation data across multiple models within the archive introduces potential challenges, including biases in mean and variance, an inflated effective sample size and the risk of spurious correlations due to model replication. This study provides analytical evidence demonstrating that the model distribution in the CMIP5 archive deviates from a random sample. To address codependency issues in the ensemble, a weighting scheme is proposed. Additionally, a method was introduced for the selection of diverse and skillful model subsets within the archive, offering a means to mitigate codependency concerns and facilitating the identification of models suitable for impact studies requiring consistent joint projections of multiple variables, including their temporal and spatial characteristics.

An investigation delved into the assessment of thirty-six GCMs based on the CMIP5, focusing on the simulation performance of T_{max} and T_{min} across 40 grid points in India by *Srinivasa Raju et al., (2017)*. Three performance indicators—CC, Normalized Root Mean Square Error (NRMSE) and SS—were utilized for GCMs evaluation. The entropy method was utilized to determine weights for these indicators, with equal weights being employed in sensitivity analysis. The CP, a distance-based decision-making technique, was adopted to amalgamate ranking patterns acquired for individual grid points, and a straightforward yet efficacious ensemble approach was proposed.

2.2 Drought Indices and its properties

The imperative necessity for comprehensive research encompassing diverse facets of expansive continental droughts, with the objective of establishing methodologies for their definition, was underscored by *Yevjevich & Ica Yevjevich, (1967).* The proposal advocated the utilization of runs as statistical parameters to delineate the temporal and spatial distribution of water deficits in the context of drought definition. Three specific types of runs are identified as pivotal parameters for drought definitions: (1) Run length of negative deviations within a time series (duration of drought): This parameter focuses on quantifying the temporal extent of droughts by measuring the

length of continuous periods featuring negative deviations from the norm. (2) Run-sum of negative deviations between a downcross and an upcross of a time series (severity of a drought): This parameter evaluated the severity of a drought by summing the negative deviations between the points where the time series crossed below and then above a defined threshold and (3) Area-run as the deficit of water over a specific time duration (run-length) and area of drought: This parameter integrates both temporal and spatial aspects of drought by assessing the deficit of water over a designated time duration and the corresponding geographical area. Analytical and data generation methods were proposed to determine runs based on known properties of hydrologic time series and the interdependence between them. These methodologies were employed at Colorado State University over a span of 4 to 5 years to investigate the properties of precipitation, effective precipitation, and runoff, thereby influencing drought descriptions. In essence, the research outlook encompasses the prediction of large continental droughts and the elucidation of potential causal factors underlying their occurrences.

A streamflow series was comprehensively analyzed for multiyear drought events by *Dracup et al., (1980)*. These tests, applied to both high-flow and drought event parameters, encompassed the examination of (1) stationarity concerning linear trends, (2) randomness in relation to lag-1 serial correlation and (3) correlation and cross-correlation among critical parameters, including the duration, magnitude and severity of drought events. The outcomes of these statistical examinations were carefully analyzed to elucidate their significance in characterizing both high-flow and drought event series. Furthermore, the assessment of high-flow and drought event series introduces two distinct types of envelopes designed for drought duration and severity. These envelopes utilized inequality principles to offer an exceptional representation of the maximum watershed response concerning drought duration and severity across the entire record period. The presentation of these envelopes contributed valuable insights into understanding the watershed's behavior in terms of drought characteristics over time.

Delving into several critical considerations for formulating a pragmatic and analytical definition of droughts provided by *Dracup et al., (1980b)*. Key aspects discussed encompass: (1) The delineation of the specific nature of the water deficit under scrutiny, distinguishing between hydrological, meteorological, or agricultural droughts. (2) The selection of the averaging period utilized to discretize the continuous time series, considering options such as months, seasons, or

years. (3) the determination of the truncation level applied to separate drought events from the remaining time series, whether based on mean or median values. and (4) the methodology employed for standardization. These assessments are thoroughly examined considering their implications on diverse approaches to drought frequency analysis. Within the scope of this research, drought events were conceptualized as intricate phenomena characterized by distinct components, namely, duration, magnitude (quantifying average water deficiency), and severity (measuring cumulative water deficiency). The study subsequently applied the proposed drought definition procedure in a practical context, exemplified through a case study involving the frequency analysis of multiyear hydrologic droughts. This comprehensive exploration aimed to contribute to the refinement and standardization of analytical frameworks for drought characterization, fostering a more nuanced understanding of drought dynamics in diverse contexts.

A novel climatic drought index, termed the SPEI was introduced aiming to enhance the existing methodologies by incorporating both precipitation and temperature data by *Vicente-Serrano et al., (2010)*. The SPEI offered the advantage of integrating multiscale characteristics with the ability to consider temperature variability in the assessment of drought conditions. The computation of the index entailed a meticulous procedure that integrated a climatic water balance, the aggregation of deficit or surplus at various time scales and an adjustment to a log-logistic PDFs. Although sharing mathematical similarities with the SPI, the SPEI uniquely incorporated temperature effects. Incorporating a water balance, the SPEI allows for a meaningful comparison with the SC_PDSI. Comparative analyses of time series data for these indices was conducted across various observatories located in distinct climatic regions worldwide. The results under conditions of global warming reveal that, unlike SPI, both the SC_PDSI and SPEI accurately depict an intensification in drought severity attributable to heightened water demand resulting from increased evapotranspiration. Notably, the SPEI, boasting multiscale attributes

, outperforms the SC_PDSI in terms of versatility, proving invaluable for comprehensive drought analysis and monitoring.

Drought, a stochastic natural hazard induced by prolonged and intense precipitation deficits, manifested significant and delayed impacts on agriculture and hydrology reviewed by *Zargar et al., (2011)*. Droughts exhibited distinctive features, characterized by dynamic dimensions such as severity and duration, contributing to a complex and subjective network of consequences. Effective

drought management necessitates comprehensive characterization, enabling both retrospective analyses (e.g., severity-impact assessment) and forward-looking planning (e.g., risk evaluation). Drought indices, offering a simplified approach, have facilitated this characterization, with over 100 indices proposed to date. Some are operational, providing gridded maps for regional and national drought assessment, addressing meteorological, agricultural, and hydrological drought types. This paper critically reviewed 74 operational and proposed drought indices, emphasizing their distinctions and tracing their developmental trends. The diverse array of indices enabled the quantification of severity levels and identification of drought onset and cessation, supporting various applications such as early warning systems, monitoring efforts and contingency planning.

A streamflow simulations derived from the Variable Infiltration Capacity (VIC) model is used to characterize droughts over the period 1950–2000 was employed by *Goyal & Sharma, (2016)*. The focus of the study is on regionalization for the state of Texas, with a specific emphasis on annual drought severity levels and durations. Recognizing the regional nature of droughts, the identification of homogeneous drought regions becomes imperative for a nuanced exploration of their characteristics. In this study, the concept of entropy is employed to delineate homogeneous regions based on both drought severity and duration. Directional information transfer, represented by a standardized version of mutual information, is utilized for station grouping, and the homogeneity of regions is rigorously assessed through L-moments. The outcomes of this analysis reveal the formation of eight regions based on drought severity and nine regions based on drought duration. Notably, regions in west Texas exhibited heightened severity, in contrast to east Texas, which manifested the least severity. South Texas and lower valley zones endured the longest drought durations, while east Texas and the upper coast experienced the least prolonged droughts. The study highlighted that critically severe and extremely dry droughts are predominantly concentrated in the western and central parts of Texas, underscoring the spatial variability of drought characteristics across the state.

2.3 Teleconnections

The temporal patterns of precipitation and the influence of large-scale climate anomalies within the Pearl River basin in South China particularly on subbasin scale is investigated by *Niu, (2013)*. Utilizing three prominent data analysis techniques—wavelet analysis, principal component analysis (PCA) and rank correlation—the research, encompassing hydrological factors, water

resource activities and large-scale climate data, intricately subdivides the entire basin into ten sub-basins, with the analysis conducted on monthly data. The wavelet analysis revealed distinct differences in the temporal scales of fluctuation embedded in monthly precipitation anomalies across the basin. PCA identified three coherent regions that demonstrate a similar distribution of variability across scales. Employing cross-wavelet transform and wavelet coherence to analyze linkages between precipitation and teleconnection patterns, the study indicated that the dominant variabilities of precipitation are primarily characterized by the IOD, particularly in the central and eastern parts of the Pearl River basin. Regarding the influence of the El Niño-Southern Oscillation (ENSO) signal on precipitation, a more significant correlation was observed in the eastern part of the basin. Long-term relationships within the 4–8 years band are identified in the western part, while the central part appears to serve as a transition zone. Rank correlations of scale-averaged wavelet power between regional precipitation and climate indices for the dominant low-frequency variability band (0.84–8.40 years) provide additional support for varying precipitation-climate relationships across different regions.

The influence of large-scale climate drivers on drought is imperative for a more profound understanding and effective management of these widespread and often prolonged natural hazards was quantified by *Kingston et al., (2015*). This study significantly contributed to advancing our understanding of drought dynamics at the continental scale, with a specific focus on Europe. Drought events were identified utilizing two key indices: the 6-month cumulative Standardized Precipitation Index (SPI-6) and the Standardized Precipitation Evapotranspiration Index (SPEI-6). These indices were computed based on the gridded Water and Global Change (WATCH) Forcing Dataset, covering the period from 1958 to 2001. By correlating monthly time series of the percentage of the European area experiencing drought with geopotential height for the same period, the study revealed an association between the onset of drought and a weakening of the prevailing westerly circulation. This atmospheric condition was intricately linked to variations in the eastern Atlantic/western Russia (EA/WR) and North Atlantic Oscillation (NAO) patterns. Through event-based analysis of the most widespread European droughts, the study observed that the SPEI-6 identifies a higher number of events compared to the SPI-6. Moreover, SPEI-6 drought events exhibit a greater diversity in spatial locations and onset dates. The atmospheric circulation drivers also differ between these two types of events, with EA/WR-type variation frequently associated with SPEI-6 droughts and NAO associated with SPI-6. This distinction underscored the

sensitivity of these drought indices to the underlying drought type- meteorological water balance versus precipitation, respectively- and the consequential variations in their timing and spatial distribution.

An advanced forecasting scheme designed to enhance the relevance, timeliness and reliability of climate information was introduced by *Manatsa et al., (2017)*. Departing from traditional precipitation-only indices such as the SPI, the study adopts the SPEI, incorporating temperature and other climatic factors in its formulation. Notably, the SPEI demonstrated a more robust connection to the ENSO compared to the SPI. The developed ENSO-SPEI prediction scheme provides a quantitative assessment of the spatial extent and severity of predicted drought conditions, aligning more closely with the risk profile in the context of global warming in the sub-region. However, the study established that the substantial regional impact of ENSO was confined to the period December–March. This prompted a reevaluation of traditional ENSO-based forecast schemes, particularly those dividing the rainfall season into October to December and January to March. Despite advancements in numerical models for ENSO prediction, this research underscores that anticipating drought impacts associated with ENSO is feasible based solely on observations. A notable temporal lag is observed between the development of ENSO phenomena (typically in May of the preceding year) and the identification of regional SPEI-defined drought conditions. The study demonstrates that using the Southern Africa Regional Climate Outlook Forum's (SARCOF) traditional 3-month averaged Nino 3.4 Sea Surface Temperature (SST) index (June to August) as a predictor does not offer significant advantages over using only the May SST index values.

A comprehensive analysis of monthly and seasonal maximum daily precipitation (MMDP and SMDP) across 131 stations in Canada was conducted by *Tan et al., (2016)*. Employing various adaptations of wavelet analysis, the research revealed that interannual oscillations (1–8 years) manifest more pronounced significance compared to interdecadal oscillations (8–30 years) across all selected stations. These oscillations exhibited spatial and temporal dependence. The wavelet coherence and phase difference between leading principal components of monthly precipitation extremes and climate indices are found to be highly variable in both time and periodicity. Notably, a singular climate index accounts for less than 40% of the total variability. Partial wavelet coherence analysis unveils that both ENSO and PDO modulate the interannual variability, while

PDO specifically influences interdecadal variability in MMDP across Canada. NAO exhibits correlation with western MMDP at interdecadal scales and eastern MMDP at interannual scales. Through composite analysis, it was evident that precipitation extremes at approximately three-fourths of the stations are significantly influenced by ENSO and PDO patterns, while around half of the stations are impacted by NAO patterns. Examining extreme El Niño and extreme PDO events of positive phase, the study revealed that the magnitude of SMDP is generally lower (higher) over the Canadian Prairies in summer and winter (spring and autumn) during extreme El Niño years and vice versa in extreme La Niña years.

The impact of large-scale climatic teleconnections on meteorological events in Iran through an analysis of three prominent climatic indices: Arctic Oscillation (AO), North Atlantic Oscillation (NAO) and SOI. Spanning the period from 1960 to 2014, the assessment employs wavelet coherence (WCO) within a time-frequency space across 30 synoptic stations was investigated by *Araghi et al., (2017)* . The investigation yields insights into the substantial influence of climatic indices on precipitation patterns in Iran. Specifically, the SOI emerges as the most influential, with noticeable effects also attributed to AO and NAO The dominant effective period of AO on precipitation is equal to or greater than 32 months at most stations, whereas NAO's major effective period is equal to or greater than 64 months. In the case of SOI, the impact duration is generally less than 64 months for most regions, except for the northwestern area where a predominant period greater than 64 months is observed. Phase differences between the three climatic indices and precipitation were found to be random, with no consistent patterns. Notably, an anti-phase situation was identified at most stations for long-term periods of SOI. The study underscores the efficacy of Wavelet Coherence Analysis (WCO) as a potent and flexible method for analyzing the relationship between multiple time series in a time–frequency space. The application of WCO in hydrological and meteorological research was anticipated to witness significant growth in the near future.

Hydro-meteorological variables, including precipitation and streamflow, were intricately influenced by diverse climatic factors and large-scale atmospheric circulation patterns was explored by *Rathinasamy et al., (2017)*. Achieving efficient water resources management necessitates a profound comprehension of the impact of climate indices on the precise predictability of precipitation. This study focused on elucidating the standalone teleconnection between precipitation patterns across India and four prominent climate indices: Niño 3.4, Pacific

Decadal Oscillation (PDO), SOI and IOD. The investigation employed partial wavelet analysis, considering the cross-correlation between the climate indices while estimating their relationship with precipitation. Unlike prior studies that overlooked the interdependence among these climate indices when analyzing their effects on precipitation, our study delves into these interrelationships. The findings underscore that precipitation was primarily influenced by Niño 3.4 and IOD, indicating a non-stationary relationship between precipitation and these two climate indices. Moreover, the partial wavelet analysis revealed that SOI and PDO do not significantly impact precipitation independently; however, their apparent influence may be attributed to their interdependence on Niño 3.4. Notably, the study observes that partial wavelet analysis robustly unveils the standalone relationship of climatic factors with precipitation after mitigating the influence of other potential factors. This nuanced understanding enhances our ability to discern the direct teleconnections between specific climate indices and precipitation in the Indian context.

2.4 Drought Frequency Analysis

Definition of drought was deliberated both practically and analytically was formulated *Dracup et al., (1980b)*. The key considerations encompassed (1) focus on nature of the water deficit that specified hydrological, meteorological, or agricultural aspects (2) averaging period for discretize a continuous time series that helps to analyze data at monthly, seasonal, or yearly intervals are deemed crucial in capturing the temporal dynamics of drought (3) truncation level for separate droughts helps to delineate drought time series (mean or median) emphasizing its impact on drought frequency analysis (4) method of regionalization or standardization. These considerations explain their impacts on various approaches to drought frequency analysis. To summarize, drought events were characterized in terms of duration, magnitude and severity. The proposed methodology was applied in a case study featuring a frequency analysis of multiyear hydrologic droughts. The study concluded that the definition of drought significantly affects the sample size, drought severity, magnitude and duration and the areal extent considered in the analysis. Hydrologists and meteorologists were advised to consider the advantages and disadvantages of a chosen drought definition in the context of their specific analysis.

The spatio-temporal characteristics of drought for sustainable water resource management in the Conchos River Basin, Mexico was explored by *Kim et al., (2002)*. The Palmer Drought Severity Index (PDSI) served as indicator to assess the drought characteristics. Frequency analysis method

was employed to investigate the spatio-temporal variations of drought based on drought intensity. The kriging estimator was then utilized to examine the spatial distribution of drought. This study incorporated the spatial and temporal characteristics of PDSI in developing drought intensity-areal-frequency curves. These curves explain drought severity and area w.r.t the return period and to describe the spatial and recurrence patterns of droughts. The analysis highlighted that a severe drought in the year 1990 with a substantial areal extent and a return period of 80 to 100 years.

A theoretical derivation for univariate and bivariate distribution return periods through a stochastic approach, was particularly focused on extreme hydrological event *Shiau, (2003)* presented. Understanding the nature of complexity of drought and flood events, the bivariate distribution was considered as a better approach to represent these events (droughts and floods) compared to the univariate distribution. Return periods were defined using either two joint random variables or separate single variables for bivariate distribution. The study employed Gumbel marginal distributions to model the flood peak and flood volume in Pachang River, Southern Taiwan based on daily streamflow data. The properties associated with both univariate and bivariate distributions was discussed and a good agreement between the models and observed streamflow data.

A comprehensive analysis of spatial and temporal variations of drought in the Kansabati River Basin, India was conducted by *Mishra & Desai, (2005)*. Utilizing the SPI at multiple timescales (1, 3, 6, 9, 12 and 24 month), the basin was divided into 25 grid cells. The inverse distance method was employed at each grid for spatial interpolation of precipitation dataset and monthly SPI was evaluated using the rain gauge station data for the period 1965–2001. Drought severity, duration and frequency were assessed at various timescales. Then, SAF curves were developed using the spatio-temporal characteristics of SPI. The SAF curves showed drought severity and area at different return periods to describe the spatial and recurrence patterns of drought. The results highlighted high short-term droughts in 1979 with return periods of 80 to 100 years over the entire basin, while Medium and long-term droughts were frequent in the 1980's with a return period of 50 to 100 years, significantly impacting agriculture, reservoir storage and groundwater in the basin.

A two-dimensional copula for drought severity and duration was constructed by *Shiau, (2006).* Copula parameters were estimated using the Inference Function for Margins (IFM) method, assuming gamma and exponential distributions for drought severity and duration. Further various

copulas were tested for drought severity and duration, Galambos copula identified as the best fit for observed drought. The study applied this approach to determine the severity and duration of droughts using SPI for Wushantou, Taiwan. The results indicated a well-fitted copula for the drought severity and duration, considered its utility as a valuable tool for exploring the relationships among drought variables.

A comprehensive examination of hydrological droughts using copulas in the Yellow river, China, employing copulas to jointly model drought severity and duration was conducted by *Shiau et al., (2007)*. Monthly streamflow data was used to evaluate drought characteristics. As droughts were complex in nature, the study applied a bivariate distribution for drought assessment by utilizing the clayton copula to describe the joint behavior of drought severity and duration. to model drought severity and duration jointly and copulas was used to achieve this purpose. Further, bivariate return periods was also calculated to identify significant historic droughts. The results conclude that a severe drought occurred during 1930-1933 with a return period of 105 years and a low return period of 4.4 years during 1997–1998 drought, attributed to significantly reduced streamflow in the Yellow River due to human activities.

Spatial characteristics of drought over Razavi and Southern Khorasan provinces in Iran using SPI12 was assessed by *Bondarabadi et al., (2008)*. Drought maps were generated through the thin plate smoothing splines method and classified into clusters. PDFs were fitted to different SPI categories and SAF curves corresponding to different return periods were developed for the study region. The results indicated that droughts with 2-to-5-year return periods were expected to cover approximately 30% of the region, while severe droughts with 20-to-50-year return periods may cover around 70% of the region, emphasizing the expectation of severe droughts with high return periods and less areal coverage.

The assessment of climate change impact on SPI over the Kansabati River Basin, India, as conducted by Mishra & Singh (2009), involves a comprehensive analysis. Historical drought events were juxtaposed with SAF curves derived from projected rainfall data, incorporating select General GCMs and accounting for scenario uncertainties. The Bayesian Neural Network (BNN) downscaling method was deployed to extrapolate precipitation patterns from six GCMs, subsequently assessing SPI at 3 and 12-month temporal scales. The results indicated an increase

in severe droughts during 2001-2050 as compared to the droughts 1980. The developed SAF curves were deemed useful for anticipating drought severity with the percentage of areal extent over future periods and the author suggested utilizing multiple GCMs helps to ease biases and uncertainties in simulations and scenarios.

To assess multi attributes of drought, SDF curves were developed using copulas for two rain gauge stations in Iran by *Shiau & Modarres, (2009)*. Using rainfall series from 1954-2003, SPI3 calculated and used to define drought properties severity, duration, and frequency. A joint distribution function was employed for drought severity and duration using copulas and the drought frequency was related to the copula-based distribution function to develop SDF curves. The analysis revealed that for a given return period and duration, Anzali station experienced greater drought severity compared to Abadan station, with the SDF curves concave downwards indicating an increase in drought severity increases with duration.

SDF curves were developed using a copula-based bivariate probabilistic approach over Western Rajasthan, India by *Janga Reddy & Ganguli, (2012)*. In this study, SPI at 6-month time scale is utilized to analyze the drought characteristics. The joint distribution of severity and duration are modelled using Plackett, Archimedean, Elliptical and Extreme Value copula families were employed to model the joint distribution of severity and duration. The Gumbel-Hougaard and Extreme Value copulas functioned better in modelling the drought characteristics, based on upper tail dependence coefficients and statistical techniques. SDF curves were further derived, with the conditional return periods assessed using the most effective copula. The study concluded that these SDF curves hold potential for aiding in the planning and management of water resources at drought prone areas.

A study was conducted to assess the effectiveness of two metaheuristic methods namely Particle Swarm Optimization (PSO) and Genetic Algorithm (GA) in estimating the copula parameters and developing SDF curves over Trans Pecos, which was an arid region in Texas, USA by *Reddy & Singh, (2014)* . Drought characteristics was analysed using SPI and drought risk is assessed using copula methods. To enhance the accuracy of copula model estimation accurate estimation, GA and PSO techniques were applied. Initially, the drought characteristics: severity and duration were modelled separately by using various PDFs and the best-fitted models selected for copula modelling. Three copula families, namely Extreme Value, Plackett and Student's-t were employed

to capture the joint dependence between drought severity and duration. The performance of these copulas was evaluated using Kolmogorov–Smirnov (KS), Akaike Information Criteria (AIC) and tail dependence tests. The results of these performance measures indicated that the Gumbel-Hougaard copula was fitted as the best model and subsequently employed for development of SDF curves. The findings conclude that the use of meta-heuristic techniques helps in accurate estimation of copula parameters and derivation of SDF curves.

Development of hydrologic drought atlas aimed at delineating the spatial variation of severity for durations of 3, 6, 12 and 24-months, corresponding to return periods 10, 25, 50 and 100-year across Texas state by *Rajsekhar et al., (2015)*. Drought characteristics are derived using the Variable Infiltration Capacity (VIC) model applied to monthly stream flow data. The Standardized Stream Flow Index (SSFI) is employed to evaluate drought severity and duration and appropriate marginal distributions is chosen from gamma, exponential, Weibull and log - normal distributions. The study further modeled the joint dependence between drought severity and duration using various copula families. Subsequently, SDF curves are developed using the best performed copula. These SDF curves are used in constructing the drought atlas for Texas, illustrating drought severity for specific durations and return periods. The findings of the research conclude that SDF curves showed convex (concave) pattern in arid and semiarid (humid and semi humid) regions. Also, a decreasing trend in drought severities is noticed from West to East of Texas.

A study focusing on the Lake Urmia Basin in Iran was conducted and developed SPI and SAF curves based on one month SPI data for the years 1971 to 2013 by *Amirataee et al., (2018)*. The joint PDFs of drought severity and drought area was subsequently modeled using seven copula functions from distinct families: Clayton, Gumbel, Frank, Joe, Galambos, Plackett and Normal copulas. Frank copula was chosen as the most suitable copula for constructing the joint probability distribution. considering various criteria Akaike Information Criteria (AIC), Bayesian Information Criteria (BIC) and Root Mean Square Error (RMSE). Frank copula was further used to develop SAF curves. The findings underscore the substantial influence of both severe/extreme drought and non-drought (wet) behaviors across the majority of the Urmia basin.

A spatiotemporal analysis of drought occurrence, frequency and hazard in different parts of India was conducted by *Gupta et al., (2020)*. They utilized meteorological data from a selected regional

climate model for RCP 8.5 to compute the Standardized Precipitation Evapotranspiration Index (SPEI) at a 12-month timescale. The study introduced an improved methodology for generating Severity-Duration-Frequency (SDF) curves under a Bayesian framework. This novel approach, employing copulas, utilized Markov Chain Monte Carlo simulation for parameter estimation. Furthermore, the researchers developed Spatially Averaged Frequency (SAF) curves for different homogeneous drought regions of India. The study also introduced the Modified Drought Hazard Index (MDHI), an enhanced metric for fuzzy drought hazard assessment based on clustering. The results of the analysis suggest that, except for Region 2 (Western Ghats), drought frequency increased over time in all regions of India. Moreover, drought severity associated with various durations is projected to significantly increase with an increase in duration for most regions. The study predicted that drought hazard is expected to be higher during the period 2071–2100.

2.5 Summary and Research gaps

The Summary on multivariate drought event analysis using Global climate models and teleconnections is as follows :

Selection of suitable Global climate model helps to analyze the drought conditions of any region more accurately. Global climate models are the only models available for projecting climate systems at any time scale either globally or regionally. In India, frequency of drought has increased in recent years and so there is a need to analyze drought both spatial and temporally. Regionally, a special attention is needed to characterize the likely occurrence and distribution characteristics of droughts for the future. From literature, noticeable effects of largescale teleconnections were observed on meteorological variables. Therefore, it is also necessary to analyze climate variability (large scale Teleconnections) with drought indices pattern**.**

Limited studies have been conducted to analyze climate change impacts by considering suitable specific global climate models. A gap in exploration of regional Climate change aspects in relation to projection of drought indices is noticed. India is significantly influenced by large scale oscillations; drought indices are to be investigated considering the climate indices. Studies on multivariate drought frequency analysis (Severity-duration-frequency and Severity-area-frequency) is not performed and projected using suitable GCMs.

CHAPTER 3

STUDY AREA AND DATA COLLECTION

3.1 Study Area

The Telangana region covering an area of 1,12,100 square kilometers, is characterized by a catchment area of 69% of river Krishna and 79% of river Godavari. It is a semi-arid region and has a predominantly hot and dry climate. Annual rainfall ranges from 700mm to 1500mm and average temperature varies from 22° to 42°c.

The economic foundation of Telangana is predominantly rooted in agriculture. The state benefits significantly from the presence of two major rivers in India, the Godavari and Krishna, which traverse through, providing essential irrigation support. Agriculture in Telangana relies heavily on rain-fed water sources. Primary crops include rice, with additional emphasis on cotton, sugar cane, mango, and tobacco as local staples. Notably, there has been a recent shift towards cultivating crops such as sunflower and peanuts for vegetable oil production. Ongoing developments encompass various multi-state irrigation projects, notably the Godavari River Basin Irrigation Projects and the Nagarjuna Sagar Dam, recognized as the world's highest masonry dam.

Figure 3.1 in the study provides a visual representation of the study area map.

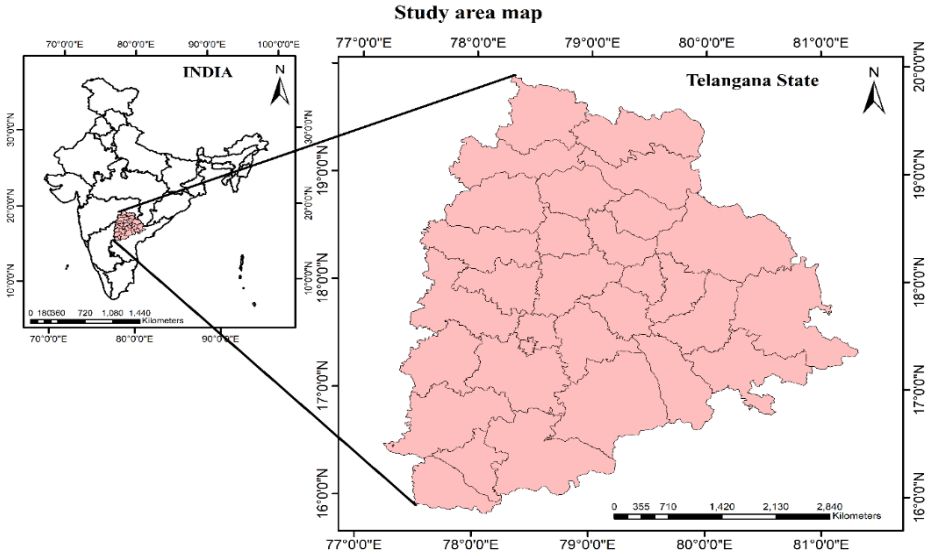

Figure 3.1. Study area map considered for the research.

Hydromorphological conditions in Telangana, India, encompass a variety of factors influenced by the state's geography, climate, and human activities mentioned below:

River Systems: Telangana is traversed by several rivers, including the Godavari, Krishna, and their tributaries. These rivers play a crucial role in the state's water resources, agriculture, and overall ecosystem health. However, their flow and health are significantly impacted by damming, irrigation projects, and diversion for urban and agricultural needs.

Groundwater: The state heavily relies on groundwater for irrigation and domestic use. However, over-extraction and inadequate recharge mechanisms have led to declining groundwater levels in several areas, exacerbating water scarcity issues, particularly during dry periods.

Reservoirs and Tanks: Telangana has numerous reservoirs and tanks (local water storage structures) that play a vital role in water management, particularly for agriculture.

Water Quality: Industrialization and urbanization have introduced pollutants into the water bodies of Telangana, affecting water quality.

Hydrological Extremes: Telangana experiences both droughts and occasional floods. The state government has implemented various measures for flood control and mitigation, including the construction of reservoirs with flood control capabilities.

Erosion and Sedimentation: Soil erosion, particularly in the catchment areas of rivers and reservoirs, contributes to sedimentation, affecting water storage capacity and water quality.

Urban Water Management: Rapid urbanization in cities like Hyderabad has placed significant pressure on water resources. Efforts are being made to improve urban water management practices and infrastructure to meet growing demands sustainably.

Climate Change: The changing climate patterns, including variations in rainfall intensity and distribution, pose challenges to water resource management in Telangana. Adaptation strategies are being explored to mitigate the impacts of climate change on water availability and quality.

Overall, the hydro morphological conditions in Telangana reflect a complex interplay of natural processes and human activities, necessitating integrated water resource management approaches for sustainable development and environmental conservation.

Telangana, like many regions in India, has experienced several notable droughts throughout its history which have significant socioeconomic and environmental impacts.

1966: This drought was severe and widespread across India, including Telangana. It led to significant agricultural losses and water scarcity.

1972: Another major drought that affected Telangana and other parts of India, causing crop failures and water shortages.

1985-1987: This was a prolonged drought period that affected Telangana, among other regions in India. It led to widespread distress in agriculture and affected rural livelihoods.

2002: Telangana experienced a severe drought in 2002, which was part of a larger drought affecting many parts of India.

2015: In recent times, Telangana faced another severe drought in 2015. This drought significantly impacted agriculture, particularly rain-fed crops.

2018: Parts of Telangana experienced drought conditions in 2018, leading to agricultural stress and water scarcity issues.

Issues associated with droughts in Telangana are mentioned

Frequency and Severity: Telangana is prone to recurrent droughts, typically caused by deficient monsoon rains. These droughts vary in severity and duration, affecting agricultural productivity, water availability, and livelihoods.

Agricultural Impacts: Agriculture is the backbone of Telangana’s economy, with a substantial portion of the population dependent on rain-fed farming. Drought leads to crop failures, reduced yields, and loss of livestock, impacting farmers' incomes and food security.

Water Stress: Droughts exacerbate water stress in Telangana, particularly in rural areas dependent on groundwater and surface water sources. Over-extraction of groundwater during droughts can lead to depleted aquifers and long-term water scarcity issues.

Livelihood Challenges: Droughts often result in economic distress and migration as farmers struggle to cope with crop failures and loss of income. Rural communities dependent on agriculture face heightened vulnerability during prolonged dry spells.

Environmental Impact: Droughts can lead to environmental degradation, including soil erosion, loss of vegetation cover, and depletion of biodiversity. Reduced water availability also affects ecosystems, wildlife, and natural habitats.

Social Implications: Droughts exacerbate social inequalities and vulnerabilities, disproportionately affecting marginalized communities, women, and children. Access to water, healthcare, and education can become compromised during severe drought periods.

Policy and Management Challenges: Effective drought management requires robust policies, early warning systems, and proactive measures such as water conservation, watershed management, and drought-resistant crop cultivation. Challenges arise in implementing these measures effectively across diverse socio-economic landscapes.

Climate Change: Changing climate patterns, including erratic rainfall and rising temperatures, pose additional challenges for drought mitigation and adaptation strategies in Telangana. Climate change projections suggest an increase in the frequency and intensity of extreme weather events, including droughts.

In response to these challenges, Telangana has implemented various drought management strategies, including drought relief measures, water conservation programs, crop insurance schemes, and investments in irrigation infrastructure. However, continued efforts are needed to enhance resilience, improve water resource management, and mitigate the impacts of future drought events on the state's population and environment.

3.2 Data Collection

3.2.1 India Meteorological Department (IMD)

In the present investigation, gridded datasets comprising precipitation, maximum temperature, minimum temperature and average temperature have been employed. These datasets originate from the India Meteorological Department (IMD) and span the temporal interval from 1975 to 2017. The data under consideration is characterized by a spatial resolution of 1°×1°, with temporal increments maintained on a monthly basis within the specified study area, as elucidated in the works of Rajeevan et al. (2008) and Srivastava et al. (2009).

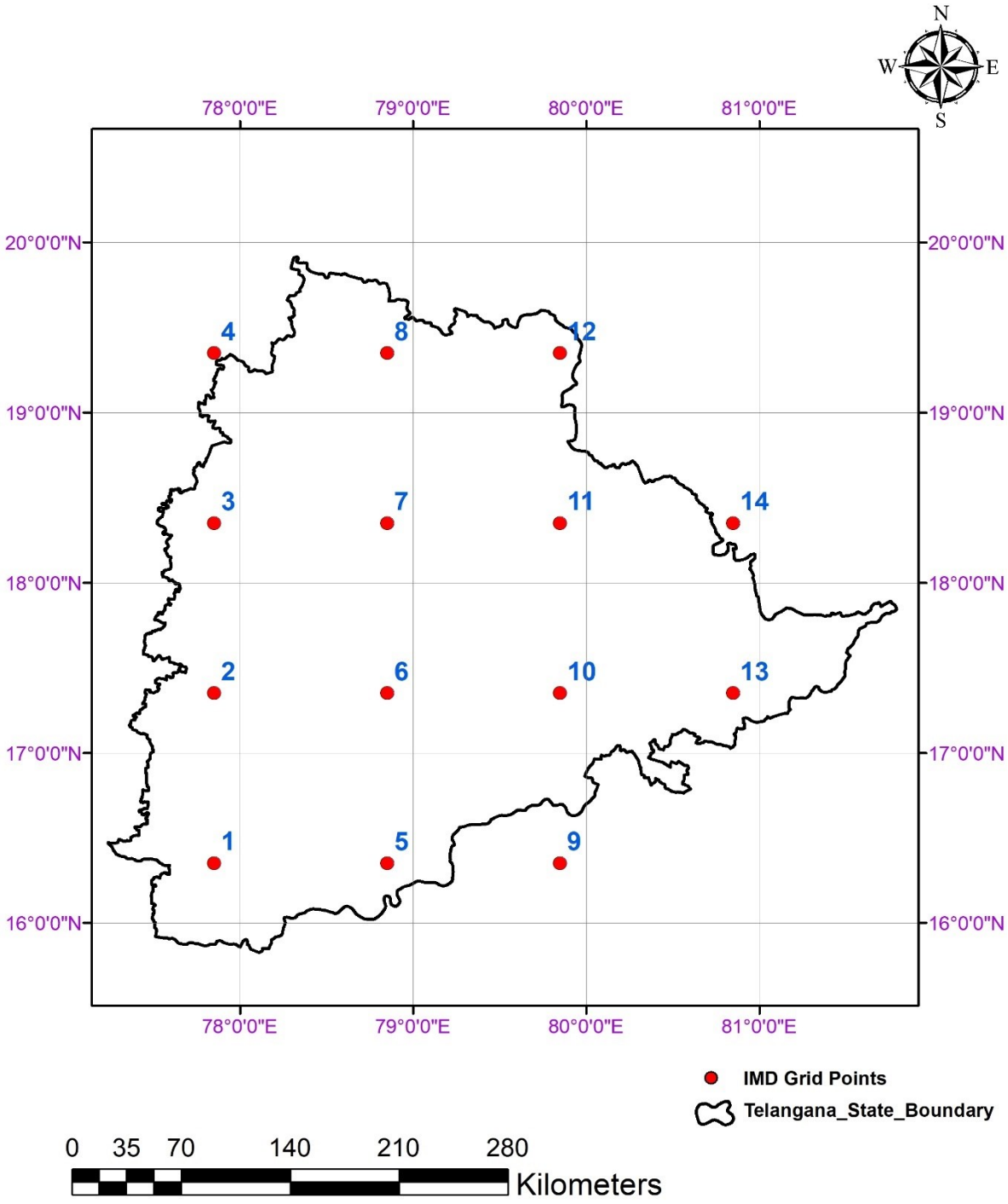

Figure 3.2. Study area map with grid points considered for the research.

Table 3.1 Global Climate Models (GCMs) considered in the study.

S.No	Model name	Resolution
1	BCC-CSM1-1	2.8°×2.8°
2	BCC-CSM1.1(m)	2.8°×2.8°
3	BNU.ESM	2.8°×2.8°
4	CanESM2	2.8°×2.8°
5	CMCC-Cm	0.75°×0.75°
6	CMCC-CMS	1.88°×1.87°
7	CNRM-CM5	1.4°×1.4°
8	ACCESS 1.0	1.25°×1.9°
9	ACCESS 1.3	1.25°×1.9°
10	CSIRO-Mk3.6.0	1.86°×1.87°
11	FIO-ESM	2.8°×2.8°
12	EC-EARTH	1.13°×1.12°
13	INMCM4.0	2.0°×1.5°
14	IPSL-CM5A-LR	1.89°×3.75°
15	IPSL-CM5A-MR	1.26°×2.5°
16	IPSL-CM5B-LR	3.75°×1.8°
17	FGOALS-g2	2.8°×2.8°
18	MIROC-ESM	2.8°×2.8°
19	MIROC-ESM-CHEM	2.8°×2.8°
20	MIROC5	1.4°×1.4°
21	HadGEM2-CC	1.88°×1.25°
22	HadGEM2-ES	1.87°×1.25°
23	MPI-ESM-LR	1.88°×1.87°
24	MPI-ESM-MR	1.88°×1.87°
25	MRI-CGCM3	1.12°×1.12°
26	GISS-E2-H	2.5°×2.5°
27	GISS-E2-R	2.5°×2.5°
28	CCSM4	1.25°×0.94°
29	CESM1(BGC)	1.25°×0.94°
30	CESM1(CAM5)	1.4°×1.4°
31	CESM1(WACCM)	2.5°×1.89°
32	NorESM1-M	2.5°×1.9°
33	HadGEM2-AO	1.88°×1.25°
34	GFDL-CM3	2.5°×2.0°
35	GFDL-ESM2G	2.5°×2.0°
36	GFDL-ESM2M	2.5°×2.0°

3.2.2 Coupled Model Intercomparison Project 5 model (CMIP5)

In this study, CMIP5 GCMs have been meticulously examined, particularly within the framework of Representative Concentration Pathways (RCP) 8.5 scenarios. The variables under scrutiny encompass precipitation, maximum temperature, minimum temperature and average temperature. The CMIP5 data, crucial to this analysis, has been sourced from the IPCC website http://www.ipcc-data.org/sim/gcm_monthly/. A total of 36 distinct dataset models derived from CMIP5, each representing an ensemble of single realizations, have been systematically incorporated into the study and are itemized in Table 3.1.

3.2.3 Self-Calibrated Palmer Drought Severity Index (SC_PDSI)

The SC_PDSI dataset employed in this investigation is acquired from the Climatic Research Unit Time Series (CRU TS) website, presenting a spatial resolution of 0.5°×0.5°. The dataset undergoes regular annual updates, with the present investigation incorporating the CRU TS 4.03 version, a recent iteration of the dataset. The dataset can be accessed at the following link: http://www.cru.uea.ac.uk/data.

3.2.4 Climate Data

The study encompasses an analysis of monthly climate oscillations namely NINO 3.4, Multivariate ENSO Index (MEI), Southern Oscillation Index (SOI) and Dipole Mode Index (DMI), during the period from 2003 to 2017. Monthly Sea Surface Temperature (SST) anomaly data for NINO3.4 is accessible at (http://www.esrl.noaa.gov/psd/gcoswgsp/Timeseries/Data/nino34.long.anom.data). MEI is selectively sourced and obtained from (https://www.esrl.noaa.gov/psd/enso/mei). SOI data is acquired from the National Oceanic and Atmospheric Administration (NOAA) Earth System Research Laboratory at (https://psl.noaa.gov/gcos_wgsp/Timeseries/SOI/). Indian Ocean Dipole (IOD) is quantified as DMI due to the dipole mode in the tropical Indian ocean and the DMI data is retrieved from (http://www.jamstec.go.jp/frcgc/research/d1/iod/DATA/dmi).

CHAPTER 4

SELECTION OF SUTIABLE GLOBAL CLIMATE MODELS

4.1 Introduction

GCMs constitute indispensable tools for projecting future climatic scenarios. Facilitated by the World Climate Research Program (WCRP), the provision of coordinated GCMs datasets contributes significantly to advancing climate science. The comprehensive nature of GCMs allows for the evaluation of physical processes across land surfaces, oceans and the atmosphere. Consequently, GCMs prove instrumental in conducting hydro-climatological studies. Recognizing their prowess, GCMs are increasingly pivotal in determining climate variables for short, medium and long-term water resource management and planning strategies. The imperative impact of climate change on hydrometeorological variables underscores their critical role in predicting phenomena such as droughts, floods and reservoir operations.

However, the efficacy of GCMs is contingent upon the scale of analysis. While they adeptly demonstrate global climate changes at a large grid scale, their accuracy diminishes progressively at smaller, local or regional grid scales (Reichler and Kim, 2008; Xu, 1999). Despite this limitation, GCMs remain the sole models capable of projecting climate systems across various temporal scales. Notably, uncertainties escalate when assessing GCMs at regional and local levels (Mujumdar and Kumar, 2012). The IPCC AR5 delineates these uncertainties, attributing them to the internal variability of short-term projections, variability at small spatial and temporal magnitudes, the dynamic nature of climate scenarios due to anthropogenic activities, the inherent physical responses governed by model equations and the predictors influencing the predictands (IPCC, 2013).

Mitigating these uncertainties necessitates an initial step – the evaluation of climate model performance within a specified study region. Given the regional and variable-specific variations in model performance, such evaluations become crucial (IPCC, 2013; McSweeney et al., 2015). Consequently, appraising the performance of climate models at both global and regional scales becomes paramount to tempering uncertainty when applying these models in climate change studies. The assessment of appropriate GCMs at the regional level proves pivotal for scrutinizing the climatic impact on hydrological, meteorological and climatological studies (Smith and Chiew,

2010; Pitman et al., 2012). Numerous studies have undertaken evaluations of GCMs, scrutinizing climatic parameters such as T_{max}, T_{min}, P and sea surface temperature across diverse global regions and temporal scales (Perkins et al., 2007; Murphy et al., 2004; Maxino et al., 2008). The performance evaluations of GCMs involve employing various statistical metrics, including Root Mean Square Error (RMSE), Normalized Root Mean Square Error (RMSE), Correlation Coefficient (CC); proposed by Galton, 1888), Skill Score (SS); proposed by Perkins et al., 2007), among others (Sun et al., 2015; Perkins et al., 2009; Maxino et al., 2008). Recommendations from various studies emphasize the adoption of simple yet significant SSPMetrics for GCM evaluations (Johnson et al., 2011; Tebaldi and Knutti, 2007; Johnson and Sharma, 2009).

Contemporary model evaluation studies employ diverse methodologies (Giorgi and Mearns, 2002; Zeleney, 1973; Raju and Kumar, 2014 a, b; Perkins et al., 2007; Sreelatha and AnandRaj, 2019). Ensemble models have proven effective in enhancing skill and consistency in climate impact studies (Tebaldi and Knutti, 2007). Consequently, within multi-model ensembles targeting various global regions, methodologies such as the equally weighted mean, weighted mean and Bayesian techniques are applied (Sanderson et al., 2017; Giorgi and Mearns, 2002; Abramowitz and Bishop, 2015).

An extensive review of the existing literature underscores the strategic advantage of evaluating the capabilities of GCMs within the realm of climate model studies, attributing this practice to its potential to mitigate uncertainty. This study is directed towards end-users of model outputs and endeavors to establish a foundational framework for the regional assessment of GCMs within the realm of climate change evaluations. The paramount objective of this investigation is to conduct meticulous regional evaluation of GCMs procured from the CMIP5, with a specific focus on P, T_{max}, T_{avg} and T_{min} and its projection using suitable models within Telangana State, situated in the southern part of India. The selection of these four variables are predicated upon their substantial impact on and reciprocal responses from meteorological, hydrological, agricultural, industrial and human activities. In the current landscape, climate models find extensive application across diverse sectors, spanning varied spatial and temporal scales. Consequently, stakeholders necessitate an acute understanding of each model's performance at regional scales relevant to their specific domains. It is crucial to acknowledge that models deemed suitable for Telangana State may not necessarily exhibit optimality when applied to other geographical regions. Considering this,

researchers are strongly encouraged to discern the most pertinent GCMs for their respective study regions by adhering to the procedural guidelines expounded in this comprehensive study. The flow chart illustrating the objective is depicted in Figure 4.1.

The sub objectives of this section are:

- Selecting the suitable global climate models using P, T_{max}, T_{avg} and T_{min} datasets from IMD and IPCC
- Projection of suitable global climate models

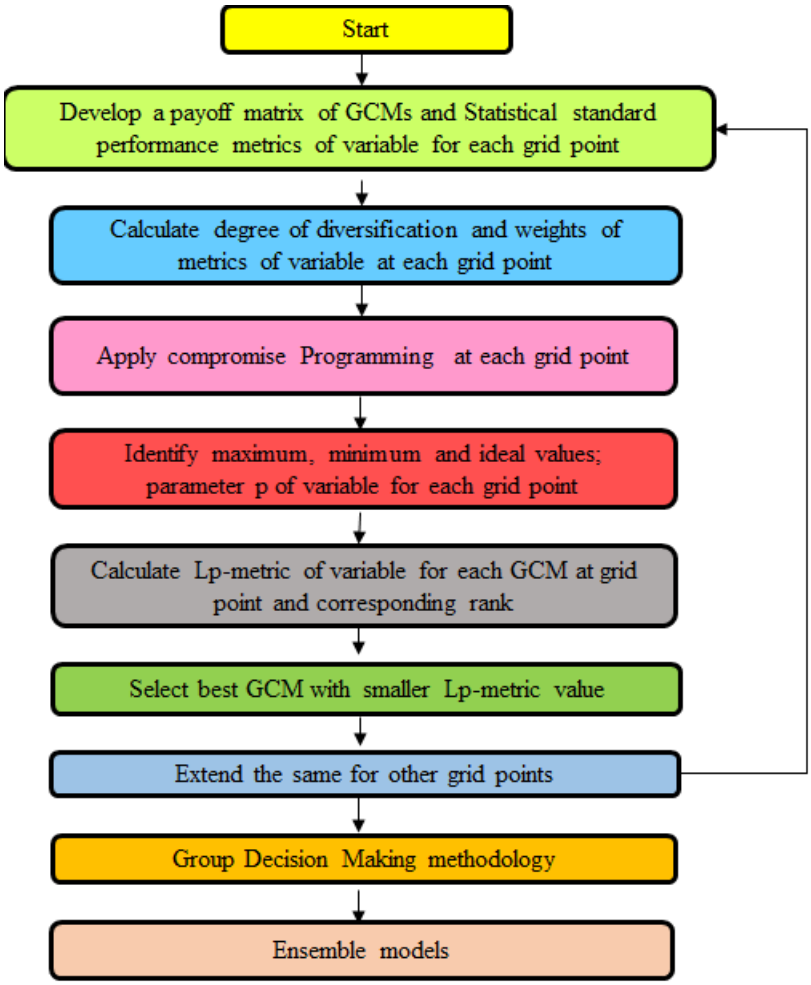

Figure 4.1: Flow chart for objective 1

4.2 Methodology

4.2.1 Processing and Analysis of data

a. The spatial resolution of the IMD datasets pertaining to the study region is precisely defined at 1°×1° obtained for the temporal scale 1975-2017. Thirty-six GCMs encompassing simulated historical monthly data for P, Tmax, Tavg and Tmin datasets.
b. To achieve coherence and congruence between the GCMs and IMD datasets, bilinear interpolation is employed to systematically re-grid the climate model datasets using Climate Data Operator (CDO) ensuring alignment with the identical grid points as those featured in the IMD data.
c. The re-gridded GCM data with the IMD data are integrated for further analysis and ensuring that all datasets (GCMs and IMD) are consistently aligned spatially and temporally.
d. Standard statistical performance metrics are calculated (NRMSD,CC,SS)
e. A payoff matrix of GCMs and SSPMetrics for variable at each grid point is developed.
f. Degree of diversification and weights are assigned to each variable at each grid point
g. Compromise programming is applied at each grid point, the lowest Lp metric is considered as the most suitable GCM at that grid point.
h. The same procedure is followed at each grid point for each variable and group decision methodology is applied to find ensemble models.

4.2.2 Normalized Root Mean Square Deviation (NRMSD)

The NRMSD quantifies the extent of variation between observed and model values, with a desirable model exhibiting NRMSD values proximal to zero. NRMSD is computed using equation 4.1.

$$NRMSD = \frac{\sqrt{[(\frac{1}{z})\sum_{i=1}^{z}(o_{i-}m_i)^2]}}{\bar{o}} \quad (4.1)$$

where o_i and m_i denote observed and model values at each point i (1,2, ... z) of the dataset.

4.2.3 Correlation Coefficient (CC)

The CC establishes a statistical relationship between observed and model values, with an ideal model exhibiting a CC value approaching 1. The CC value is determined using equation 4.2.

$$CC = \frac{\sum_{i=1}^{z}(o_i-\bar{o})(m_i-\bar{m})}{(z-1)s_o s_m} \quad (4.2)$$

where $\bar{o}$ and $\bar{m}$ represents the mean values and s_o and s_m are the standard deviations of the observed and model values, respectively.

4.2.4 Skill Score (SS)

The SS gauges the similarity measure between the observed and model-simulated PDFs, with a value of 1 indicating best performance. SS is given by equation 4.3.

$$SS = \sum_{x=1}^{ci} \min(f_o, f_s) \tag{4.3}$$

where f_o and f_s denote the frequencies of observed and model values, ci represents the number of class intervals and x indicates the number of metrics.

4.2.5 Entropy Method

The entropy method, as elucidated by Hwang and Yoon (1981), explores the disparities between data sets.

4.2.5.1 Estimation of weights

Weights for metrics are determined through the entropy method (Eq. 4.4), chosen in this study for its efficacy in ranking models in a multi-criteria decision-making context (Pomerol and Romero, 2000). The entropy of the matrix is computed using equation 4.4.

$$E_x = \frac{1}{\ln(z)} \sum_{i=1}^{z} p_{iz} \ln(p_{ix}) \tag{4.4}$$

where p_{iz} is the payoff matrix, E_x is the entropy of the metric, x is the number of SSPMetrics $(1,2,..X)$, i is the number of models. The total number of SSPMetrics is indicated by X.

4.2.5.2 Degree of Diversification

The degree of diversification denoted as D_x quantifies the outcome of criterion x from the dataset and is given by using equation 4.5.

$$D_x = 1 - E_x \tag{4.5}$$

4.2.5.3 Weights of SSPMetrics

Normalized weights of performance metrics are expressed as:

$$w_x = \frac{D_x}{\sum_{x=1}^{X} D_x} \tag{4.6}$$

where w_x signifies the weights assigned to the SSPMetrics.

4.2.6 Compromise Programming (CP)

Zeleny (1973) introduced CP as a method to identify solutions closest to an ideal solution. The distance measure matrix of SSPMetric is given by using equation 4.7.

$$L_p(a) = [\sum_{x=1}^{X} w_x{}^p \, |f_x{}^* - f_x(a)|^p]^{\frac{1}{p}} \quad (4.7)$$

where $L_p(a)$ denotes the distance measure metric for GCM a of parameter p, $f_x{}^*$ is the normalized value of SSPMetric x, $f_x(a)$ is the normalized ideal value of SSPMetric x and p represents the distance measure parameter (1, 2, … ∞).

4.2.7 Group Decision Making Approach (GDMA)

GDMA as outlined by Duckstein et al. (1989) and Stewart et al. (1992), constitutes a process for determining the optimal option when grid points are considered. In instances where a singular feasible alternative is sought, GDMA is implemented. Rankings are established in a descending order and are bifurcated into two distinct parts - upper and lower.

Within the model framework, denoted as $X = \frac{w}{2}$, where w represents the total number of GCMs. The terms within the upper part of the GCMs list are assigned rankings from 1 to X. The significance strength of the model is given by equation 4.8 and weakness is given by equation 4.9.

$$S_u = \sum_{k=1}^{m} \sum_{z=1}^{x} (x - z + 1) \, q_{uz}^{k} \forall u, k \forall z = 1, \dots x \quad (4.8)$$

where S_u signifies the strength of model u, $q_{uz}^{k} = 1$ when model u is in position z for grid k, else 0; The indices $k = 1,2, \dots m$ denote the grid points; z represent the rank position varying from 1 to x in the upper part, m denotes the grid points; u indicates the model in the upper part.

$$W_u = \sum_{k=1}^{m} \sum_{z=y}^{w} (z - y + 1) \, q_{uz}^{k} \forall u, k \forall z = y, \dots w \quad (4.9)$$

Similarly, W_u denotes the weakness of model u, $q_{uz}^{k} = 1$ when model u is in position z position for grid k, else it is 0; z is the rank position varying from 1 to y in the lower part; u indicates the model in the lower part.

The net strength of each GCM model u is articulated as:

$$N_u = S_u - W_u \quad (4.10)$$

The model exhibiting the highest net strength is deemed the preferred choice, while other models are ranked accordingly in descending order of their net strength values. This structured approach within the GDMA framework enhances the decision-making process by systematically evaluating the relative strengths and weaknesses of each GCM model.

4.3 Results and Discussions

In this study, both observed data from the IMD and simulated data from GCMs are utilized for 14 distinct grid points, characterized by latitude and longitude, to analyze P, T_{max}, T_{avg} and T_{min}. The assessment involved the computation of CC, SS and NRMSD collectively referred to as SSPMetrics. For each variable (P, T_{max}, T_{avg} and T_{min}) at every grid point, Normalized weights using the entropy method and equal weights through sensitivity analysis for each SSPMetric are calculated. The subsequent step involved assigning ranks to GCMs based on their Lp values obtained through CP. The lowest Lp value for a model is assigned a rank of 1, exemplified in Table 4.1 for P at grid point 18.35°×80.85°. Table 4.5 provides an overview of SSPMetrics with minimum and maximum values for P, T_{max}, T_{avg} and T_{min} at the same grid point, utilizing both entropy and sensitivity methods. The weight distributions for all three variables are detailed in Tables 4.6.(a) and 4.6.(b) It is noteworthy that slight variations in the Lp values lead to changes in the ranking positions of GCMs. This comprehensive procedure is systematically repeated for all grid points within the study area, with the results exemplified for grid point 18.35°×80.85°.

4.3.1 Analysis of Precipitation

Table 4.1 presents a comprehensive overview of the SSPMetrics and associated ranks for P, encompassing SS, CC and NRMSD using Entropy method across all 36 GCMs. Notably, an optimal value of 1 is sought for both SS and CC and to align NRMSD with CC and SS, a negative sign is ascribed to NRMSD. Weights are meticulously computed for each GCM with respect to every SSPMetric, employing the entropy method and a sensitivity analysis method with equal weights.

The weight distribution across the considered SSPMetrics, where SS holds a predominant position with weight percentages of 41.2% (entropy method) and 38.02% (sensitivity analysis), surpassing the weight allocations for CC (36.3% and 35.9%) and NRMSD (22.5% and 26.08%) in both entropy and sensitivity analysis methodologies, respectively.

4.3.2 Analysis of Maximum Temperature

The same procedure as that described in section 4.3.1 is repeated, to calculate the SSPMetrics and rankings with respect to the T_{max}. Using the entropy method, the minimum value of the L_p metric, 0.0047 (Table 4.2), is observed for the BCC-CSM1.1(m) model, followed by MIROC5 (0.0063) and CanESM2 (0.0085). The maximum value is observed for CCSM4 (0.0479; Table 4.2). In the sensitivity analysis, the minimum value of L_p metric, 0.0681 (Table 4.5), is observed for BCC-CSM1.1(m) and maximum value is observed for IPSL-CSM5B-LR (0.2671). Note : Column 1-S.No represents model name as of in Table 4.1. From Table 4.6.(a) and (b), In case of T_{max}, CC (46.8%) has higher percent of weightage compared to SS (40.4%) and NRMSD (12.8%) in the entropy method. The same is observed in the sensitivity analysis method : CC (43.4%), SS (37.9%) and NRMSD (18.7%).

4.3.3 Analysis of Minimum Temperature

The analysis of T_{min} in terms of SSPMetrics and rankings for grid point $(18.35° \times 80.85°)$ is presented in Table 4.3. In the entropy method, the minimum value of the L_p metric (0.0159; Table 4.3) is observed for CanESM2, followed by ACCESS1.0 (0.0166) and MRI-CGCM3 (0.0171), whereas CMCC-CMS exhibited the maximum value (0.0418; Table 4.3). In the sensitivity analysis, the minimum value of L_p metric is observed for HadGEM2-CC (0.1937; Table 4.5), while the maximum value is observed for CMCC-CMS (0.2819). Note : Column 1-S.No represents model name as of in Table 4.1. From the analysis (Table 4.6.(a) and (b)), CC (57.3%) has higher percent of weightage compared to SS (28.1%) and NRMSD (10.6%) in the entropy method. The same is observed in the sensitivity analysis, with CC, SS and NRMSD equal to 47.8%, 37.6% and 14.6%, respectively.

4.3.4 Analysis of Average Temperature

The analysis of T_{avg} in terms of SSPMetrics and rankings for grid point $(18.35° \times 80.85°)$ is presented in Table 4.4. In the entropy method, the minimum value of the L_p metric (0.0040; Table 4.4) is observed for BCC-CSM1.1(m), followed by MIROC5 (0.0040) and HadGEM2-A0 (0.0041), whereas Had-GEM2ES exhibited the maximum value (0.0227; Table 4.4). In the sensitivity analysis, the minimum value of L_p metric is observed for MIROC5 (0.0052; Table 4.5), while the maximum value is observed for ACCESS1.3 (0.0325). Note : S.No represents model name as of in Table 4.1. From the analysis (Table 4.6(a)and (b)), SS has higher percent of weightage compared to CC and NRMSD in both entropy and sensitivity method.

Table 4.1: SSPMetrics, L_p metric and rank of P at grid point $(18.35° \times 80.85°)$using entropy method.

S. No	Model name	CC	SS	NRMSD	L_p	RANK
1	BCC-CSM1-1	0.5952	0.8846	0.6891	0.0083	14
2	BCC-CSM1.1(m)	0.6053	0.8077	0.6687	0.0087	20
3	BNU.ESM	0.7943	0.6250	0.8229	0.0091	22
4	CanESM2	0.6515	0.7788	0.5568	0.0077	9
5	CMCC-Cm	0.6271	0.7821	0.6464	0.0083	16
6	**CMCC-CMS**	**0.7088**	**0.7500**	**0.6865**	**0.0068**	**2**
7	CNRM-CM5	0.1736	0.9423	0.552	0.0234	34
8	ACCESS1.0	0.5880	0.8686	0.4915	0.0087	19
9	ACCESS1.3	0.1589	0.8007	0.3259	0.0239	36
10	CSIRO-Mk3.6.0	0.2488	0.9103	0.7614	0.0207	31
11	FIO-ESM	0.7493	0.7083	0.6975	0.0071	5
12	EC-EARTH	0.7440	0.6538	0.7543	0.0086	17
13	**INMCM4.0**	**0.8021**	**0.6987**	**0.5494**	**0.0070**	**3**
14	IPSL-CM5A-LR	0.5417	0.8462	0.6293	0.0105	25
15	IPSL-CM5A-MR	0.6410	0.8077	0.2991	0.0075	8
16	IPSL-CM5B-LR	0.1688	0.8109	0.7859	0.0238	35
17	**FGOALS-g2**	**0.7650**	**0.7276**	**0.7944**	**0.0064**	**1**
18	MIROC-ESM	0.8147	0.6506	0.7857	0.0083	15
19	MIROC-ESM-CHEM	0.7985	0.6699	0.4475	0.0078	10
20	MIROC5	0.2129	0.6667	0.3063	0.0233	33
21	HadGEM2-CC	0.4266	0.8558	0.4255	0.0145	28
22	HadGEM2-ES	0.5375	0.8269	0.6542	0.0108	26
23	MPI-ESM-LR	0.7366	0.6827	0.6354	0.0080	11
24	MPI-ESM-MR	0.7409	0.6763	0.392	0.0081	13
25	MRI-CGCM3	0.4257	0.8686	0.7139	0.0145	27
26	GISS-E2-H	0.3564	0.7596	0.5497	0.0176	30
27	GISS-E2-R	0.2584	0.7660	0.7596	0.0210	32
28	CCSM4	0.7351	0.6571	0.7963	0.0087	18
29	CESM1(BGC)	0.7725	0.6955	0.7561	0.0072	6
30	CESM1(CAM5)	0.7094	0.6090	0.7835	0.0103	24
31	CESM1(WACCM)	0.7986	0.5865	0.7051	0.0101	23
32	NorESM1-M	0.7378	0.7147	0.57	0.0071	4
33	HadGEM2-AO	0.4041	0.7853	0.6578	0.0158	29
34	GFDL-CM3	0.7662	0.6891	0.6987	0.0074	7
35	GFDL-ESM2G	0.7089	0.6987	0.6975	0.0080	12
36	GFDL-ESM2M	0.6627	0.7115	0.552	0.0087	21

Table 4.2: SSPMetrics values of T_{max} (NRMSD-CC-SS), L_p metric and Rank at grid point (18.35° × 80.85°) for entropy method. S.No represents model name as of in Table 4.1.

S.No	NRMSD	CC	SS	L_p	RANK
1	0.0747	0.8378	0.7372	0.0118	5
2	**0.0833**	**0.8454**	**0.8429**	**0.0047**	**1**
3	0.1034	0.8152	0.5897	0.0258	16
4	**0.0903**	**0.8367**	**0.7724**	**0.0085**	**3**
5	0.0880	0.8982	0.6699	0.0179	10
6	0.0971	0.8731	0.6378	0.0210	13
7	0.0810	0.8478	0.7404	0.0114	4
8	0.1142	0.8132	0.5577	0.0289	22
9	0.1795	0.6483	0.5641	0.0289	21
10	0.1258	0.7382	0.6731	0.0180	11
11	0.0997	0.9000	0.4968	0.0348	28
12	0.1409	0.8324	0.4199	0.0423	34
13	0.1652	0.8717	0.3814	0.0460	35
14	0.1436	0.6705	0.6571	0.0200	12
15	0.1277	0.6870	0.7340	0.0129	6
16	0.2018	0.4549	0.5673	0.0304	23
17	0.1189	0.7770	0.5801	0.0268	18
18	0.1130	0.8526	0.5064	0.0339	27
19	0.1110	0.8792	0.5096	0.0335	25
20	**0.0590**	**0.8456**	**0.8141**	**0.0063**	**2**
21	0.0793	0.8161	0.6891	0.0164	8
22	0.0827	0.8239	0.6795	0.0172	9
23	0.1138	0.8583	0.6346	0.0212	14
24	0.1141	0.8740	0.5833	0.0263	17
25	0.1167	0.8040	0.7083	0.0142	7
26	0.1343	0.8175	0.5064	0.0339	26
27	0.1359	0.7404	0.5641	0.0285	19
28	0.1469	0.8928	0.3622	0.0479	36
29	0.1312	0.8945	0.4551	0.0388	29
30	0.1192	0.9126	0.4487	0.0395	31
31	0.1167	0.8748	0.5160	0.0329	24
32	0.1207	0.8887	0.4519	0.0392	30
33	0.1040	0.8683	0.6186	0.0229	15
34	0.1094	0.8862	0.5577	0.0288	20
35	0.1577	0.8912	0.4327	0.0410	33
36	0.1496	0.8913	0.4423	0.0401	32

Table 4.3: SSPMetrics values of T_{min} (NRMSD-CC-SS), L_p metric and Rank at grid point (18.35° × 80.85°) for entropy method. S.No represents model name as of in Table 4.1.

S.No	NRMSD	CC	SS	L_p	RANK
1	0.0930	0.8713	0.8590	0.0171	4
2	0.1321	0.8796	0.7179	0.0211	10
3	0.0844	0.9272	0.8462	0.0173	5
4	**0.1547**	**0.8010**	**0.8173**	**0.0159**	**1**
5	0.0926	0.9408	0.8077	0.0178	7
6	0.5572	0.5584	0.4483	0.0418	36
7	0.2604	0.9114	0.5801	0.0300	28
8	**0.1676**	**0.8104**	**0.7853**	**0.0166**	**2**
9	0.1238	0.8057	0.7147	0.0218	11
10	0.1154	0.8168	0.7019	0.0229	17
11	0.0801	0.9312	0.8141	0.0180	8
12	0.2217	0.9346	0.4968	0.0381	34
13	0.5561	0.5524	0.4583	0.0413	35
14	0.2439	0.8116	0.5641	0.0319	30
15	0.2072	0.8419	0.5994	0.0291	27
16	0.3209	0.7290	0.5769	0.0301	29
17	0.0999	0.7962	0.6891	0.0242	24
18	0.0875	0.8790	0.7179	0.0223	13
19	0.0885	0.8814	0.7051	0.0231	19
20	0.0776	0.9329	0.8526	0.0175	6
21	0.2295	0.8784	0.6603	0.0234	20
22	0.1780	0.8737	0.6859	0.0224	14
23	0.1465	0.9354	0.6859	0.0230	18
24	0.1420	0.9335	0.6763	0.0238	21
25	**0.0943**	**0.8918**	**0.8429**	**0.0171**	**3**
26	0.1315	0.7713	0.6859	0.0239	22
27	0.1353	0.7828	0.6987	0.0228	16
28	0.2229	0.7643	0.5353	0.0349	33
29	0.2263	0.7818	0.5673	0.0319	31
30	0.2016	0.8671	0.5385	0.0346	32
31	0.1482	0.8165	0.7404	0.0195	9
32	0.1564	0.8135	0.6699	0.0243	25
33	0.2307	0.8840	0.6410	0.0250	26
34	0.1295	0.9242	0.7051	0.0220	12
35	0.1206	0.9398	0.6795	0.0241	23
36	0.1093	0.9244	0.7051	0.0225	15

Table 4.4: SSPMetrics values of T_{avg} (NRMSD-CC-SS), L_p metric and Rank at grid point $(18.35° \times 80.85°)$ for entropy method. S.No represents model name as of in Table 4.1.

S.No	NRMSD	CC	SS	Lp	Rank
1	0.8267	0.7212	0.0769	0.0053	8
2	**0.8560**	**0.8269**	**0.0729**	**0.0040**	**1**
3	0.8743	0.6186	0.0886	0.0067	13
4	0.8509	0.7404	0.0857	0.0045	6
5	0.9022	0.6859	0.0764	0.0052	7
6	0.8267	0.7115	0.0769	0.0054	9
7	0.8758	0.7853	0.0612	0.0042	4
8	0.8399	0.8173	0.0715	0.0042	5
9	0.6513	0.5160	0.1981	0.0115	31
10	0.7454	0.6923	0.1129	0.0067	14
11	0.9049	0.5353	0.0955	0.0086	18
12	0.8565	0.3590	0.1544	0.0131	34
13	0.9042	0.4455	0.1377	0.0107	27
14	0.6679	0.6667	0.1332	0.0086	19
15	0.6957	0.6763	0.1291	0.0079	17
16	0.4733	0.5994	0.1842	0.0140	35
17	0.8442	0.6635	0.0921	0.0059	11
18	0.8905	0.5192	0.1044	0.0090	20
19	0.8949	0.4968	0.1075	0.0095	25
20	**0.8704**	**0.8077**	**0.0638**	**0.0041**	**3**
21	0.8210	0.6987	0.0717	0.0058	10
22	0.8418	0.0021	0.0651	0.0227	36
23	0.8912	0.5737	0.1079	0.0075	16
24	0.8806	0.6058	0.1045	0.0068	15
25	0.7769	0.6987	0.1175	0.0059	12
26	0.8011	0.5256	0.1330	0.0092	24
27	0.7565	0.5577	0.1268	0.0091	21
28	0.9047	0.4455	0.1283	0.0107	28
29	0.9267	0.4199	0.1221	0.0114	30
30	0.9182	0.4006	0.1338	0.0119	32
31	0.8948	0.5096	0.1101	0.0092	23
32	0.8961	0.4712	0.1191	0.0101	26
33	**0.8585**	**0.7949**	**0.0748**	**0.0040**	**2**
34	0.9105	0.5096	0.1172	0.0091	22
35	0.9178	0.3974	0.1489	0.0119	33
36	0.9170	0.4391	0.1417	0.0108	29

Table 4.5: SSPMetrics, L_p metric and rank of P, T_{max}, T_{min} and T_{avg} at grid point (18.35° × 80.85°) using Entropy (E) and Sensitivity (S) method.

Variable	Minimum Lp Value	Model name	Maximum Lp Value	Model name
P(E)	0.064	FGOALS-g2	0.0239	ACCESS1.3
P(S)	0.1098	CMCC-CMS	0.3423	ACCESS1.3
T_{max}(E)	0.0047	BCC-CSM1.1(m)	0.0479	CCSM4
T_{max}(S)	0.0681	BCC-CSM1.1(m)	0.2671	IPSL-CSM5B-LR
T_{min}(E)	0.0159	CanESM2	0.0418	CMCC-CMS
T_{min}(S)	0.1937	HadGEM2-CC	0.2819	CMCC-CMS
T_{avg} (E)	0.0040	BCC-CSM1.1(m)	0.0227	HadGEM2-ES
T_{avg} (S)	0.0052	MIROC5	0.0378	ACCESS 1.3

Table 4.6.(a): Weight distribution of P, T_{max}, T_{min} and T_{avg} over 14 grid points of Telangana State from entropy method

Variables	SSPMetrics	Weights in %				
		0-20	20-40	40-60	60-80	80-100
P	CC	3	4	7	-	-
	SS	-	1	11	2	-
	NRMSD	1	2	7	4	-
T_{max}	CC	3	7	4	-	-
	SS	2	7	5	-	-
	NRMSD	9	2	3	-	-
T_{min}	CC	-	9	5	-	-
	SS	2	9	3	-	-
	NRMSD	2	8	4	-	-
T_{avg}	CC	5	5	4	-	-
	SS	4	6	4	-	-
	NRMSD	5	7	2	-	-

Table 4.6.(b): Weight distribution of P, T_{max}, T_{min} and T_{avg} over 14 grid points of Telangana State from sensitivity method

Variables	SSPMetrics	Weights in %				
		0-20	20-40	40-60	60-80	80-100
P	CC	2	6	5	1	-
	SS	1	3	7	3	-
	NRMSD	2	3	5	4	-
T_{max}	CC	3	6	5	-	-
	SS	4	5	5	-	-
	NRMSD	6	4	2	2	-
T_{min}	CC	3	8	3	-	-
	SS	3	7	4	-	-
	NRMSD	4	5	5	-	-
T_{avg}	CC	5	8	1	-	-
	SS	4	6	4	-	-
	NRMSD	3	8	3	-	-

4.3.5 Application of GDMA, Ensemble Method and Spatial Projections

The net strength for the 36 GCMs using the entropy method. For P, FGOALS-g2 and INMCM4.0 have net strengths of 86 and 85, respectively, ranking first and second among the models. On the other hand, ACCESS1.3 ranks last with a net strength of -96. For T_{max}, CanESM2, BCC-CSM1-1(m), and ACCESS1.3 rank first, second and last, respectively, with net strengths of 80, 79 and -88. For T_{min}, CanESM2 and BCC-CSM1.1(m) rank first and second with scores of 82 and 81, respectively, while ACCESS1.3 ranks last with a score of -88. For T_{avg}, net strength of first occupied GCM is observed as MIROC5 with 73 followed to BCC-CSM1.1 (m) with 69 whereas IPSL-CM5B-LR has occupied last position with net strength -51. The finalized ensemble GCMs are represented in Table 4.7

Table 4.7: Finalized ensemble models of P, T_{max}, T_{min} and T_{avg} in this study.

Variable	Finalized ensemble models
P	FGOALS-g2, CMCC-CMS, INMCM4.0
T_{max}	BCC-CSM1.1(m), CanESM2, MIROC5
T_{min}	CanESM2, BCC-CSM1-1(m), ACCESS 1.0
T_{avg}	MIROC5, BCC-CSM1-1(m),CNRM-CM5

Results showed that Compromise Programming has the ability to find suitable GCMs. GDMA is performed for multi model ensemble. The present study provided evaluation of an optimal model and ensemble multi model selection for the Telangana region which can be used further in different applications of hydrology or hydrologic studies are represented in Figure 4.2.(a),(b),(c)and(d). Climate change projections for Telangana State are presented for P, T_{max}, T_{avg} and T_{min} for three future time intervals (1: 2006–2035, 2: 2036–2065 and 3: 2066–2095) using RCP 8.5 scenarios. The spatial representation of the long-term projection (for the three-time intervals) of is shown in Figure 4.3. Low amounts of rainfall are observed in relation to high temperatures for both the RCP 8.5 scenarios. The climate change projections in the study area are overall consistent. However, precisely locating the variations of a variable is difficult. The climate projections for future scenarios are shown in Figure 4.3.

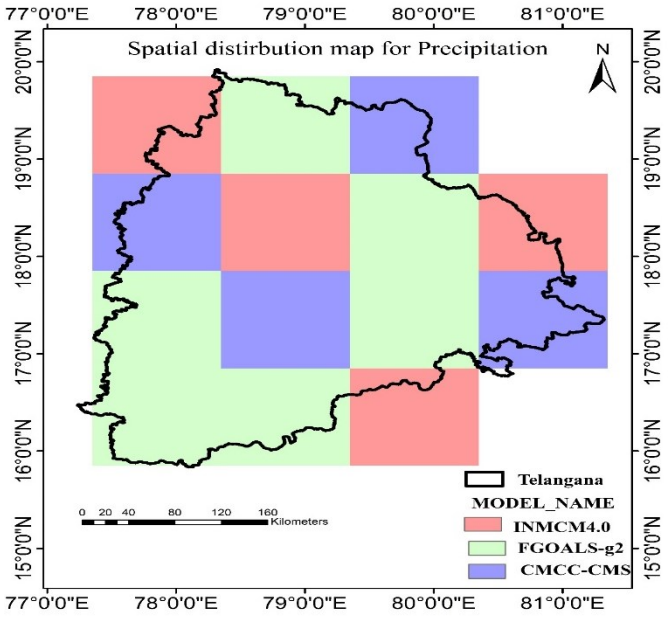

Figure 4.2 (a) Precipitation

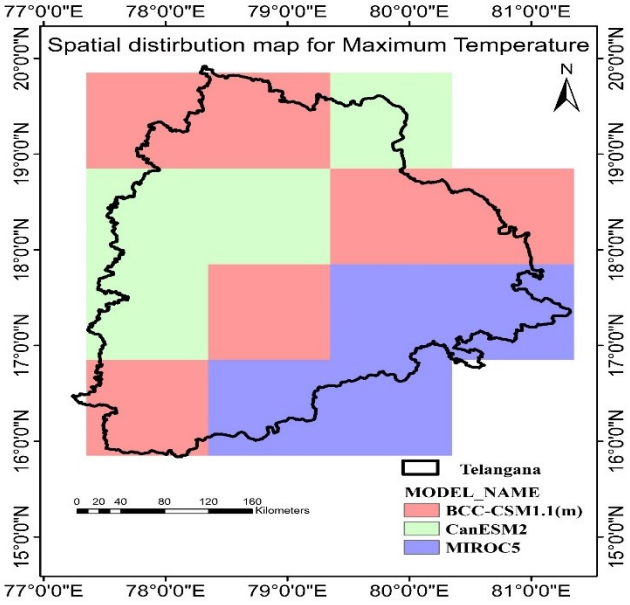

Figure 4.2 (b)Maximum Temperature

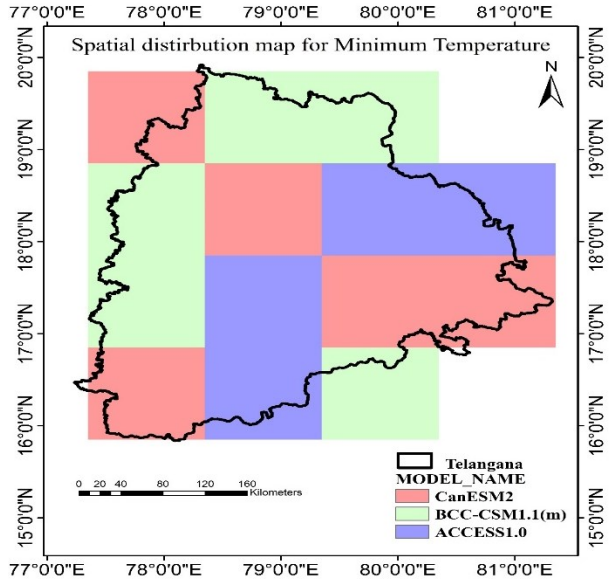

Figure 4.2 (c) Minimum Temperature

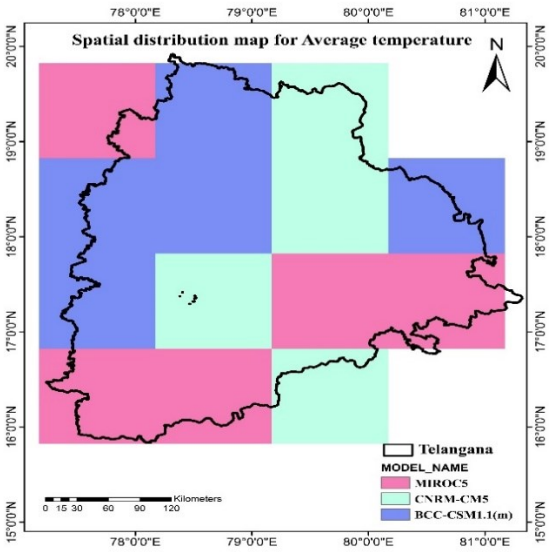

Figure 4.2 (d) Average Temperature

Figure 4.2.(a),(b), (c) & (d) presents spatial distribution of ensemble models of P, T_{max}, T_{min} & T_{avg}.

For 2006-2035

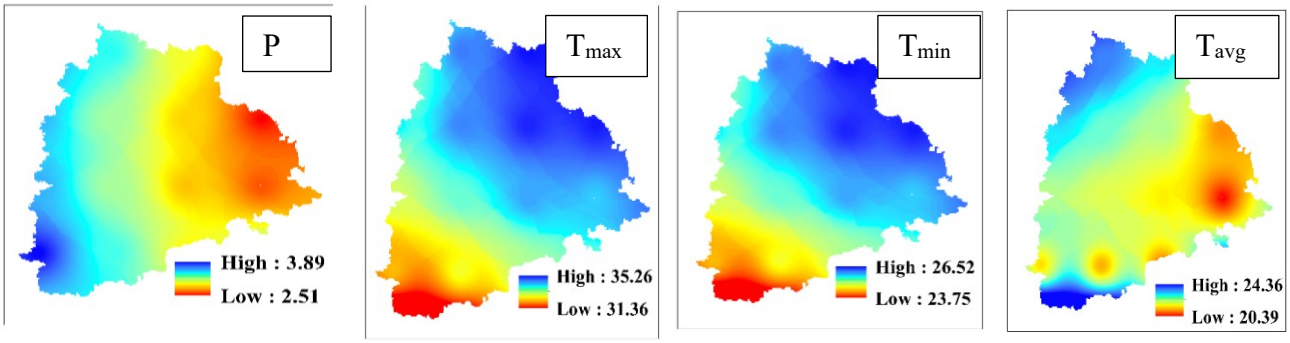

For 2036- 2065

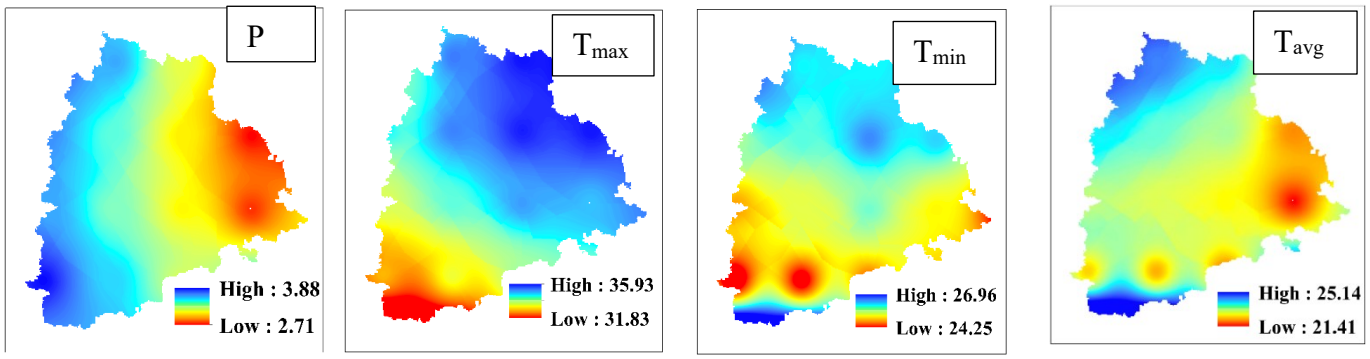

For 2066-2095

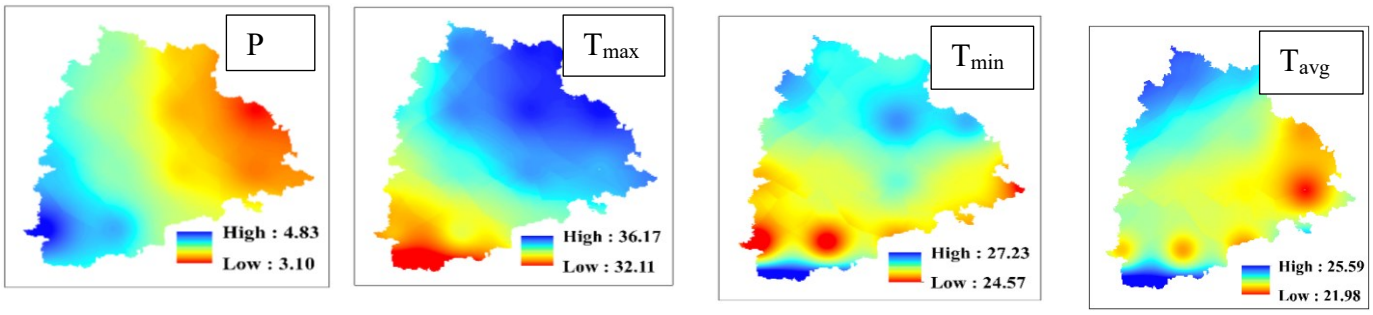

Figure 4.3 Climate Projections for RCP 8.5 future scenarios P (mm), T_{max}, T_{min} & T_{avg}(degree celsius)

4.4 Conclusions

Three SSPMetrics (CC, SS and NRMSD) for four variables (P, T_{max}, T_{min} and T_{avg}) are evaluated to compare 36 GCMs against observed data of IMD at 14 grid points in Telangana State, southern India. Using entropy and sensitivity analysis, the weights of the SSPMetrics are determined for the four variables. These weights are found to vary at each grid point remarkably, affecting the rankings of the considered variables. CP and GDMA are performed to identify suitable individual and ensemble GCMs for applications in climate-related impact assessments in the study region. Spatial distribution maps of ensemble models and spatial projections are projected to future scenarios.

The study yields the following conclusions.

- The identified suitable ensemble models for P include FGOALS-g2, CMCC-CMS and INMCM4.0. BCC-CSM1.1(m), CanESM2, and MIROC5 are deemed suitable GCMs for T_{max}. For T_{min}, the recommended ensemble comprises CanESM2, BCC-CSM 1-1(m) and ACCESS1.0. For T_{avg}, MIROC5, CNRM-CM5 and BCC-CSM1.1 (m) emerge as the suitable models.
- If a single GCM is to be used, then FGOALS-g2 for P and BCC-CSM1.1(m) for T_{max}, Tavg and T_{min} should be considered.

- In the analysis of SSPMetrics for precipitation (P), SS holds a predominant position with percentages of 41.2% (entropy) and 38.02% (sensitivity), surpassing CC (36.3% and 35.9%) and NRMSD (22.5% and 26.08%) in both methods.
- In the analysis of SSPMetrics for Tmax, Tmin and Tavg: CC receives higher weightage in entropy (46.8%, 57.3% and 42.3%) and sensitivity (43.4%,47.8% and 46.8%) compared to SS and NRMSD.
- From spatial projections of GCMs, a rise in temperature can be expected for the future periods (2036-2065 and 2066-2095), which leads to an increase in evaporation rate.

The proposed method for identifying the optimal individual model or ensemble model Telangana State can be helpful in various applications, such as in hydrological, meteorological, and climatic model studies. This study offers a clear and quantitative method for selecting suitable GCMs, thereby reducing the uncertainty associated with the use of GCMs for climate impact studies at regional scale.

CHAPTER 5

REGIONALIZATION OF STUDY AREA AND EVALUATING DROUGHT INDICES AND ITS CHARACTERSITICS

5.1 Introduction

Droughts stand out as intricate and profoundly impactful natural occurrences observed annually across various regions, it inflicts substantial losses both in terms of economic resources and human lives (Goyal et al., 2017; Wilhite, 2000). Compared to other hydrological phenomena characterized for brief durations, droughts manifest as enduring disasters spanning from several months to multiple years. Their gradual onset and protracted nature further compound the challenge of precisely delineating the commencement and conclusion of drought events. Droughts, affecting both surface and subsurface water resources, play a pivotal role in significantly diminishing the overall water availability. Moreover, the repercussions extend beyond mere quantity, encompassing adverse impacts on water quality, agricultural yield failures, reduced power generation and the degradation of riparian habitats (Goyal & Ojha, 2012; Riebsame et al., 1991). Empirical evidence substantiates the intensification of extreme hydrological events, such as floods and droughts, in recent times, marked by a notable reduction in their return periods across diverse geographical domains (D.P. Lettenmaier et al., 1996). The escalating threats posed by global warming and climate change further accentuate the likelihood of heightened drought intensity and increased frequency, a prediction facilitated by advanced downscaling approaches (e.g., Vasiliades et al., 2009).

Drought, as a phenomenon, exhibits a distinctly regional character. Numerous researchers have embraced a regional perspective to scrutinize and comprehend drought dynamics, with seminal contributions from Clausen & Pearson, (1995); Goyal & Sharma, (2016); Hisdal & Tallaksen, (2003); Liu et al., (2015); Mirakbari et al., (2010); Mishra et al., (2009); Rajsekhar et al., (2011); Sen, (1980). The inherent spatial variability in drought intensity assumes paramount importance, particularly in the context of water transfer operations management within drought-affected regions. Conducting a regional analysis of droughts is imperative for a nuanced understanding of this phenomenon, given its incremental and pervasive nature. The principal objective of such an

analysis resides in delineating homogeneous regions, characterized by analogous drought behaviors. A homogeneous region, defined as a cluster of stations demonstrating comparable drought behavior or possessing akin frequency distribution patterns for drought occurrences (Mirakbari et al., 2010), serves as a foundation for devising coherent drought management and mitigation policies tailored to the specific characteristics of each identified region. This regional approach contributes substantively to the enhancement of precision in drought analysis and the formulation of targeted strategies for effective water resource management. The flowchart of chapter 5 is presented in Figure 5.1. (a) and (b)

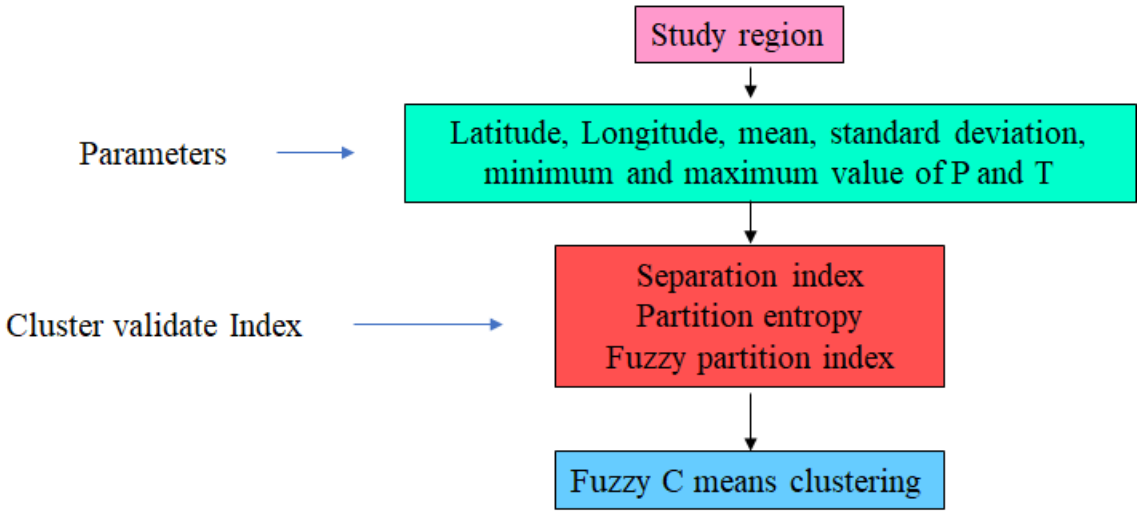

Figure 5.1.(a). Flowchart for regionalization of study area

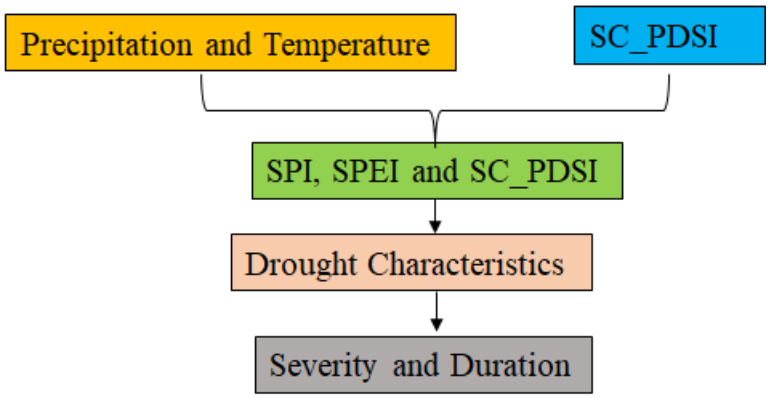

Figure 5.1.(b) Flowchart for evaluating drought indices and their characteristics.

5.2 Methodology

5.2.1 Step by procedure used

a. To delineate homogenous regions, parameters – latitude, longitude, mean, standard deviation, minimum and maximum value of precipitation and temperature datasets are considered.

b. Cluster validate index namely separation index, partition entropy and fuzzy partition index are used to find optimum number of clusters.

c. Monthly precipitation, temperature and SC_PDSI data is considered for time period of 1975-2017.

d. SPI is computed at SPI12. Further SPEI is calculated incorporating potential evapotranspiration (PET), calculated.

e. A drought severity threshold (-0.8) is established and applied to identify drought events based on SPI, SPEI and SC_PDSI series exceeding the established threshold.

f. Characteristics analysis – severity and duration is determined regionally.

5.2.2 Fuzzy C-Means clustering

The conceptualization of FCM is introduced by Dunn 1973 and subsequently extended by Bezdek in 1981. Let us consider cluster c with M objects where Y_k is the data vector for k_{th} $(k = 1, 2 \ldots M)$ object. The FCM technique aims to minimize the following objective function 5.1.

$$J(U, C) = \sum_{j=1}^{M} \sum_{i=1}^{c} u_{ik}^{\theta} ||Y_k - C_i||^2 \qquad (5.1)$$

let u_{ik} denotes the membership value of the k_{th} point in the i_{th} cluster, where $C_{i\ denotes}$ the centre of the i_{th} cluster (i = 1, 2,...,c), $\|Y_k - C_i\|^2$ is the Euclidean squared distance. Here C_i and θ signify the cluster center and the fuzziness index (or fuzzifier) respectively, where θ can assume any value >1. In the FCM algorithm, the number of clusters and centers are stochastically determined. Subsequently, the membership matrix is computed using the following expression 5.2.

$$u_{i<k}^{t} = \left[\sum_{j=1}^{c} \left(\frac{||Y_k - C_i||}{||Y_k - C_j||} \right)^{\frac{2}{\theta - 1}} \right]^{-1} \qquad (5.2)$$

with an updated membership value, new cluster centers are calculated using C_i

$$C_i = \frac{\sum_{k=1}^{M} u_{ik}^{\theta} y_k}{\sum_{k=1}^{M} u_{ik}^{\theta}} \quad (5.3)$$

using new cluster centers, the membership matrix is updated to following equation 5.4.

$$u_{i<k}^{t+1} = \left[\sum_{j=1}^{c} \left(\frac{||Y_k - C_i||}{||Y_k - C_j||} \right)^{\frac{2}{\theta-1}} \right]^{-1} \quad (5.4)$$

if $\|U^{t+1} - U^t\| < \varepsilon$ the algorithm will stop. If not, it goes back to step 1. Three validity indices are used to check the efficiency of clustering.

5.2.2.1 Separation index (*Si*)

The compactness and separation function (Si) proposed by (Xie & Beni, 1991) is defined as the ratio of variance within clusters to the variance between clusters. The Si value is lower, the clustering is better. *Si* is represented as in the following equation 5.5.

$$S_i(U, V: X) = \frac{\sum_{i=1}^{c} \sum_{k}^{M} (u_{ik}^{a}) ||c_i - y_k||^2}{M \min_{i \neq k} ||v_i - y_k||^2} \quad (5.5)$$

5.2.2.2 Fuzziness partition index (*Fpi*)

The membership (fuzziness) that various classes share (J. C. Bezdek, 1974; James C. Bezdek, 1973) is calculated by the Fuzziness partition index and is presented in the following equation 5.6.

$$F_{pi}(U) = \frac{1}{m} \sum_{i=1}^{c} \sum_{k=1}^{M} u_{ik}^2 \quad (5.6)$$

5.2.2.3 Partition entropy (*Pe*)

Partition entropy is represented as

$$P_e(U) = \frac{1}{m} \sum_{i=1}^{c} \sum_{k=1}^{M} u_{ik} log_a (u_{ik}) \quad (5.7)$$

Lower the *Pe* value, better the clustering and it varies between 0 and log(c). The FCM clustering analysis is performed using *R* software (package: ppclust; version 3.5.1; https://www.r-project.org/)

5.2.3 Standardized Precipitation Index (SPI)

SPI is a dimensionless meteorological drought index which requires single hydrological variable i.e., precipitation to characterize drought events. SPI is simple to analyse, spatially invariant and can be applied to evaluate meteorological, hydrological and agricultural drought phenomenon. Using SPI, the temporal analysis of drought events can be evaluated at 3, 6, 9, 12, 24, 36 and 48-month time scales. To evaluate SPI for a given year *i*, month *j* and for time scale of *k*, the following steps are used:

- For a specific period of interest *j*, cumulative precipitation series is evaluated X_{ij} ($i = 1,2,...,n$), where each term denotes the sum of precipitation of $k-1$ previous successive months.
- The aggregated monthly precipitation series (say $k = 12$ months) is fitted with cumulative PDFs (for e.g., gamma distribution). The gamma distribution function is defined as $g(x) = \frac{1}{\beta^{\alpha}\Gamma(\alpha)} x^{\alpha-1} e^{\frac{-x}{\beta}}$; where, $\Gamma(\alpha)$ = gamma function, α = shape parameter and β = scale parameter. The shape and scale parameters are estimated using method of maximum likelihood.
- For a specific month and time, the estimated parameters are utilized in finding the cumulative PDFs of the precipitation event.
- A mixed (containing zero values and continuous precipitation amount) two parameter gamma distribution function is employed and the corresponding Cumulative Distribution Function (CDF) is given as $F(x) = q + (1 - q)\ G(x)$; where, q = probability of zero precipitation and $G(x)$ = distribution function calculated for non-zero precipitation.
- An equiprobability transformation Panofsky & Brier, (1968) is carried out from the CDF of mixed distribution to the CDF of standard normal distribution (zero mean and unit variance), which is given as SPI = $\psi^{-1}(F(x))$. This transformed probability is the SPI. The negative SPI value specifies that the precipitation is below average (dry condition) and positive SPI value indicates above average precipitation (wet condition).

A drought period is defined as the successive number of SPI values below a threshold (approximately 0.8). According to Mckee et al., (1993), droughts are classified into four categories namely mild (D0), moderate (D1), severe (D2) and extreme (D3) droughts as given in Table 5.1. In this study, SPI is computed over 12-month timescales with monthly gridded precipitation data at a spatial resolution of 1°×1° from 1975 to 2017.

Table 5.1: SPI - Drought categories under Dry (D) conditions.

Drought Category	SPI
D0: Mild (abnormal) Drought	0 to -0.99
D1: Moderate Drought	- 1.00 to -1.49
D2: Severe Drought	-1.50 to -1.99
D3: Extreme Drought	≤ -2

5.2.4 Standardized Precipitation Evapotranspiration Index (SPEI)

To characterize droughts several drought indexes have been developed by considering one or more climatic variables like precipitation, temperature, runoff, evapotranspiration and soil moisture. To quantify meteorological drought, SPI is considered as the most widely used drought index because it is less data intensive and simple to calculate. As SPI can be calculated at different time scales, it helps in understanding the effect of rainfall deficit on various hydrological components (Mckee et al., 1993). The limitation of SPI is that it does not consider other climate variables like evapotranspiration in quantifying droughts. Therefore, SPI may not reproduce the true water deficit that is intensified by climate change. By considering all the advantages of SPI, Vicente-Serrano et al., (2010) developed SPEI which can be calculated at 1 to 48-month time scale representing hydrological, agricultural and meteorological droughts (Maccioni et al., 2015). For calculating SPEI, Potential Evapotranspiration (PET) is evaluated first. For the estimation of PET, Penman-Monteith, Thornthwaite and Hargreaves are the most widely used methods. In the present study, Hargreaves method is adopted to calculate PET because of its simplicity and lower data requirement. Then, the difference between precipitation and PET is estimated as shown in Eq. 5.8.

$$D_i = P_i - PET \tag{5.8}$$

where, P_i = precipitation at i_{th} month, D_i = surplus or deficit in the i_{th} month.

The D_i values are then aggregated, PDFs are fitted and the best fitted distribution is chosen using L-moments method. In this study, L-moments method is adopted in finding the best PDFs because it is more robust for outliers and is effective in characterizing various distribution functions compared to other methods. The CDF of the best fitted distribution is then normalized to evaluate SPEI for the selected region. Henceforth, the SPEI is computed at a 12-month scale utilizing *P* and *T* data from IMD. The dataset, spanning from 1975 to 2017, exhibits a resolution of 1°×1°. Positive SPEI values denote wet conditions, while negative values signify dry conditions. The SPEI demonstrates efficacy in assessing drought characteristics, owing to its consistent and adaptable nature in spatial and temporal dimensions, enabling the replication of water deficiencies across diverse timescales.

5.2.5 Self-Calibrated Palmer Drought Severity Index (SC_PDSI)

In 1965, Wayne C. Palmer introduced PDSI, a metric designed to assess the equilibrium between moisture demand and supply by employing a two-layer soil water balance model. Subsequently, within the PDSI framework, Wells et al., (2004) formulated the SC_PDSI model, which autonomously adjusts climatic characteristics (K) and duration factors based on historical climate data specific to a given location. The SC_PDSI is derived from time series data of precipitation and temperature, utilizing fixed parameters corresponding to the soil/surface characteristics at each geographical location. In this investigation, global gridded monthly SC_PDSI values (0.5°×0.5°) spanning from 1975 to 2017 are considered for analysis.

5.3 RESULTS

5.3.1 Formation of Homogenous Regions

The application of the FCM involves the utilization of a matrix comprising latitude, longitude, mean, standard deviation, minimum and maximum values of precipitation and temperature series. Prior to subjecting these selected variables to cluster analysis, normalization is performed to mitigate the impact of unit variations. The efficacy of FCM is contingent upon the choice of the fuzzifier index and the optimal number of clusters. In accordance with Urcid and Ritter (2012), the

cluster range systematically varied from 2 to 5, employing a fuzzifier index of 2, as advocated by Pal and Bezdek (1995). The selection of the optimal number of clusters is guided by validity indices, specifically Si, Pe and Fpi, outlined in the methodology Figure 5.1.(a). Notably, the values of Si, Pe and Fpi collectively indicate a minimum at three clusters detailed in Table 5.2. Consequently, the optimal number of clusters is determined to be three, as demonstrated in Figure 5.2

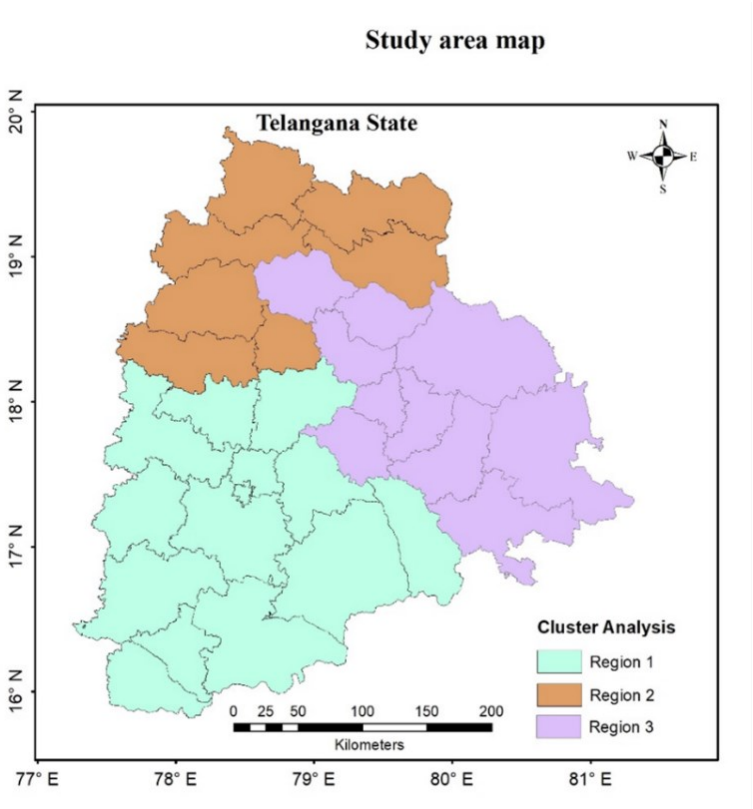

Figure 5.2: Homogenous regions identified by Fuzzy C-Means clustering.

Table 5.2: Statistics of the validity indices

Clusters	*Si*	*Fpi*	*Pe*
2	0.64	0.83	0.85
3	**0.37**	**0.67**	**0.73**
4	0.45	0.65	0.73
5	0.43	0.65	0.78

From the three homogenous regions delineated within Telangana State, the districts comprising Region 1 (South Zone) includes Sangareddy, Medak, Siddipet, Medchal Malkajgiri, Hyderabad, Vikarabad, Rangareddy, Yadagiri Bhuvangiri, Suryapet, Nalgonda, Narayanpet, MahabubNagar, Nagarkurnool, Jogulamba Gadwal. In Region 2 (North zone), the districts encompass Adilabad , Kumurambheem asifabad, Nirmal, Mancherial, Nizambad, Kamareddy, Rajanna Siricilla. Region 3 (east zone) comprises Jagtial, Peddapalli, Karimnagar, Hanumakonda, Jangaon, jayashankar Bhupallapally, Mulugu, Warangal, Mahububabad, Khammam, Bhadradri kothagudem. This geographical categorization serves as the foundational basis for subsequent analyses within the research framework, acknowledging the intrinsic heterogeneity and climatic intricates across these demarcated regions within Telangana State.

5.3.2 Characterization of SPI12 Drought Indices

The computation of SPI12 values for each homogeneous region in Telangana State is conducted utilizing the IMD monthly precipitation dataset spanning the years 1975 to 2017. Subsequently, the Method of Runs, as delineated by Yevjevich (1967), is applied to the SPI series, employing a threshold of - 0.8 to assess drought characteristics, including severity, duration and events of severe drought, across the three homogeneous regions. Table 5.3 presents the top five severe drought events for each region in Telangana State. Notably, the most severe and protracted drought event occurs in region 2 from June 2001 to August 2005, exhibiting a severity of 44.43 and a duration spanning 51 months. Region 1 experienced its lengthiest drought period between September 1984 to September 1987 with a duration of 37 months and a severity of 34.9 during between August 2011 and September 2013. Region 3 encounters its most severe drought from August 1984 to August 1986, registering a severity of 38.5 and a duration of 27 months during July 2014 to September 2016. Remarkably, all regions exhibit drought events during the periods 1984-1987, 2001-2003 and 2011-2012, underlining the temporal consistency and recurrent nature of drought occurrences within the study timeframe. Figure 5.3.(a), (b) and (c) presents Timeseries of most severe droughts event of SPI12 for the period 1975-2017 for each homogenous region.

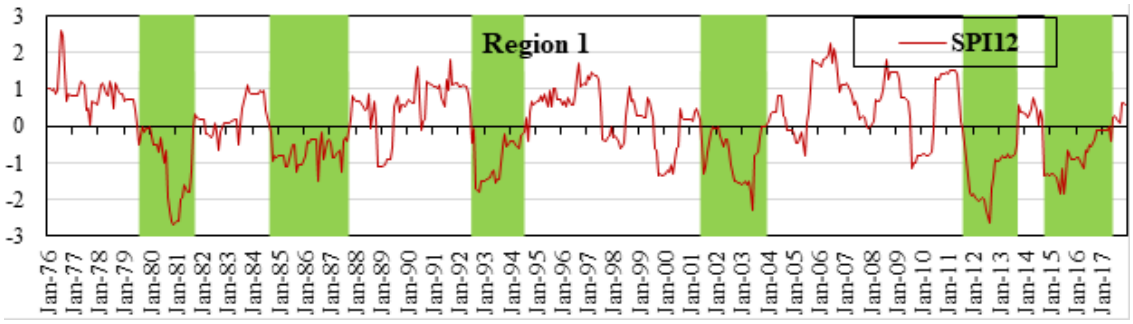

Figure 5.3.(a) Timeseries of severe drought of SPI12 (region 1)

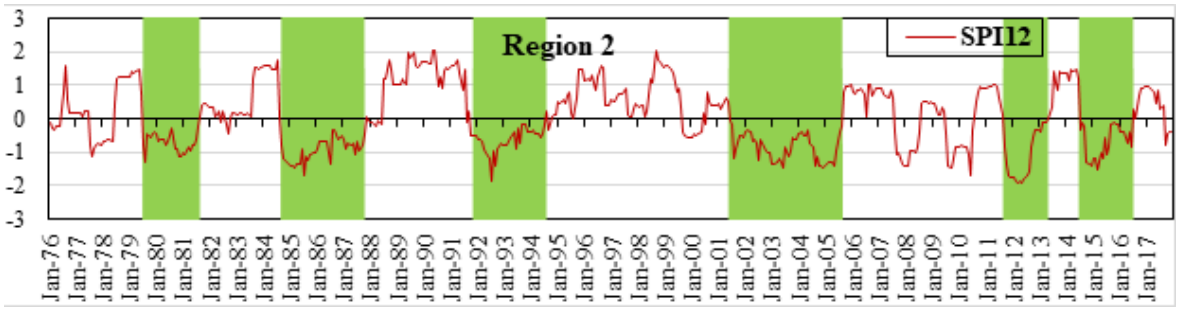

Figure 5.3.(b) Timeseries of severe drought event of SPI12 (region 2)

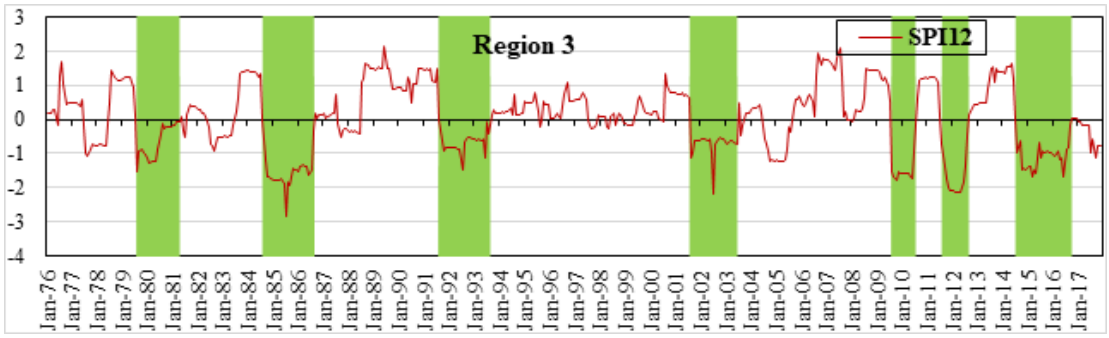

Figure 5.3.(c) Timeseries of severe drought of SPI12 (region 3)

Table 5.3: SPI12- severe drought events (IMD)

Regions	Starting month	Ending month	Severity	Duration (months)
Region 1	August1979	September 1981	30.19	26
	September 1984	**September 1987**	26.4	**37**
	June 2001	December 2003	25.5	31
	August 2011	**September 2013**	**34.9**	26
	October 2014	May 2017	26.89	32
Region 2	July 1979	August 1981	18.92	26
	September 1984	October 1987	35.68	38
	November 1991	July 1994	21.88	33
	June 2001	**August 2005**	**44.43**	**51**
	September 2011	April 2013	22.87	20
Region 3	**August 1984**	**August 1986**	**38.5**	25
	August 1991	August 1993	17.02	25
	August 2001	June 2003	17.19	23
	August 2011	August 2012	22.28	13
	July 2014	**September 2016**	29.23	**27**

5.3.3 Characterization of SPEI12 Drought Indices

The computation of SPEI12 values for each homogeneous region in Telangana State is conducted utilizing the IMD monthly precipitation and temperature dataset during the years 1975 to 2017. To calculate SPEI, Potential Evapotranspiration (PET) is initially determined and for this purpose, various estimation of PET, Penman-Monteith, Thornthwaite and Hargreaves are the most widely used methods. In the present study, Hargreaves method is adopted to calculate PET because of its simplicity and lower data requirement. Subsequently, the Method of Runs, as delineated by Yevjevich (1967), is applied to the SPEI series, employing a threshold of -0.8 to assess drought characteristics, including severity, duration and events of severe drought, across the three homogeneous regions. Table 5.4 presents the top five drought events for each region in Telangana State. Notably, the most severe and protracted drought event occurs in region 1 from August 2006 to September 2013, exhibiting a severity of 81.07 and a duration spanning 86 months. Region 2 experienced its lengthiest drought period between August 2006 to June 2013, with a severity of

75.1 and a duration of 83 months. Region 3 encounters its most severe drought from March 2014 to December 2017, registering a severity of 68.02 and a duration of 51 months during March 2007 to May 2011. Remarkably, all regions exhibit drought events during the periods 1984-1986, 1992-1994, 2006-2013 and 2014-2017, highlighting the temporal consistency and recurrent nature of drought occurrences within the study timeframe. Figure 5.4.(a),(b) and (c) Timeseries of homogenous regions for the most severe drought event of SPEI12 for the period 1975-2017.

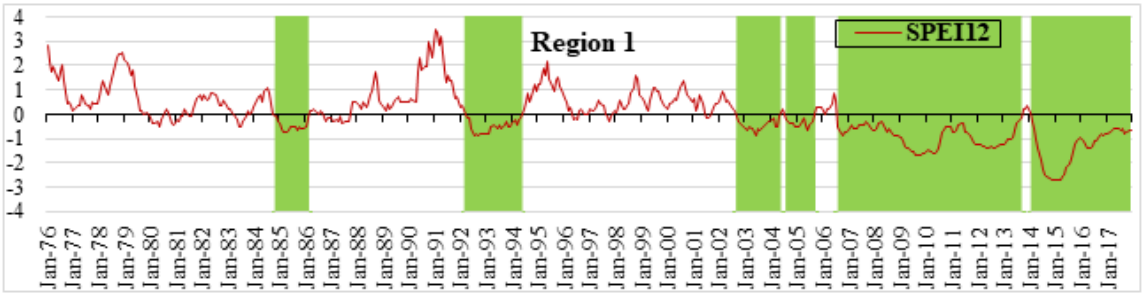

Figure 5.4.(a) Timeseries of severe drought event of SPEI12 (region 1)

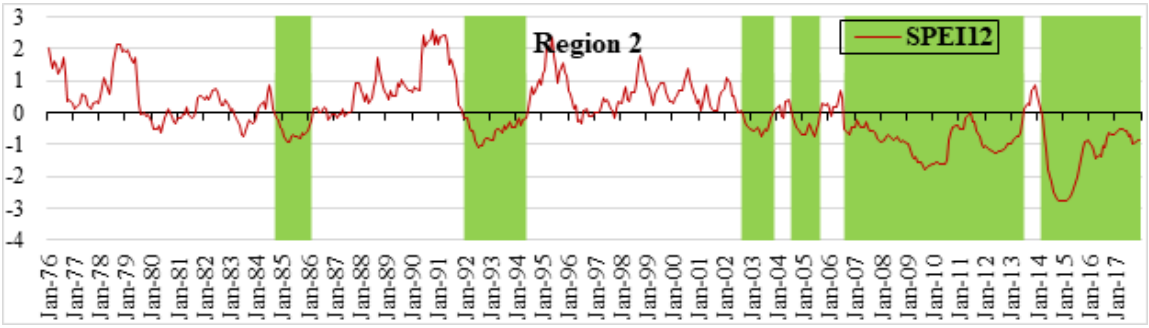

Figure 5.4.(b) Timeseries of severe drought of SPEI12 (region 2)

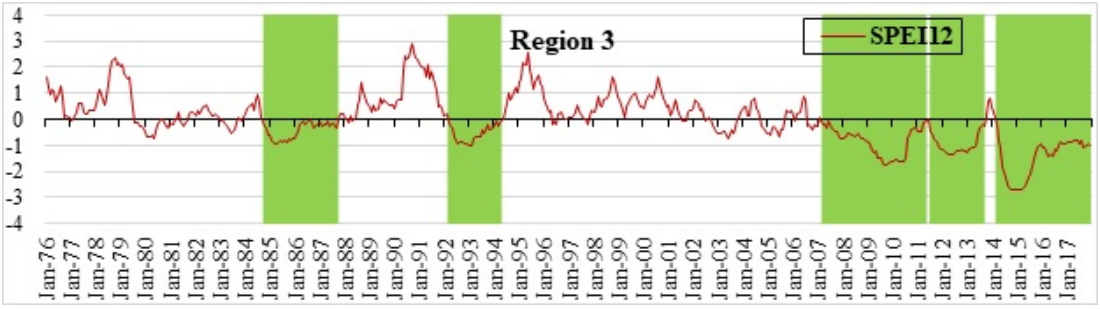

Figure 5.4.(c) Timeseries of severe drought of SPEI12 (region 3)

Table 5.4: SPEI12- severe drought events (IMD)

Region	Starting month	Ending month	Severity	Duration (months)
Region 1	November 1984	February 1986	8.18	16
	March 1992	May 1994	13.98	27
	September 2002	May 2004	9.87	21
	August 2006	**September 2013**	**81.07**	**86**
	February 2014	December 2017	66.15	47
Region 2	October 1984	February 1986	10.52	17
	January 1992	May 1994	16.65	29
	August 2004	August 2005	6.68	13
	August 2006	**June 2013**	**75.1**	**83**
	March 2014	December 2017	64.6	46
Region 3	October 1984	September 1987	15.66	36
	March 1992	April 1994	14.49	26
	March 2007	**May 2011**	43.67	51
	June 2011	September 2013	26.77	27
	March 2014	**December 2017**	**68.02**	46

5.3.4 Characterization of SC_PDSI Drought Indices

This study considered global grided monthly SC_PDSI12 values from 1975 to 2017. Same as SPI12 and SPEI12, the Method of Runs, as delineated by Yevjevich (1967), is applied to the SC_PDSI12 series, employing a threshold of -0.8 to assess drought characteristics. Table 5.5 presents the top five severe drought events for each region in Telangana State. Notably, the most severe and protracted drought event occurred in region 3 from March 1979 to April 1988, exhibiting a severity of 227.75 and a duration of 108 months. Followed by Region 1 experienced its lengthiest drought period between September 2000 and June 2013, with a severity of 79.77 and a duration of 33 months. Region 2 encounters its most severe drought from February 1984 to September 38.92 and duration of 19 months. Remarkably, all regions exhibited drought events during the periods 1992-1994, 2008-2010 and 2014-2017. Figure 5.5 (a), (b) and (c) represents the most severe drought event of SC_PDSI.

5.3.5 Intercomparison of Characterization of SPI12, SPEI 12 and SC_PDSI Drought Indices

Comparing the SPI12, SPEI12, and SC_PDSI12 results across homogeneous regions in Telangana State reveals distinct drought characteristics:

SPI12 Analysis:

Region 2 had the most severe drought from June 2001 to August 2005, with a severity of 44.43 and a duration of 51 months. Region 1 experienced a severe drought from September 1984 to September 1987, with a severity of 34.9 and a duration of 37 months. Region 3 encountered a severe drought from August 1984 to August 1986, with a severity of 38.5 and a duration of 27 months. Consistent drought events were observed during the periods 1984-1987, 2001-2003, and 2011-2012.

SPEI12 Analysis:

Region 1 had the most severe drought from August 2006 to September 2013, with a severity of 81.07 and a duration of 86 months. Region 2 experienced a severe drought from August 2006 to June 2013, with a severity of 75.1 and a duration of 83 months. Region 3 encountered a severe drought from March 2014 to December 2017, with a severity of 68.02 and a duration of 51 months. Consistent drought events were observed during the periods 1984-1986, 1992-1994, 2006-2013, and 2014-2017.

SC_PDSI12 Analysis:

Region 3 had the most severe drought from March 1979 to April 1988, with a severity of 227.75 and a duration of 108 months. Region 1 experienced a severe drought from September 2000 to June 2013, with a severity of 79.77 and a duration of 33 months. Region 2 encountered a severe drought from February 1984 to September 1985, with a severity of 38.92 and a duration of 19 months. Consistent drought events were observed during the periods 1992-1994, 2008-2010, and 2014-2017.

In summary, while SPI12 emphasizes moderate to severe droughts across all regions, SPEI12 incorporates temperature effects, showing longer and more severe droughts. SC_PDSI12, focusing

on moisture balance, indicates prolonged and extreme droughts, particularly notable in Region 3. All indices highlight recurrent drought periods, underscoring the temporal consistency and severity of drought occurrences in Telangana State from 1975 to 2017.

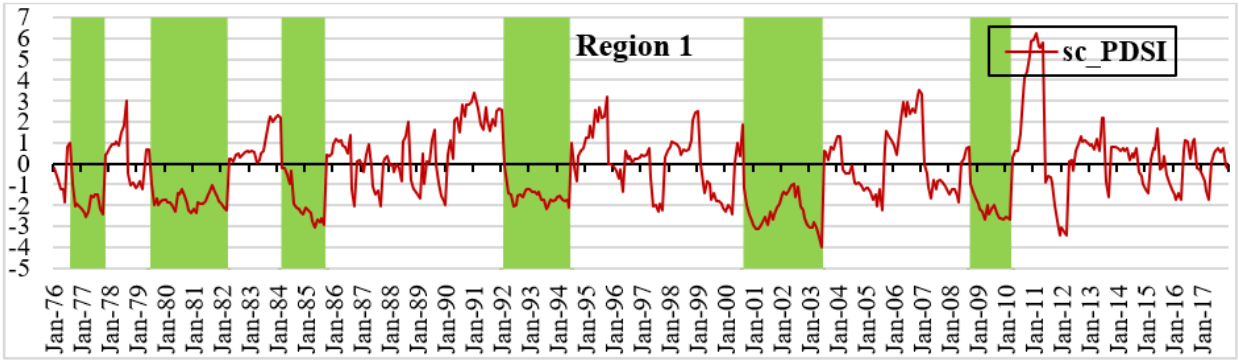

Figure 5.5.(a) Timeseries of severe drought of SC_PDSI (region 1)

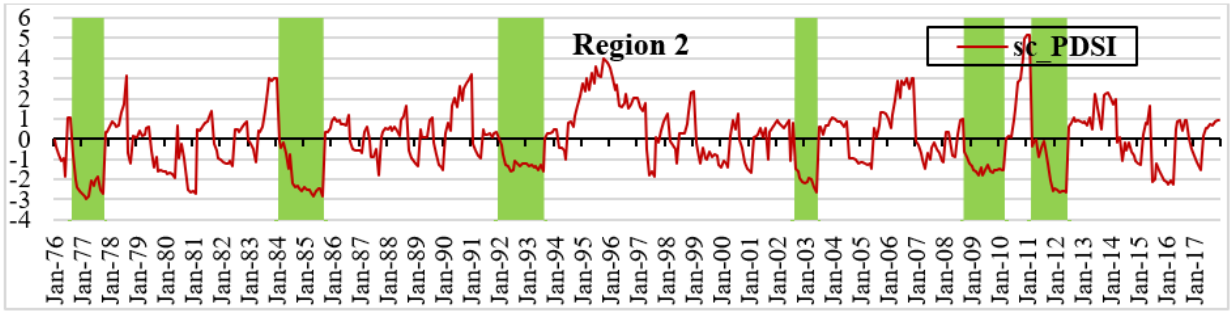

Figure 5.5.(b) Timeseries of severe drought of SC_PDSI (region 2)

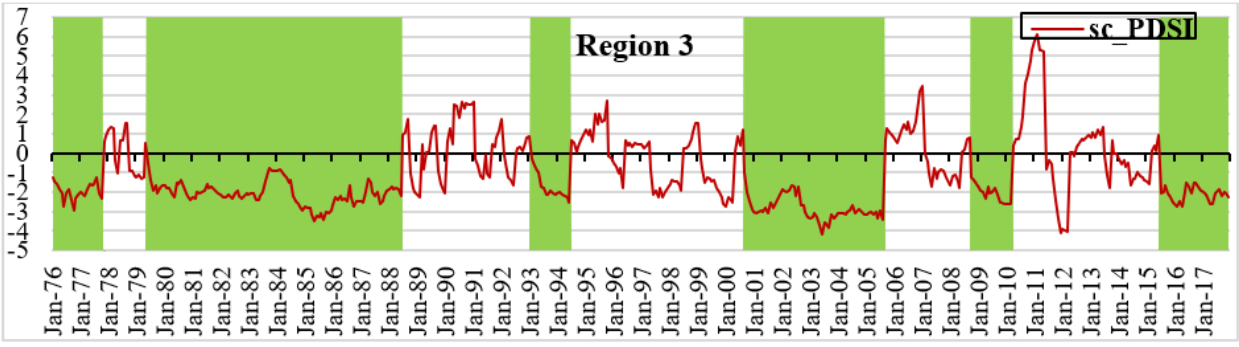

Figure 5.5.(c) Timeseries of severe drought of SC_PDSI (region 3)

Table 5.5: SC_PDSI- severe drought events (IMD)

Region	Starting month	Ending month	Severity	Duration (months)
Region 1	July 1979	March 1982	58.84	32
	March 1984	September 1985	36.73	18
	February 1992	June 1994	44.82	28
	September 2000	**June 2003**	**79.77**	**33**
	October 2008	March 2010	39.71	17
Region 2	September 1976	October 1977	32.72	13
	February 1984	**September 1985**	**38.92**	**19**
	January 1992	August 1993	23.89	18
	October 2008	March 2010	26.01	17
	March 2011	June 2012	23.95	15
Region 3	January 1976	October 1977	43.5	22
	March 1979	**April 1988**	**227.75**	**108**
	March 2007	May 2011	172.83	59
	July 2011	September 2013	37.83	18
	March 2014	December 2017	63.68	29

5.4 Discussions

This research endeavors to delineate homogenous regions within the study area, examining the distinctive characteristics of three drought indices. Subsequently the assessment of drought characteristics, specifically severity and duration, involves the calculation and examination of SPI, SPEI and SC_PDSI. This comprehensive approach enables a nuanced exploration of the diverse climatic conditions inherent in the study area. The SPI12, emphasizing precipitation patterns, the SPEI12, encapsulating both precipitation and evapotranspiration dynamics and the SC_PDSI12, integrating soil moisture considerations, collectively contribute to a holistic understanding of the spatiotemporal evolution of drought events. A precipitation-based drought index in the context of India is intricately linked with diverse physical processes, encompassing topography, atmospheric and oceanic circulation, as well as local phenomena. Employing a singular precipitation indicator becomes intricate when assessing the Indian monsoon cycle due to the influence of factors such as moisture, terrain and vegetation, contributing to the variability in precipitation at both regional and meso-scales (Wang et al., 2015b). The SPEI serves as an indicator of water availability, akin to the PDSI. SPEI represents the summation of precipitation and evapotranspiration, quantifying normalized fluctuations in moisture availability. Several studies have attested to the utility of SPEI in temporally assessing variations (Li et al., 2012). In the computation of the SC_PDSI, soil

moisture is evaluated through the integration of evapotranspiration (demand) and precipitation (supply), utilizing the water balance equation. Recognized as a multifactorial water budget indicator, SC_PDSI incorporates monthly precipitation, temperature, and soil properties into its calculations.

The drought characteristics of the drought indices are calculated and the most severe drought events are identified and presented in Table 5.3, 5.4 and 5.5. Despite the disparities among drought indices and the diverse methodologies employed in their computation, it becomes evident that a more comprehensive understanding of droughts can be attained through the synergistic application of multiple indices. SPI12 and SPEI12 exhibit heightened sensitivity to precipitation and evapotranspiration dynamics. This contrasts with SC_PDSI12, where the model algorithm incorporates soil moisture content as a primary component, distinguishing it from the former indices.

5.5 Conclusions

In this study, delineation of homogenous regions are identified. During the period between 1975-2017, this study examined and evaluated the drought conditions for three homogenous regions of Telangana state. Multiple drought indices are used to investigate drought conditions. Moreover, the assessment of regional-scale drought events is conducted through the utilization of three key drought indices: SPEI12, SPI12 and SC_PDSI12. The primary focus is on evaluating and understanding drought characteristics, with a specific emphasis on severity and duration across all regions. The following conclusions are made from this chapter:

- The optimal number of clusters is determined to be three for the study region.
- South zone of region 1 comprises of 14 districts of Telangana, North zone of region 2 comprises 7 districts; east zone of region 3 comprises 10 districts.
- SPI has experienced droughts during the periods 1984 -1987; 2001-2003 and 2011-2013 for all regions; SPEI faced drought events during 1984-1986; 1992-1994; 2006-2017; SC_PDSI, experienced drought for all regions during 1992 to 1994 and 2008-2011.
- The most severe and protracted drought event for SPI occurred in region 2 from June 2001 to August 2005, exhibiting a severity of 44.43 and a duration spanning 51 months followed by region 3 and 1.

- SPEI exhibited the most severe drought event with a severity of 81.07 and a duration of 86 months for region 1 from August 2006 to September 2013.
- SC_PDSI major drought event occurred in region 3 from March 1979 to April 1988, exhibiting a severity of 227.75 and a duration of 108 months.

Overall, these valuable insights of severity and duration of SPI, SPEI and SC_PDSI are found to be effective for analysing and assessing the regional drought conditions.

CHAPTER 6

ASSESSING THE RELATIONSHIP BETWEEN DROUGHT INDICES AND TELECONNECTIONS

6.1. Introduction

The intricate interplay of large-scale climate variations in India engenders significant spatio-temporal distribution of water resource exhibits significant heterogeneity thereby influencing the agricultural and industrial productivity of the nation (Bhuvaneswari et al., 2013). A noteworthy instance is the 2016 drought, which impacted 330 million people, resulting in a substantial economic loss exceeding $100 billion, underscores the critical importance of comprehending monsoon precipitation variations, water vapor demand and their interconnection with teleconnections in India. In the context of water resource conservation, gaining insights into these dynamics is paramount for effective management and sustainable utilization of water resources in the region.

The impact of climatic circulation exhibits a diverse influence on dry and wet conditions across various global regions. Numerous investigations have delved into the examination of the El Niño-Southern Oscillation (ENSO) phenomenon and its effects on drought occurrences, both on a global scale and within specific regions. These studies contribute valuable insights into the nuanced interactions between ENSO dynamics and drought events, offering a comprehensive understanding of the regional and global implications of climatic circulation patterns. While agriculture significantly contributes to India's GDP, as evidenced by studies there remains a dearth of comprehensive investigations into the nexus between the ENSO and drought occurrences in the Indian subcontinent. This gap in research represents an opportunity for enhancing drought prediction models. Ganguli (2014) utilized a probabilistic framework to quantify drought risk in western India, specifically examining the impact of ENSO-induced climatic variability. Additionally, Kumar et al., (2013) demonstrated the substantial influence of sea surface temperature variability on monsoon droughts in India. The limited existing research underscores the need for more extensive studies to elucidate the intricate relationship between ENSO dynamics and drought patterns in the Indian context, thereby contributing to the refinement of predictive modeling for drought events in the region.

The practical utility of teleconnections is encapsulated in the construction of teleconnection maps, providing a visual representation of the linkages of a specific concerned region with all other locations within the province. Table 6.1 enumerates commonly utilized climate indices, including their full names and acronyms. In the present study, the influence of four prominent climate oscillations namely MEI, SOI, DMI and NINO3.4 on drought indices (SPI, SPEI and SC_PDSI) is scrutinized across Telangana State. Figure 6.1 delineates the regions monitored for NINO3.4, SOI, MEI and DMI events, contributing to a comprehensive understanding of the teleconnected dynamics shaping hydrological patterns in the study area.

Table 6.1: List of climate indices (full names and acronyms)

Index full name	Acronym
El Nino Southern Oscillation˜	ENSO
Southern Oscillation Index	SOI
Multivariate ENSO Index	MEI
North Atlantic Oscillation	NAO
Oceanic Nino Index	ONI
Pacific Decadal Oscillation	PDO
Arctic Oscillation	AO
Pacific North America	PNA
Antarctic Oscillation	AAO
Indian Ocean Dipole	IOD
Sea Surface Temperature	SST
Indian Summer Monsoon Index	ISMI

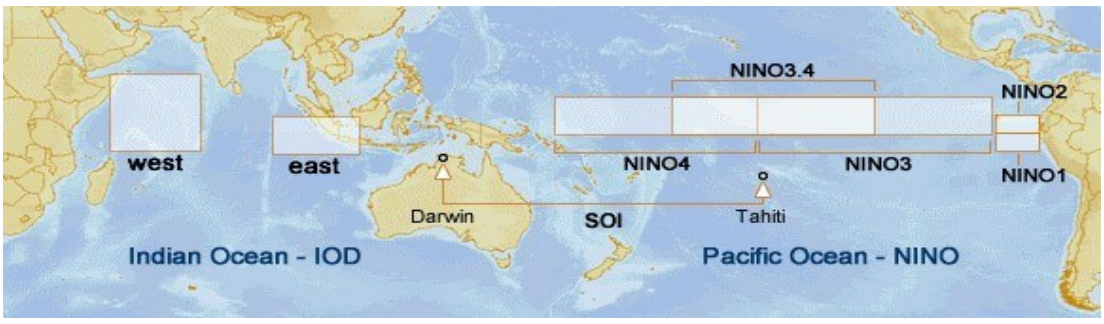

Figure 6.1: Climate indices regions. (Chowdhury, M.R. (2022))

6.2 Methodology

6.2.1 Teleconnections

The atmospheric circulation, arising from the dynamic interplay between the ocean-atmosphere and land-atmosphere interactions, facilitates the transfer of energy and water mass across vast distances, exerting a profound influence on climatic conditions (Wallace & Gutzler, 1981). This intricate system transmits climatological variations through the conveyance of heat, moisture and momentum fluxes, manifesting as precipitation and evaporation within the expansive continental water cycle and ocean circulation. The atmospheric circulation emerges as a primary driver impacting both terrestrial and marine environments, thereby contributing significantly to climate fluctuations (Alexander et al., 2002). These variations exhibit discernible patterns across diverse temporal scales, encompassing diurnal, daily, weekly and monthly intervals as well as intra-seasonal, seasonal and interannual epochs. Teleconnections, in this context, serve as a conceptual framework elucidating atmospheric interactions and transport processes, offering a means to distill climate variability into a set of indices. Coined by Walker in 1924, the term "teleconnection" is introduced to assess correlations among atmospheric pressure, temperature and rainfall.

ENSO represents a recurring phenomenon characterized by periodic variations in sea surface temperature (El Niño) and atmospheric air pressure (Southern Oscillation) over the equatorial Pacific Ocean. Regarded as a pivotal driver of global inter-annual climate fluctuations, ENSO significantly influences weather patterns in numerous regions across the globe. The manifestation of El Niño or its counterpart, La Niña, markedly alters the atmospheric circulation, impacting local and regional weather conditions. It is typically indicated by four indices: Nino 1+2, 3, 4 and 3.4. These indices delineate sea surface temperature (SST) anomalies within specific regions of the equatorial Pacific. Among these, Nino 3.4 stands out as the most widely utilized index, spanning latitudes between 5°S-5°N and longitudes between 170°W-120°W. Positive values of the Nino 3.4 signify El Niño conditions, indicative of elevated sea surface temperatures, while negative values denote La Niña conditions, reflecting colder sea surface temperatures. The prominence of ENSO indices, particularly Nino 3.4, underscores their significance in quantifying and characterizing the phases of El Niño and La Niña events, contributing to a comprehensive understanding of their climatic implications.

The SOI serves as a standardized metric derived from observed alterations in sea level pressure between Tahiti and Darwin, Australia. Specifically designed to capture large-scale air pressure oscillations during El Niño and La Niña phases, the SOI quantifies the atmospheric pressure differentials across the western and eastern tropical Pacific. Smoothed time series of the SOI exhibit significant correlations with variations in ocean temperatures within the eastern tropical Pacific region. The negative phase of the SOI, observed at Tahiti, signifies below-normal air pressure, whereas at Darwin, it indicates above-normal air pressure. The persistence of negative (positive) SOI values during El Niño (La Niña) occurrences is indicative of prolonged periods characterized by exceptionally warm (cold) ocean waters in the eastern tropical Pacific. The SOI, through its nuanced assessment of atmospheric pressure dynamics, offers valuable insights into the manifestation and progression of El Niño and La Niña events, contributing to a comprehensive understanding of the associated climatic phenomena.

The MEI constitutes a methodological approach that integrates both oceanic and atmospheric variables to quantitatively characterize the intensity of an ENSO event. This comprehensive index is derived from the first principal component of six key observed variables, including sea level pressure, sea surface temperature, zonal and meridional components of surface wind, surface air temperature and total cloudiness fraction of the sky across the tropical Pacific. The data utilized for MEI computation is sourced from the Comprehensive Ocean Atmosphere Data Set (COADS). The MEI is calculated for each of the twelve-sliding bi-monthly periods, such as December/January, January/February and so forth. Positive MEI values indicate the presence of El Niño conditions, signifying an intensified ENSO event, while negative MEI values denote the occurrence of La Niña conditions, indicative of an augmented ENSO event in the opposite phase. The MEI, through its multidimensional integration of diverse climatic variables, facilitates a nuanced and robust assessment of ENSO intensity, contributing to an enhanced understanding of the climatic variations associated with El Niño and La Niña events.

The DMI is instrumental in discerning IOD events, which are characterized by fluctuations in the tropical Indian Ocean. These events are delineated by prolonged changes in SSTs across the tropical Western and Eastern Indian Oceans. The IOD is quantitatively evaluated through an index, also known as the DMI, which is calculated as the disparity between two SST anomalies in the tropical Indian Ocean. The IOD West region encompasses the area between 50°E to 70°E and 10°S to 10°N, while the IOD East region covers the expanse from 90°E to 110°E and 10°S to 0°S, as

depicted in Figure 6.1. A positive DMI indicates cooler water in the tropical Eastern Indian Ocean and warmer water in the tropical Western Indian Ocean compared to the respective averages. Conversely, a negative DMI denotes warmer water in the tropical Eastern Indian Ocean and cooler water in the tropical Western Indian Ocean relative to the averages. The DMI, by virtue of its polarity, provides a nuanced representation of the temperature anomalies within the specified regions, contributing to a comprehensive understanding of the Indian Ocean Dipole dynamics.

Correlation analysis stands as a widely employed technique for elucidating teleconnection patterns. As a methodological approach to construct teleconnection maps, correlation analysis is distinguished by its simplicity and directness. The teleconnection map, in this context, serves as a graphical representation of the correlation between two geographical points, offering insights into the relationships between atmospheric or oceanic phenomena. A notable illustration of this methodology is evidenced in the work of Wallace and Gutzler in 1981, where correlation analysis is applied to investigate teleconnections associated with the North Atlantic Oscillation (NAO), the North Pacific Oscillation (NPO) and the Pacific-North America (PNA). This analytical tool facilitates the identification and visualization of significant correlations, thereby contributing to the comprehension of interrelated climatic variables and patterns on a global scale. In contemporary research endeavors, the Wavelet transform methodology has emerged as a potent analytical tool for discerning intricate relationships within the realm of meteorological phenomena and their interplay with large-scale climatic oscillations (Han et al., 2019).

6.2.2 Wavelet Transform

Fourier transform serves as a valuable instrument for analyzing the components of a stationary signal, wherein the signal parameters remain constant. Nonetheless, natural observations often yield non-stationary signals, demanding a more nuanced understanding of frequency variations over time. While the Fourier transform exclusively offers information pertaining to the frequency domain, the Wavelet transform, as articulated by (Farge, 1992), presents a spectrum that is not only localized in frequency but also in the time domain, thus offering a more comprehensive depiction of signal characteristics.

Wavelet transform, while conceptually akin to Fourier transformations, offers heightened versatility in analyzing frequencies within a time series. Its applicability extends across a spectrum from stationary to non-stationary and short to long-term components, providing a more nuanced

approach to frequency analysis (Percival and Walden, 2000). Widely adopted in hydro-climatology and signal processing domains (Z. Jiang et al., 2003; L. Xu et al., 2019), Wavelet Transformations (WT) manifest in two primary forms: Continuous WT (CWT) and Discrete WT (DWT). These two methods of WT exhibit notable distinctions, succinctly outlined herein. In the current study, the time-frequency spectrum derived from Continuous WT (CWT) is employed to scrutinize the relationship between climate indices and drought indices.

A wavelet is characterized as a wave-like oscillation with an amplitude that initiates from zero, undergoes growth and subsequently returns to zero. In accordance with Farge (1992), a fundamental component of wavelet transformation, known as the mother wavelet basis function ψ(t), adheres to the following condition:

$$C_\psi = 2\pi \int_\infty^\infty \frac{|\Psi(\omega)|^2}{|\omega|} d\omega < 0 \qquad (6.1)$$

where, C_ψ = admissibility constant. Integral is considered over all frequencies ω. $\Psi(\omega)$ = Fourier transform of the wavelet $\psi(t)$. The wavelet function oscillates along time axis and decays rapidly in both directions of time. Therefore, CWT with respect to wavelet $\psi(t)$, for a time series $x(t)$ is defined as given below (Farge, 1992).

$$W_S(\tau, s) = \int_\infty^\infty x(t) \frac{1}{\sqrt{s}} \psi^* \frac{t-\tau}{s} dt = 0 \qquad (6.2)$$

where, $W_s(\tau,s)$ = wavelet transform, with τ = time shift and s = scale factor. ψ = wavelet function and ψ^* = complex conjugate. $(\tau,s) = (0,1)$ represents basic or mother wavelet.

The basic or mother wavelet is denoted by $\tau = 0$ and $s = 1$. The wavelet transform's flexibility comes from the scale variations in a time series, which allow it to capture both long and short frequencies. Also, the time series can be divided into high and low frequencies with $s > 1$ corresponds to high frequency of ψ. In general, by varying s and τ values, we obtain the wavelet spectrum at various time and frequency scales. The Morlet wavelet is one of the most widely used wavelet functions in hydro-climatology and is represented by the equation below.

$$\varphi_0(\theta) = \pi - \frac{1}{4ei\omega^0\theta_e - \frac{\theta^2}{2}} \qquad (6.3)$$

where, φ_0 represents mother wavelet; ω_0, θ denotes frequency and time; higher ω_0 time resolution decreases, scale resolution increases and vice versa.

6.2.3 Wavelet Coherence

Within the time-frequency space, wavelet coherence can be used to determine the relationship between two time series by estimating the correlation between them that varies between 0 and 1. In accordance with Torrence & Webster (1999) coefficient of wavelet coherence between the two sets of time series data can be denoted as follows:

$$R^2(s,\tau) = \frac{\left|s\left(s^{-1}W_{xy}(s,\tau)\right)\right|^2}{s(s^{-1}|W_x(s,\tau)|^2 . s(s^{-1}|W_y(s,\tau)|^2)} \quad (6.4)$$

where, $R^2(s,\tau)$ = coherence coefficient minimum and maximum coherence at 0 and 1. $W_{xy}(s,\tau)$ = cross wavelet transforms between two series. The wavelet coherence varies between 0 and 1 (Liu, 1994). s= smoothing operator represented as given below

$$S(W) = S_{scale}\ (S_{time}\,(W(s,\tau))) \quad (6.5)$$

The smoothing along wavelet axis (scale and time) are represented as S_{scale} and S_{time} respectively. Designing the smoothing operator so that it has a similar footprint as the wavelet used is a common process and Torrence & Webster (1999) proposed a suitable smoothing operator for the Morlet wavelet, details can be found in Grinsted et al., (2004). Using Monte Carlo method, the statistical significance level is estimated using 1000 ensemble surrogate pairs with AR1 coefficients as the input datasets. Then we evaluate wavelet coherence for each pair and for each scale calculate the significance level using only values outside the cone of influence. Grinsted et al., (2004) specified that resolution chosen when computing the scale smoothing has a major impact on the significance level. Therefore, the number of scales per octave should be high enough to capture the rectangle shape of the scale smoothing operator while minimizing computing time. In the present study, the wavelet coherence is examined at 5% significance level or at the confidence interval > 95%.

6.2.4 Step by procedure used

a. SPI12, SPEI12 and SC_PDSI are computed using R software tool
b. Severity i.e., minimum value of drought index during each drought event is calculated
c. Duration number of consecutive months below the threshold -0.8 is measured.
d. Teleconnection indices (ENSO, MEI, SOI and NINO3.4) data is considered and standardized.
e. Correlation coefficients are computed between drought indices and teleconnection indices are computed using MATLAB.
f. The significance of teleconnection indices in predicting drought events is evaluated.
g. Overlap of drought indices with teleconnections are identified using timeseries plot.

6.3 RESULTS

6.3.1 Correlation between Drought Indices and Teleconnection Factors

Previous studies have shown that droughts are closely related to climate variables (Mishra & Singh, 2010). In this study, MEI, NINO3.4, SOI and DMI are chosen to describe the influences of teleconnections over droughts. Moreover, Wavelet coherence is employed to evaluate the link between drought indices (SPI.SPEI and SC_PDSI) and climate factors during 1975-2017. The 95% confidence level is presented as thick contour and the relative phase relationship is represented by arrows with anti-phase pointing left and in-phase pointing right as shown in Figure. 6.2, 6.3, 6.4 and 6.5.

The Wavelet coherence analysis between SPI and various climate factors (DMI, MEI, NINO3.4 and SOI) is depicted in Figure 6.2. A sustained coherence in interannual variability is discerned throughout the temporal spans of 1980-1995 and 2002-2017, primarily evident at time scales ranging from 20 to 40 months. Notably, intermittency is observed between 4 to 16 months during different years for SOI. For NINO3.4, intermittency is noticed between 1978-1992 and 2002-2015 for time scales spanning 18 to 40 months, with intermittent coherence observed at varying years within the range of 4 to 10 months. Regarding the SOI, interannual coherence is evident between 1975-1990 and 1995-2017, spanning time scales from 10 to 20 months. MEI interannual coherence is evident between 1982-1994 and 1995-2017, spanning time scales from 16-40 months and intermittency is observed between 4-12 months. In contrast, DMI exhibited comparatively weaker effects across various scales during diverse years when compared to other teleconnections.

For SPEI, the Wavelet coherence analysis between SPEI and various climate factors(DMI, MEI, NINO3.4 and SOI) is presented in Figure 6.3. The impact of the DMI is notably observed across time scales spanning 6 to 20 months during the period of 1990-2000. In the case of MEI, interannual variability manifests within the 4–12 month time scale, while annual variability is discerned at the 16-32 month time scale over the interval of 2002-2012. Annual variability of the NINO3.4 index is evident between 2002-2015, spanning an 18–50 month time scale, with interannual variability observed at the 6-16 month time scale. The SOI exhibits a highly significant influence within the time scale range of 14-40 months during the period 2002-2014.

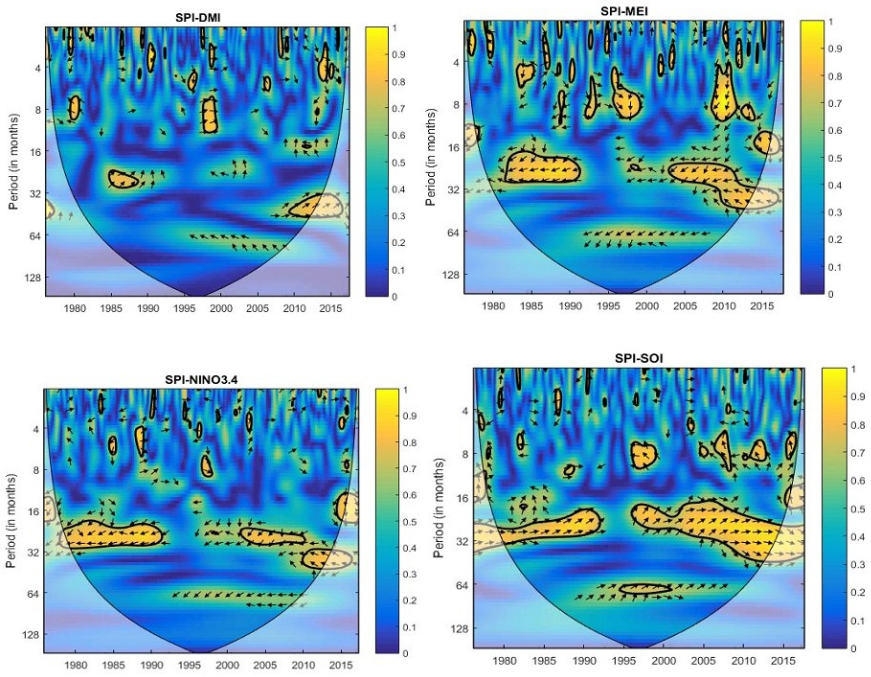

Figure 6.2: Wavelet coherence between SPI with (a) DMI (b) MEI (c) NINO 3.4 and (d) SOI

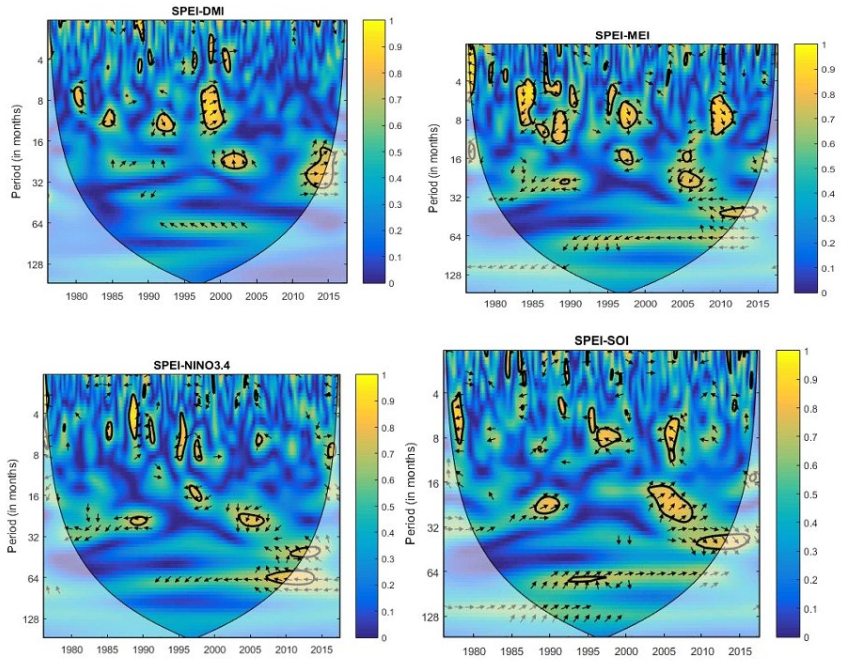

Figure 6.3: Wavelet coherence between SPEI with (a) DMI (b) MEI (c) NINO 3.4 and (d) SOI

The Wavelet coherence analysis between the SC_PDSI and various climate factors (DMI, MEI, NINO3.4 and SOI) is represented in Figure 6.4. SC_PDSI, annual variability demonstrates notable insufficiency in coherence with DMI. For the SOI, where it is observed intermittently across different years within the time scale range of 8-32 months. Interannual variability is discerned in the time scale range of 4-10 months at different years for SOI. Furthermore, the impact of interannual variability spans is observed between the time scales of 4-32 months for all climate factors. Notably, the annual variability of DMI is relatively less pronounced when compared with the MEI, SOI and NINO3.4. For MEI, interannual variability is observed between the time scales of 20-32 months across diverse years within the span of 1980-1990. The annual variability of NINO3.4 exhibits high significance within the 12–32 month time scales. In the case of SOI, interannual variability is discerned across time scales ranging from 4 to 32 months for different years.

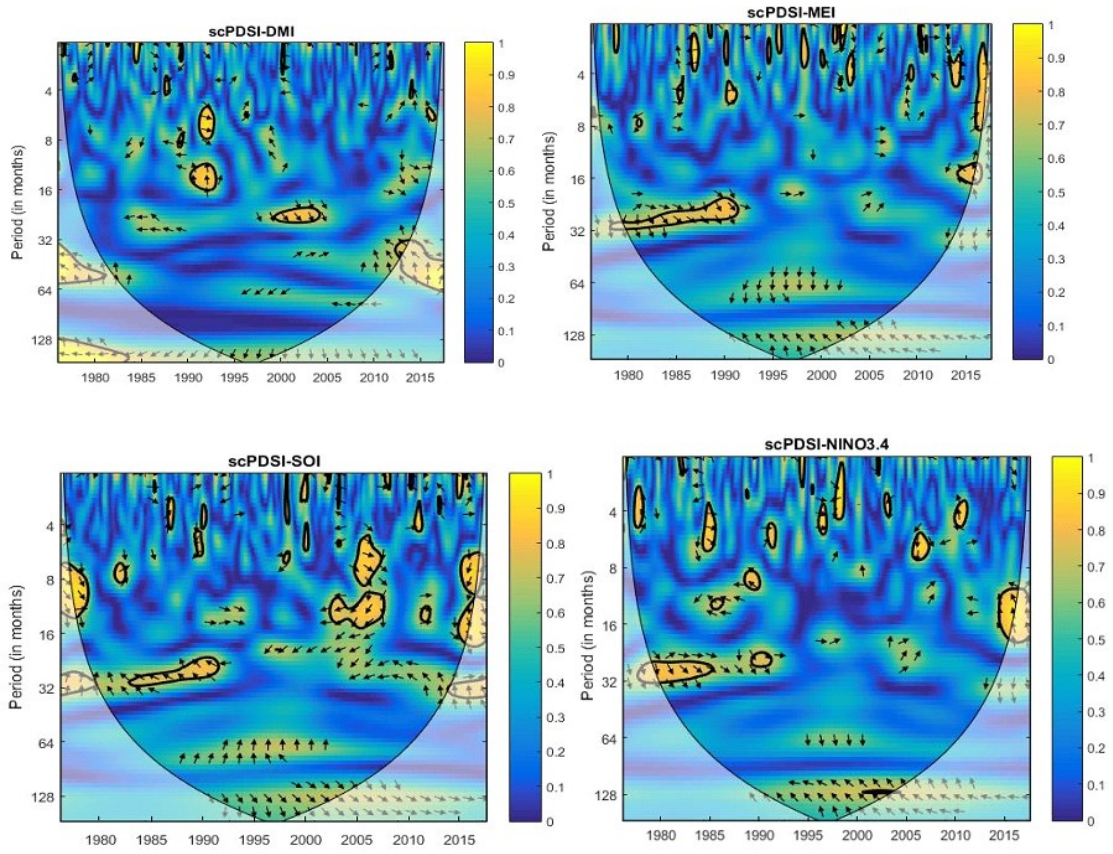

Figure 6.4: Wavelet coherence between SC_PDSI with (a) DMI (b) MEI (c) SOI & (d) NINO 3.4

6.3.2 Analysis of Annual Time Series of Teleconnections with Drought Indices

For DMI, the annual time series reveals noticeable overlap periods with SPI12 during 1979-1982, 1984-1987 and 1992-1994. Similarly, for SPEI12, a substantial correlation in overlap periods is observed in 1984-1987, 1992-1994 and 2004-2007. In the case of SC_PDSI, notable overlap with DMI is identified during the periods 1979-1982, 1984-1987, 1992-1994 and 2004-2006. It is noteworthy that SC_PDSI exhibited overlaps at different time intervals, followed by SPI12 and SPEI12. Fig 6.5 represents the annual time series of DMI with Drought indices.

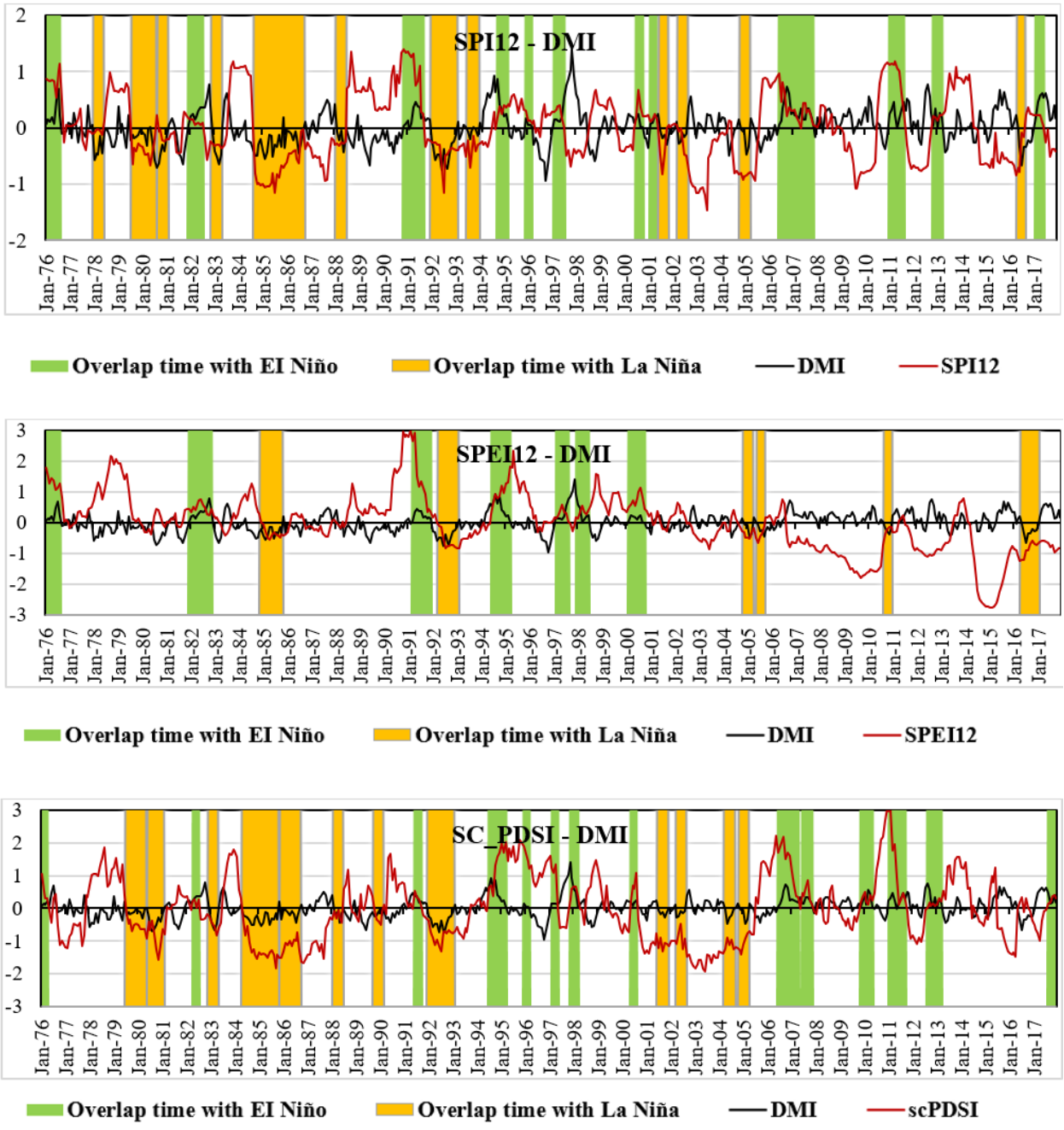

Figure 6.5 Annual series of DMI with Drought indices

For MEI, the annual time series reveals discernible overlap periods with SPI12 during 1984-1987 and 2011-2013. Likewise, SPEI12, a substantial correlation in overlap periods is observed in 1984-1987, 2007-2009, 2010-2013 and 2016-2017. In the case of SC_PDSI, notable overlap with DMI is identified during the periods 1980-1982, 1984-1987, 1999-2002, 2008-2009 and 2016-2017. It

is noteworthy that SPEI12 exhibits overlaps at different time intervals, followed by SC_PDSI and SPI12. Figure 6.5 visually represents the annual time series of MEI with drought indices.

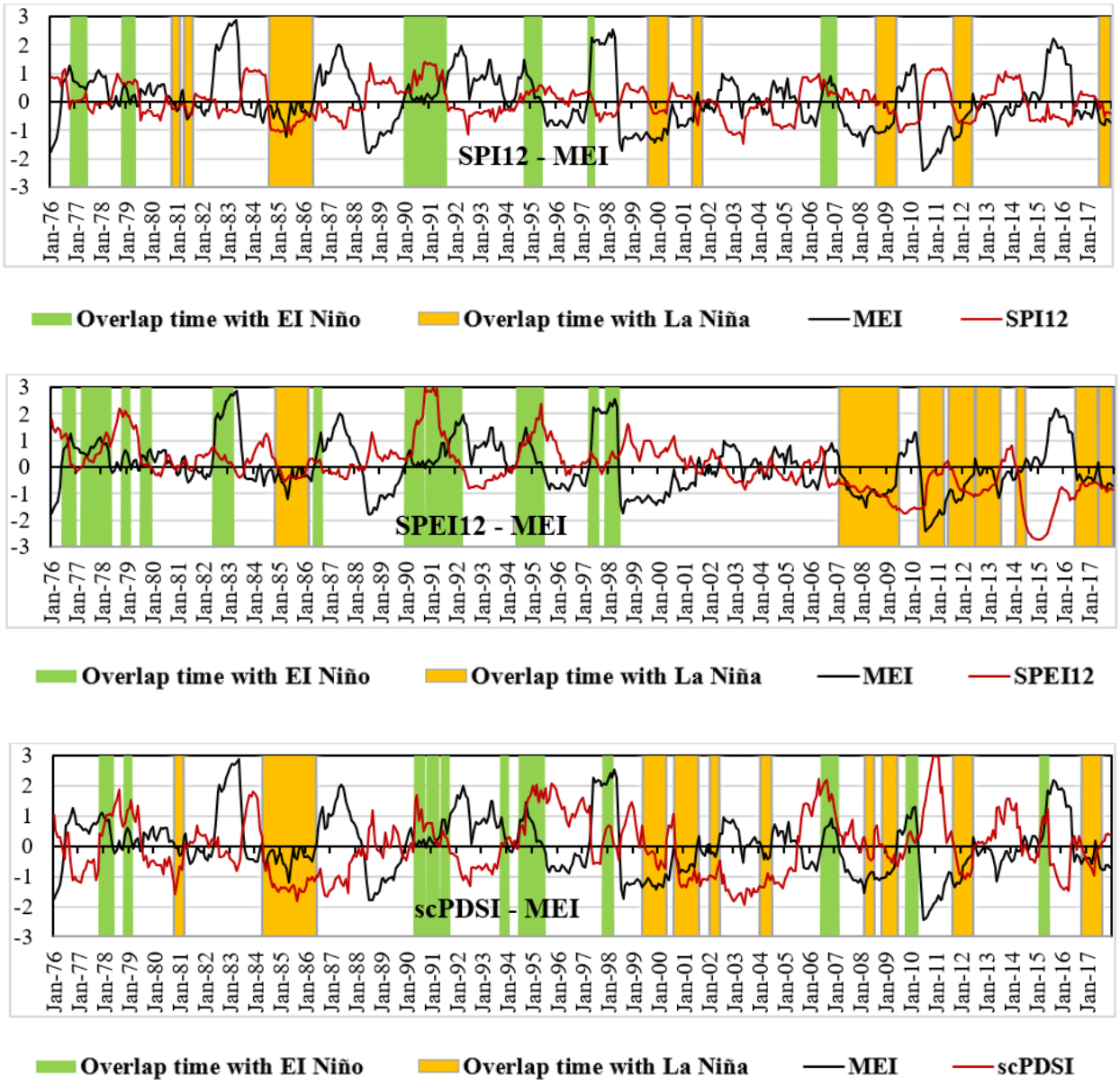

Figure 6.6 Annual series of MEI with Drought indices

The annual time series unveils that SOI overlap periods with SPI12 during 1977-1979, 1980-1981, 1986-1988,1991-1995,1997-1999, 2002-2004 and 2014-2017. Similarly, for SPEI12, a substantial correlation in overlap periods is observed in 1980-1981, 1986-1988, 1992-1994, 2002-2004, 2007-2009, 2010, 2012 and 2014-2016. In the case of SC_PDSI notable overlap with DMI is identified

during the periods 1977-1979, 1980-1981, 1982-1984, 1987-1989, 1993-1994, 2002-2006, 2008-2009 and 2014-2016. SOI demonstrates robust overlaps at different time intervals for all drought indices. Figure 6.7 visually represents the annual time series of SOI with drought indices

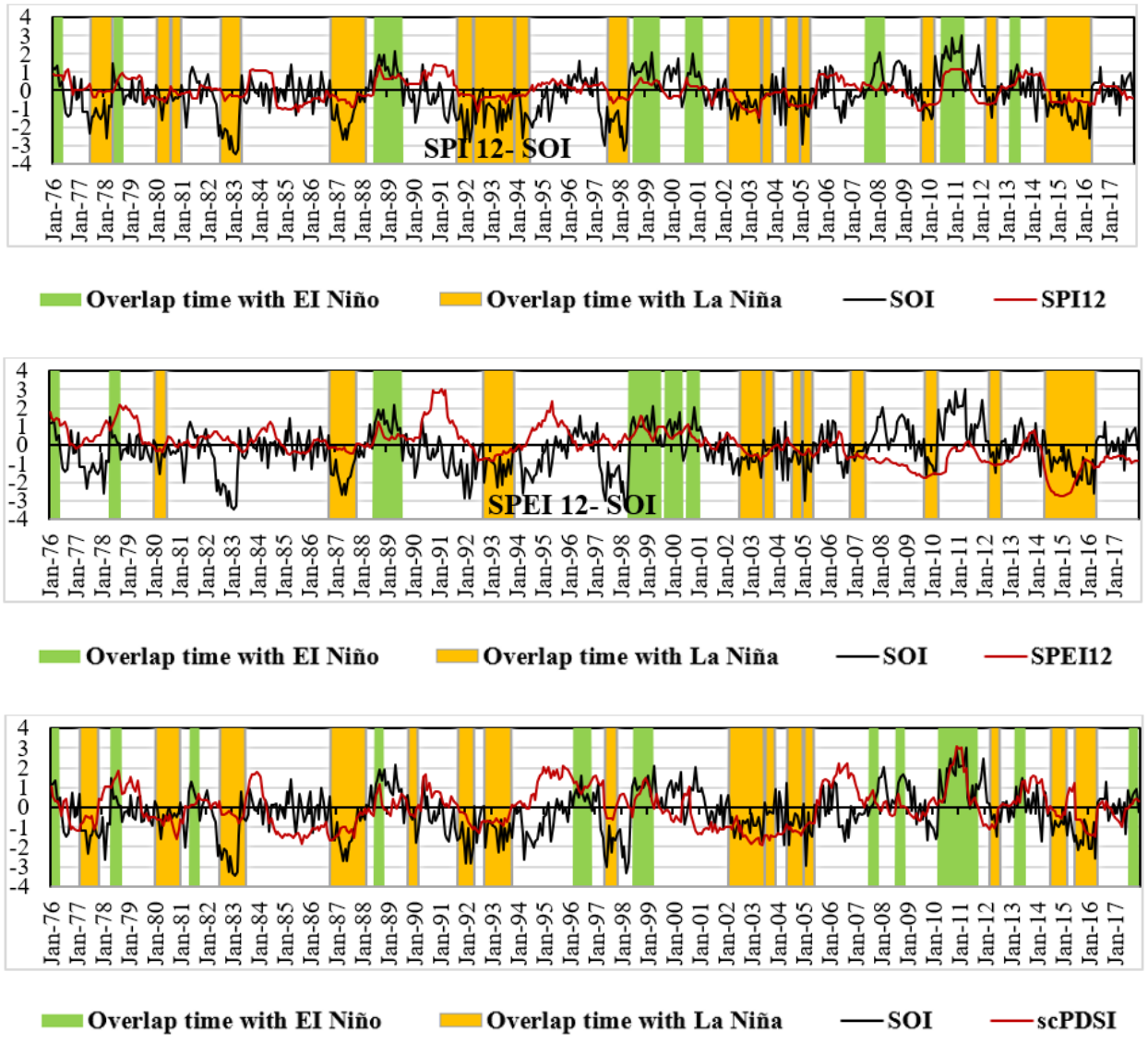

Figure 6.7 Annual series of SOI with Drought indices

The annual time series of NINO 3.4 reveals discernible overlap periods with SPI12 during 1980-1982, 1984-1987, 1999-2001, 2000-2009, 2012 and 2017. Similarly SPEI12, a substantial correlation in overlap periods is observed in 1984-1987, 1992-1993, 2007-2009, 2010-2013 and 2016-2017. In the case of SC_PDSI, notable overlap with NINO 3.4 is identified during the periods

1984-1987, 1989, 1999-2000, 2001-2002 and 2011-2012. Figure 6.8 visually represents the annual time series of NINO 3.4 with drought indices.

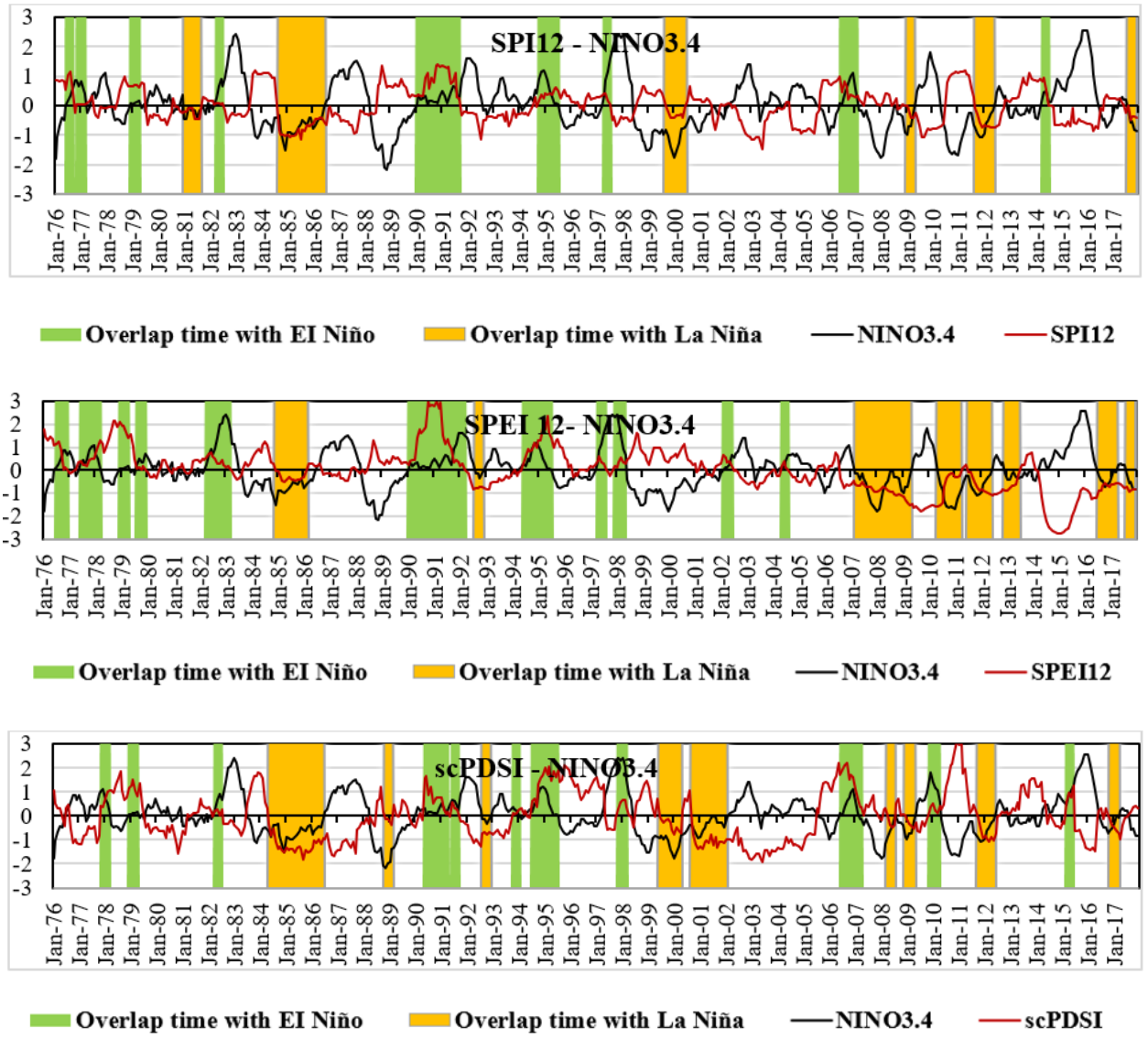

Figure 6.8 Annual series of NINO 3.4 with Drought indices

6.3.3. Intercomparison of Drought Indices with Teleconnections

The intercomparison of SPI12, SPEI12, and SC_PDSI with various climate indices reveals significant overlap periods indicating drought correlations:

1. SPI12 Overlaps:

Significant overlaps with DMI during 1979-1982, 1984-1987, and 1992-1994. MEI shows overlaps in 1984-1987 and 2011-2013. SOI overlaps during 1977-1979, 1980-1981, 1986-1988, 1991-1995, 1997-1999, 2002-2004, and 2014-2017. NINO 3.4 overlaps in 1980-1982, 1984-1987, 1999-2001, 2000-2009, and 2012.

2. SPEI12 Overlaps:

Significant overlaps with DMI in 1984-1987, 1992-1994, and 2004-2007. MEI shows overlaps in 1984-1987, 2007-2009, 2010-2013, and 2016-2017. SOI overlaps during 1980-1981, 1986-1988, 1992-1994, 2002-2004, 2007-2009, 2010, 2012, and 2014-2016. NINO 3.4 overlaps in 1984-1987, 1992-1993, 2007-2009, 2010-2013, and 2016-2017.

3. SC_PDSI Overlaps:

Significant overlaps with DMI in 1979-1982, 1984-1987, 1992-1994, and 2004-2006. MEI shows overlaps in 1980-1982, 1984-1987, 1999-2002, 2008-2009, and 2016-2017. SOI overlaps during 1977-1979, 1980-1981, 1982-1984, 1987-1989, 1993-1994, 2002-2006, 2008-2009, and 2014-2016. NINO 3.4 overlaps in 1984-1987, 1989, 1999-2000, 2001-2002, and 2011-2012.

These overlaps indicate consistent periods of drought conditions as measured by SPI12, SPEI12, and SC_PDSI with variations in intensity and duration influenced by different climate indices across the studied periods.

6.4 Discussions

Researchers have established that climate factors significantly contribute to the initiation of drought events (Dai, 2011). Moreover, the results obtained from Wavelet coherence analysis reveal an impactful association between climate factors, namely the MEI, SOI, DMI, NINO3.4 and the evolution of drought. Notably, in the context of Indian regions, MEI, SOI and NINO3.4 exhibit the most pronounced influence on drought patterns (Fig. 6.2, 6.3 and 6.4). Multiple teleconnections exert their influence on drought indices, encompassing various components across India. While earlier studies predominantly focused on the impact of the ENSO, relying on a single indicator to encapsulate the diverse climatic variability features across extensive regions is deemed inadequate (Zhu et al., 2017). In the present study, four widely acknowledged climate factors are considered

and their connections with drought indices are meticulously assessed. The outcomes underscore substantial variations in the influence of each teleconnection on different drought indices. The coherence observed in drought indices with teleconnections (MEI, SOI, DMI and NINO3.4) at approximately 8-32 months may be attributed to the correlation existing among climate indices, as depicted in Figure. 6.2, 6.3 and 6.4. Consequently, a comprehensive analysis, isolating the standalone impact of teleconnection factors on drought indices after mitigating the effects of other influential time series, may yield a more robust correlation (Tan et al., 2016).

6.5 Conclusions

In the present study, during 1975-2017, the time series of drought indices are examined climate indices. Then, using the Wavelet coherence method, the relationship between drought indices and climate factors is evaluated. This reliable and robust quantitively results helps to understand the relation between the climate and drought indices and new insights for further investigating the drought. The key findings from this study are given as follows:

- A sustained coherence for SPI interannual variability is discerned throughout the temporal spans of 1980-1995 and 2002-2017, primarily evident at time scales ranging from 20 to 40 months. Notably, intermittency is observed between 4 to 16 months during different years for MEI. The SOI, interannual coherence is evident between 1975-1994 and 1995-2017 spanning time scales from 16 to 40 months.
- The SOI exhibits a highly significant influence within the time scale range of 14-40 months during the period 2002-2014 in the case of SPEI.
- Annual variability of DMI with SC_PDSI is relatively less pronounced when compared with the MEI, SOI and NINO3.4.
- A substantial correlation in overlap periods is observed in 1984-1987, 2010-2013 and 2016-2017 among all drought indices with climate factors.
- The Wavelet coherence analysis effectively demonstrated the connection between climate indices and drought events. The influence of SOI on drought is significantly high followed by NINO3.4 and MEI with all drought indices. SOI has the strongest impact in detecting the progression of drought compared to other climate indices.

CHAPTER 7

INVESTIGATIONG MULTIVARIATE FREQUENCY ANALYSIS USING SEVERITY-DURATION-FREQUENCY AND SEVERITY-AREA-FREQUENCY CURVES

7.1 Introduction

Evaluation of SDF and SAF regional drought curves is conducted within the context of drought manifestations within three homogenous regions in Telangana, where the predominant reliance on rainfed source of irrigation is observed. Presently, the Copula concept finds widespread application for quantifying bivariate and multivariate joint probability distributions within the realms of Hydrology and engineering (Ganguli, 2014; Thilakarathne & Sridhar, 2017). In the modeling of characteristics pertaining to two or more dependent variables encompassing dimensions such as severity, duration and the spatial extent, Copula functions emerge as potent and resourceful analytical tools. This efficacy is attributed to Copula's capacity to maintain a robust correlation between the variables under consideration, unhindered by the requirement for identical marginal probability distributions in the context of long-term predictions. The ensuing section provides a comprehensive delineation of the methodology employed in the derivation of SDF and SAF curves.

Within the confines of this chapter, the analytical framework relies upon the IMD precipitation and temperature dataset for the evaluation of the 12-month Standardized Precipitation Index (SPI) and Standardized Precipitation Evapotranspiration Index (SPEI) for the temporal span between 1975 and 2017. In parallel, Suitable GCMs datasets (FGOALS-g2 and BCC-CSM1.1(m)) pertaining to precipitation and temperature variables are harnessed to compute SPI and SPEI for the time span from 1975 to 2095. Leveraging the computed SPI12 and SPEI12 indices, the derivation of SDF and SAF curves unfolds across homogeneous regions, encapsulating the entire temporal continuum from 1975 to 2095. Furthermore, the ensuing section provides an elucidation on the projection of these SDF and SAF curves, offering insights into their future trajectories and implications within the stipulated timeframe. The methodology for developing SDF and SAF involves a systematic approach to data collection, preprocessing and statistical analysis represented in Figure 7.1.

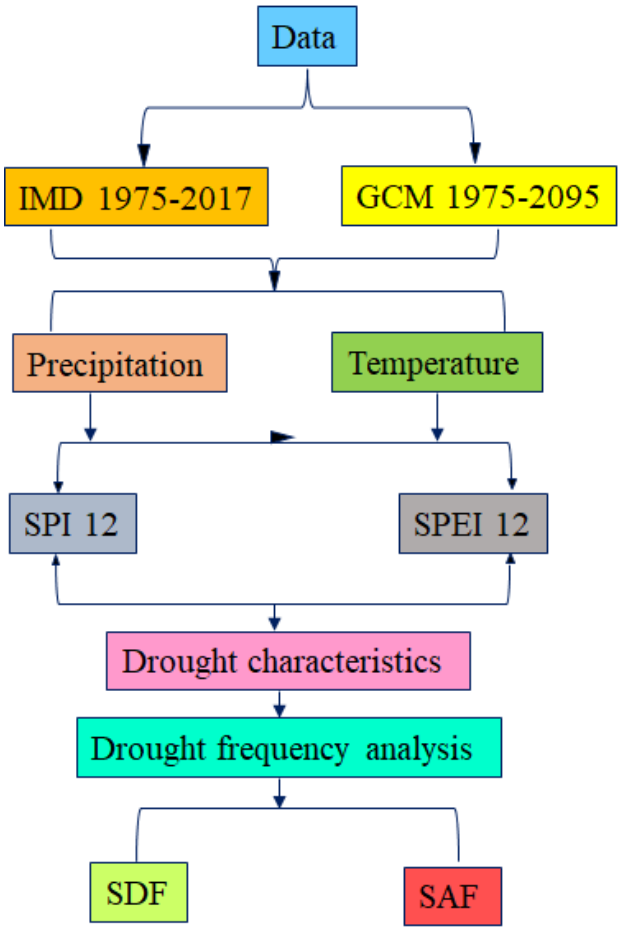

Figure 7.1: Methodology for the development of SDF and SAF curves.

7.2. METHODOLOGY

The investigation in this section encompasses the following components: (i). quantification of alterations in drought climatology utilizing the SPI12 and SPEI12 through the analysis of the precipitation and temperature dataset (IMD and GCMs(RCP 8.5 Scenario)) (ii). A copula-based methodology is employed to formulate SDF curves. This involves scrutinizing modifications in the joint return period concerning drought characteristics. (iii) derivation of SAF curves is conducted, scrutinizing alterations of return periods that encapsulate areal extent (percentage) alongside corresponding severity.

Step by procedure followed is mentioned below

a. Monthly precipitation and temperature data for the study area is obtained with timescales (IMD dataset (1975-2017) and GCMs (1975-2095).

b. SPI is computed at SPI12 further SPEI is calculated incorporating potential evapotranspiration (PET), calculated.
c. A drought severity threshold (-0.8) is established and applied to identify drought events based on SPI and SPEI series exceeding the established threshold.
d. Characteristics analysis – number of droughts, mean interarrival time , mean severity, maximum severity, mean duration and maximum duration is analysed.
e. Frequency of occurrence is further calculated
f. Characteristics of drought and frequency of occurrence is further compared regionally over the study region.

7.2.1 Copula function

The Copula function, introduced by Sklar, (1959), serves as a pivotal tool for associating or coupling two or more random variables. This mathematical construct inherent ability to uphold a robust correlation among the considered variables, irrespective of the demand for identical bivariate or multivariate marginal distributions, especially in the context of long-term predictions.. Consider a pair of random variables, X and Y, each characterized by marginal cumulative distribution functions $F_X(x)$ and $F_Y(y)$. Sklar's theorem establishes that the joint distribution function $F_{XY}(x,y)$ for these dependent random variables can be succinctly expressed using the Copula function C:

$$P(X \leq x,\ Y \leq y) = F_{XY}(x,y) = C\big(F_X(x), F_Y(y)\big) \qquad (7.1)$$

Here, $F_{XY}(x,y)$ represents the joint Cumulative Distribution Function (CDF) of the considered random variables X and Y and u and v are uniformly distributed random variables defined as $u = F_X(x)$ and $v = F_Y(y)$The bivariate copula is characterized by the distribution function $C(\bullet)$, with the mapping $C: [0,1]^2 \rightarrow [0,1]$. Each element (u,v) in the domain adheres to the following properties:

$$C(u,0) = 0 = C(0,v)\ \forall\ u,v \in [0,1]^2$$

$$C(u,1) = u; C(1,v) = v\ \forall\ u,v \in [0,1]^2$$

If $C(u,v)$ is a joint distribution function, then

$$C(u_2,v_2) - C(u_2,v_1) - C(u_1,v_2) + C(u_1,v_1) > 0;$$

for $0 \leq u_1 \leq u_2 \leq 1 \; and \; 0 \leq v_1 \leq v_2 \leq 1.$

Various copula families, with distinct properties, are established and a comprehensive exposition of these families is available in Nelsen, (2007). Prominent among copula classes are Archimedean, Extreme, Elliptical and Plackett. In the current investigation, copulas from the Archimedean class (specifically Clayton, Gumbel and Frank), Galambos from the Extreme class and Plackett copulas are applied to model the joint dependence of drought variables. Expressions for Cumulative Distribution Functions (CDFs), corresponding PDFs and pertinent copula family set parameters are presented in Table 7.1.

Table 7.1. Expressions for CDF ($C(u,v)$) of copula families.

Copula family	$\boldsymbol{C(u,v)}$	**Parameter space**
Clayton	$(u^{-\theta} + v^{-\theta} - 1)^{-\frac{1}{\theta}}$	$\theta \geq 0$
Frank	$-\frac{1}{\theta} ln\left[1 + \frac{(e^{-\theta u} - 1)(e^{-\theta v} - 1)}{(e^{-\theta} - 1)}\right]$	$\theta \neq 1$
Gumbel	$\exp\left\{-\left[(-lnu)^{\theta} + (-lnv)^{\theta}\right]^{\frac{1}{\theta}}\right\}$	$\theta \geq 1$
Galambos	$uv \exp\left\{\left[(-lnu)^{-\theta} + (-lnv)^{-\theta}\right]^{-\frac{1}{\theta}}\right\}$	$\theta \geq 0$
Plackett	$\frac{1}{2(\theta - 1)}(s - q)$	$\theta \geq 0$

Note: u and v represent two dependent CDFs, θ is the copula parameter,

$s = 1 + (\theta - 1)(u + v)$ and $q = \sqrt{s^2 - 4uv\,\theta(\theta - 1)}$

7.2.1.1 Copula parameter estimation

The primary methodologies employed for copula parameter estimation encompass (i) Method of Moments (MoM) expounded by Genest & Rivest, (1993) (ii) Inference from Margins (IFM) introduced by Joe, (1997) (iii) Exact Maximum Likelihood (EML) and (iv) Maximum Pseudo-Likelihood (MPL) methods as outlined by C. Genest et al., (1995). In this present analysis, copula parameter estimation is conducted using Maximum Pseudo-Likelihood (MPL) method is adopted for.

Within the MPL framework, the estimation of copula parameters is predicted on the utilization of a pseudo log-likelihood function. Let $X \in X_i, 1, X_i, 2, \ldots, X_i, d$ represent observations from a d-dimensional random vector X. The pseudo-observations are constructed based on the ranks of the observed data and the empirical Cumulative Distribution Function (CDF) is estimated using the following expression. This approach ensures a rigorous and technically sound methodology for copula parameter estimation within the context of the present study.

$$\mathrm{U} = U_{i,d} = \frac{Ranked\ data\ of\ X_{i,d}}{n+1}\ \forall\ i = 1,2, \ldots \ldots, n \tag{7.2}$$

$$U_{i,d} = \frac{1}{n+1} \sum_{j=1}^{n} 1\{X_{j,d} \leq X_{j,d}\}\ \forall\ i = 1,2, \ldots \ldots, n; j \neq i; d = 1,2, \ldots., n \tag{7.3}$$

In the context of this study, where U_i, d represents the vector of pseudo-samples, particularly in the bivariate scenario denoted as U = {Ui,1, Ui,2} for all i = 1, 2, ..., n, the integration of empirical Cumulative Distribution Functions (CDFs) into the bivariate copula density yields a log-likelihood function in accordance with the formulation proposed by Christian Genest & Favre, (2007). This log-likelihood function serves as a pivotal element in the analytical framework, encapsulating the statistical underpinnings of copula parameter estimation.

$$L_U(\theta) = \sum_{i=1}^{n} \log\left[c_\theta\left(U_{i,1,} U_{i,2,}\right)\right] = \sum_{i=1}^{n} \log\left[c_\theta\left(\frac{R_i}{n+1}, \frac{S_i}{n+1}\right)\right]\ \forall\ i\epsilon\{1, \ldots., n\} \tag{7.4}$$

Here, c_θ as the bivariate copula density and acknowledging R_i and S_i as the ranks corresponding to the observed data, the derivation of the copula parameter θ involves the maximization of the rank-based pseudo log-likelihood function. This endeavor yields the parameter θ through the

utilization of the following expression. The optimization of the pseudo log-likelihood function constitutes a fundamental step in the estimation of copula parameters, embodying the statistical foundation of this analytical procedure.

$$\hat{\theta} = arg\ max[lnL_U(\theta)] \tag{7.5}$$

7.2.1.2 Goodness of Fit

The discernment of a suitable copula model is executed through the application of distance-based statistical measures, such as Anderson–Darling (AD) and Akaike Information Criterion (AIC) which helps to identify best fit copula. The formulae of AD and AIC statistics are given as follows

$$\text{AD} = \max_{1\le i\le n, 1\le j\le n} \frac{|\widehat{C_n}\left(\frac{i}{n'n}\right) - C_{p\theta}\left(\frac{i}{n'n}\right)|}{\sqrt{C_{p\theta}\left(\frac{i}{n'n}\right)[1 - C_{p\theta}\left(\frac{i}{n'n}\right)]}} \tag{7.6}$$

where, i and j denotes order statistics of the random variable u and v.

$$AIC(m) = n\,log(MSE) + 2m \tag{7.7}$$

where, *m*= number of fitted parameters; *n*= number of observations; *MSE*= mean square error of the fitted copula model and is expressed as follows

$$MSE = \frac{1}{n-m}\sum_{i=1}^{n}(O_i - P_i)^2 \tag{7.8}$$

where, O_i, P_i are the observed and simulated variables. the lowest *AD* and *AIC* is considered as best copula (Amirataee et al., 2018; Janga Reddy and Ganguli, 2012).

7.2.1.3 Drought Frequency analysis

In the current study, the quantification of drought characteristics, encompassing severity and duration, adheres to the runs theory as outlined by Yevjevich & Ica Yevjevich, (1967). Let X_t represent a drought variable with a time series denoted by t. Accordingly, a run is identified as a segment within the time series wherein all values either exceed or fall below a predetermined threshold X_0. Consequently, values surpassing (or falling below) this threshold are termed positive runs (negative runs). Notably, the properties of drought are intricately linked to the selected threshold, which may either be constant or exhibit variability over time (Mishra & Singh, 2010).

In this study, a threshold is established with 20th percentile of the SPI and SPEI values, approximately corresponding to a threshold value of -0.8. This selection is informed by its utility in signifying drought occurrences, as values beneath this threshold indicate the onset of drought conditions (Reddy & Ganguli, 2013). This rigorous consideration of the threshold, grounded in established methodologies, ensures a nuanced analysis of drought characteristics within the defined temporal framework.

Numerous investigations into drought properties have been conducted through the lens of univariate frequency analysis by researchers Cancelliere & Salas, (2004); Tallaksen et al., (1997). Recognizing the limitations inherent in univariate approaches, Researchers such as Kim et al., (2006); Rajsekhar et al., (2015); Shiau & Shen, (2001) have advanced the field by extending their focus to bivariate frequency analysis. This extension is particularly pertinent since the joint behavior of multiple drought characteristics remains concealed within the confines of univariate analyses. Hence, a rigorous exploration of the collective dynamics inherent in drought characteristics becomes imperative for augmenting regional drought assessment and strategic planning. This transformative paradigm has engendered the formulation and application of SDF and SAF curves. These curves play a pivotal role in unraveling the intricate interdependencies and joint dynamics of various drought attributes. By adopting a bivariate frequency analysis approach, researchers can gain a more comprehensive understanding of drought occurrences, thereby facilitating improved regional assessment and strategic planning in the context of water resource management and environmental sustainability.

7.2.1.4 Severity-Duration-Frequency Analysis

SDF curves represent invaluable tools for conducting multivariate analyses of regional and global drought frequencies. A comprehensive exploration of relevant literature reveals several seminal studies that have applied SDF analysis to characterize drought features across diverse geographic regions. ISO-severity maps are developed using SDF analysis by Dalezios et al., (2000) & Saghafian et al., (2003). An alternative analytical approach utilizing copula for SDF curve derivation is presented by Shiau & Modarres, (2009). Building on these foundations, notable studies by Janga Reddy & Ganguli, (2012), Rad et al., (2017) have further contributed to the field by deriving SDF curves employing copula methodologies.

The methodological steps employed in generating Standardized Drought Frequency (SDF) curves through copula analysis in this investigation encompass the following:

- Selection of pertinent goodness-of-fit statistics to assess the optimal fitting marginal distribution for severity and duration.
- Formulation of joint and conditional marginal distributions employing a best-fit copula approach for severity and duration.
- Establishment of the interdependence among severity, duration and frequency in relation to return periods for drought events, utilizing the conditional recurrence interval methodology as proposed by Shiau et al. (2007).

$$T_{S|D}(s|d) = \frac{1}{\gamma(1-F_{S|D}(s|d))} \tag{7.9}$$

where, d = duration, s = severity, $\gamma =$ arrival rate, $F_{S|D}(s|d)$ and $T_{S|D}(s|d)$ are the conditional CDF and conditional recurrence interval of S given $D = d$ respectively. The expression for conditional CDF is given below.

$$F_{S|D}(s|d) = \frac{\partial F_{S,D}(s,d)}{\partial F_D(d)} \tag{7.10}$$

where $F_{S,D}(s,d) =$ joint CDF and $F_D(d)$ represents the CDF of drought duration.

- SDF curves are derived from Eq. 7.9 and 7.10 at various return periods.

7.2.1.5 Severity-Area-Frequency Analysis

The determination of the return period for a drought event characterized by a specified percentage of areal extent is facilitated through the application of SAF curves, serving as a decisive indicator of drought occurrence (Burke & Brown, 2010). Noteworthy antecedent studies, such as those conducted by Tase, (1976), Hisdal & Tallaksen, (2003), Santos, (1983) Loukas & Vasiliades, (2004), Bonaccorso et al., (2015), Mishra & Singh, (2009) have contributed to develop SAF curves.

The assessment of SAF curves is systematically executed through the following procedural steps:

- Annual drought severity is calculated using run theory at each grid point.

- Areal extents are subsequently delineated through the computation of distinct severity thresholds expressed as a percentage of the total area for each calendar year.
- L-moments serve as the basis for calculating distribution parameters, enabling the identification of the optimal fit among various probability distributions intended for severity values related to varied areal extents.
- Frequency analysis is conducted entailing the computation of return periods corresponding to diverse levels of drought severity associated with percentage areal extents.

Within the scope, the quantification of drought severity is conducted through the application of the run theory approach. The spatial delineation of areal extents is intricately tied to the calibration of severity metrics specific to each designated drought region. A meticulous examination of various probability distributions ensues, using Akaike Information Criterion (AIC), to discern the optimal fit that characterizes the severity values within the respective drought regions.

7.3 RESULTS

7.3.1 Characterization of Drought using SPI12 and SPEI12

7.3.1.1 SPI12

The SPI12 values are computed for each homogenous region using IMD (1975-2017) and GCM (1975-2095: 1975-2005, 2006-2035, 2036-2065 and 2066-2095) monthly precipitation dataset. The method of runs (Yevjevich, 1967) is applied to the SPI series with a threshold of -0.8 to evaluate drought characteristics (Number of drought events, mean interarrival time, maximum duration, minimum duration, maximum severity and minimum severity) for three homogeneous regions. From analysis it is noticed that number of droughts is increasing in future compared to the IMD. An increasing trend is noticed in the maximum duration and severity for future scenarios. The mean inter arrival time is gradually decreasing with an increase in the number of droughts. The graphical representation of the observed dataset, specifically a scatterplot and histogram, delineates the relationship between drought intensity and duration within the stipulated regions are shown in Fig. 7.2 (a).

7.3.1.2 SPEI12

The SPEI12 values are computed for each homogenous region using IMD (1975-2017) and GCM (1975-2095, 1975-2005, 2006-2035, 2036-2065 and 2066-2095) monthly precipitation and temperature dataset. Here in SPEI, Same as SPI a threshold of -0.8 is used to evaluate drought characteristics for three homogeneous regions. From analysis is noticed that number of droughts is increasing in future compared to the IMD. An increasing trend is noticed in the maximum duration and severity for future scenarios. The mean inter arrival time is gradually decreasing with increase in number of droughts. The graphical representation of the observed dataset, specifically a scatterplot and histogram, delineates the relationship between drought intensity and duration within the stipulated regions are shown in shown in Fig. 7.2 (b).

Table 7.2 (a): SPI12 - Drought characteristics

Region	**Drought characteristic**	**IMD**	**GCM**			
		1975-2017	**1975-2005**	**2006-2035**	**2036-2065**	**2066-2095**
Region 1	No. of droughts	18	16	19	15	18
	Mean interarrival time	24.8	22.4	19.7	23.6	20.5
	Mean severity	11.45	8.7	9.1	9.1	10.3
	Maximum severity	34.9	32.2	38.7	55.6	64.9
	Mean duration	12.35	11.2	13	13.7	12.2
	Maximum duration	37	34	58	48	61
Region 2	No. of droughts	20	20	20	13	21
	Mean interarrival time	26.31	18.3	21.4	23.5	24.2
	Mean severity	10.2	6.9	7.78	10.9	10.1
	Maximum severity	44.43	33.7	41.8	56.5	62.8
	Mean duration	13.63	9.1	9.7	12	10.8
	Maximum duration	51	37	45	72	64
Region 3	No. of droughts	21	16	23	25	18
	Mean interarrival time	23.65	22.68	24.69	26.64	26.47
	Mean severity	9.52	8.72	9.08	8.78	9.87
	Maximum severity	38.5	30.87	36.68	52.53	57.3
	Mean duration	10.9	10.93	11.08	9.6	11.64
	Maximum duration	48	44	43	51	59

The drought characteristics are evaluated using SPI12 and SPEI 12 for each homogeneous drought region. Regions 2 and 3 experienced the highest number of drought events for IMD and the same is expected for GCMs in future scenarios in both the cases. Whereas, the mean inter-arrival time is maximum for regions 3, followed by region 1. In case of maximum severity and duration, regions 1 and 3 experienced the highest values. With respect to the drought characteristics, decreasing trend is observed from region to region. Regions 1 exhibit a lower frequency of drought occurrences characterized by elevated severity levels and extended mean interarrival times. Overall, it is expected to experience a greater number of droughts with high mean arrival time, severity and duration for most part of the Region 1 and 3. This expectation aligns with the findings of Gupta and Jain (2018), who observed an escalated rate of increase in potential evapotranspiration (PET) compared to rainfall across numerous regions in the country. Consequently, a heightened proclivity towards increased aridity is envisaged in the latter portion of the 21st century, contributing to a concomitant elevation in the severity and duration of drought episodes.

The frequency of occurrence is also shown in Figure 7.3 (a) and (b) for SPI 12 and SPEI 12 . The prevalence of moderate drought events is notably elevated in both historical and projected future periods across all examined regions, constituting nearly 30% of the total drought occurrences. This heightened occurrence of moderate droughts is consistently observed throughout the study duration across all regions. Specifically, Region 1 exhibits a comparatively greater frequency of moderate droughts compared to other regions. A substantial escalation in the incidence of both moderate and severe drought events is discernible across the entirety of the three regions. Anticipations for the future indicate a pronounced likelihood of extreme drought events, particularly in Regions 1 and 3. Notably, the hydrological dynamics in India are profoundly influenced by the monsoon season (June-September), accounting for 70% of the annual precipitation. Consequently, the manifestation, progression and spatial distribution of drought events are intricately linked to the patterns of monsoonal rainfall. The anticipated rise in evaporation rates due to global warming is expected to induce drier terrestrial conditions and an augmentation of water vapor content in the atmosphere, contributing to the evolving dynamics of drought occurrences over time.

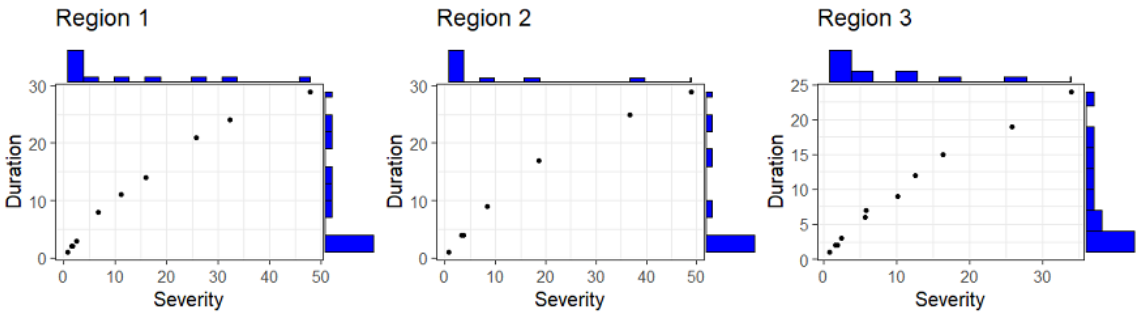

Figure 7.2 (a) SPI12 - Scatterplot and histograms

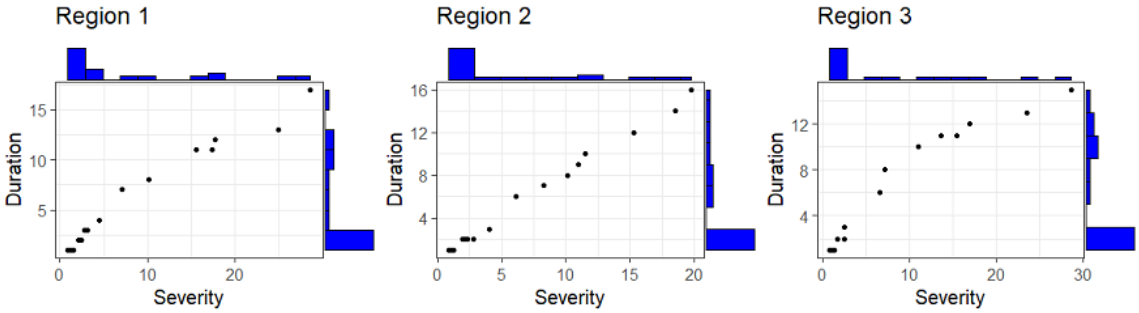

Figure 7.2 (b) SPEI12 - Scatterplot and histograms

7.3.1.3 Intercomparison of characterization of Drought using SPI12 and SPEI12

The comparison between SPI12 and SPEI12 reveals distinctive quantitative details in drought characteristics across homogeneous regions:

Frequency and Severity:

Both SPI12 and SPEI12 indicate a notable increase in the frequency of moderate drought events across historical and projected future periods, constituting nearly 30% of total drought occurrences. Region 1 shows a higher frequency of moderate droughts compared to other regions, suggesting varying susceptibility to drought conditions.

Severity and Duration:

Regions 1 and 3 consistently exhibit the highest values for maximum severity and duration of drought events, highlighting their vulnerability to prolonged and severe drought conditions. A decreasing trend in drought characteristics is observed from Region 1 to Region 3, with Region 1 typically experiencing lower frequency but higher severity and longer mean inter-arrival times of droughts.

Table 7.2 (b) : SPEI12 – Drought Characteristics

Region	**Drought characteristic**	**IMD**	**GCM**			
		1975-2017	**1975-2005**	**2006-2035**	**2036-2065**	**2066-2095**
Region 1	No. of droughts	17	18	17	14	19
	Mean interarrival time	25.63	19.27	20.76	23.64	21.47
	Mean severity	11.47	7.76	11.78	10.38	14.53
	Maximum severity	81.07	28.56	38.18	56.19	58.08
	Mean duration	13.18	9.5	9.7	12.07	12.8
	Maximum duration	86	33	41	46	51
Region 2	No. of droughts	20	20	14	17	19
	Mean interarrival time	21.84	17.35	26.07	18.83	20.38
	Mean severity	9.6	5.41	13.72	7.34	15.14
	Maximum severity	75.1	29.88	45.73	51.29	50.39
	Mean duration	11.21	8.4	7.57	9.83	14.31
	Maximum duration	83	32	43	41	61
Region 3	No. of droughts	23	19	16	16	15
	Mean interarrival time	20.27	19.10	21.87	23.68	21.64
	Mean severity	8.29	7.51	12.53	9.53	17.47
	Maximum severity	68.02	25.38	35.12	39.79	52.59
	Mean duration	9.86	9.21	8.31	11	11.83
	Maximum duration	51	23	39	54	58

Future Projections:

Future scenarios suggest an escalation in both moderate and severe drought events across all regions, with Regions 1 and 3 particularly vulnerable to extreme drought episodes. These projections align with studies indicating increased evapotranspiration rates relative to rainfall, contributing to heightened aridity and prolonged drought conditions in the latter part of the 21st century.

Hydrological Dynamics and Monsoon Influence:

The hydrological cycle in India, heavily influenced by the monsoon season, plays a crucial role in shaping drought patterns. Expected rise in evaporation rates due to global warming may intensify terrestrial dryness and atmospheric water vapor content, further influencing the spatial distribution and evolution of drought events.

In summary, while both SPI12 and SPEI12 capture similar trends in drought frequency and severity, SPEI12's incorporation of evapotranspiration data enhances understanding of drought impacts on water availability and vegetation, particularly in regions prone to increased aridity and prolonged drought episodes.

7.3.2 Drought Frequency Analysis using SPI12`and SPEI12.

7.3.2.1 Severity-Duration-Frequency analysis

The copula best fitting the frequency analysis is determined based on the distribution with the minimum values for Kolmogorov-Smirnov (K-S), Carmer Vos Mises (C-M) and Anderson-Darling (A-D) statistics, as presented in Table 7.3 (a). Specifically, for SPI12, the Clayton copula emerges as the optimal fit for Region 1, the Gumbel copula for Region 2 and the Frank copula for Region 3. Conversely, for SPEI12, the Gumbel copula is identified as the most suitable for Region 1, the Frank copula for Region 2 and once again, the Frank copula for Region 3. These determinations are made based on the evaluation of Log Likelihood (L-L) and Akaike Information Criterion (AIC) values as shown in Table 7.4 (a). for SPI12 and 7.4 (b) SPEI 12.

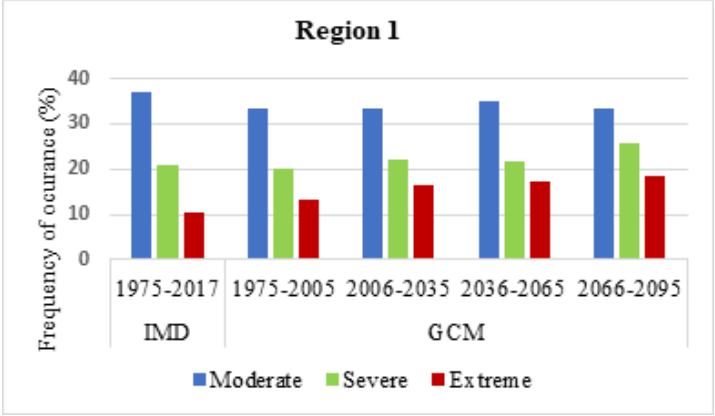

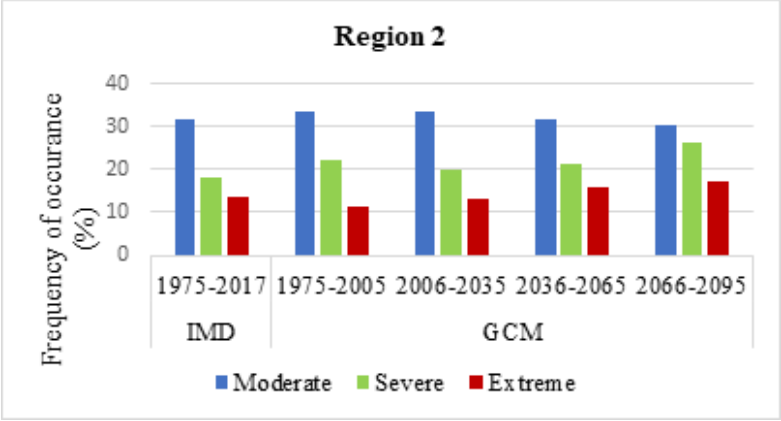

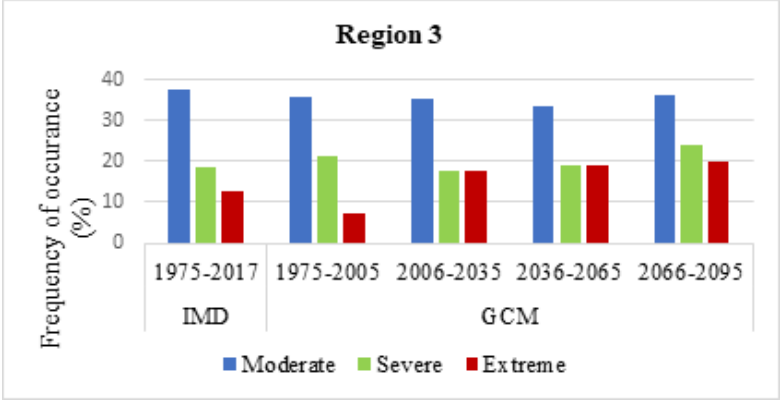

Figure 7.3 (a) SPI12 - Frequency of occurrence

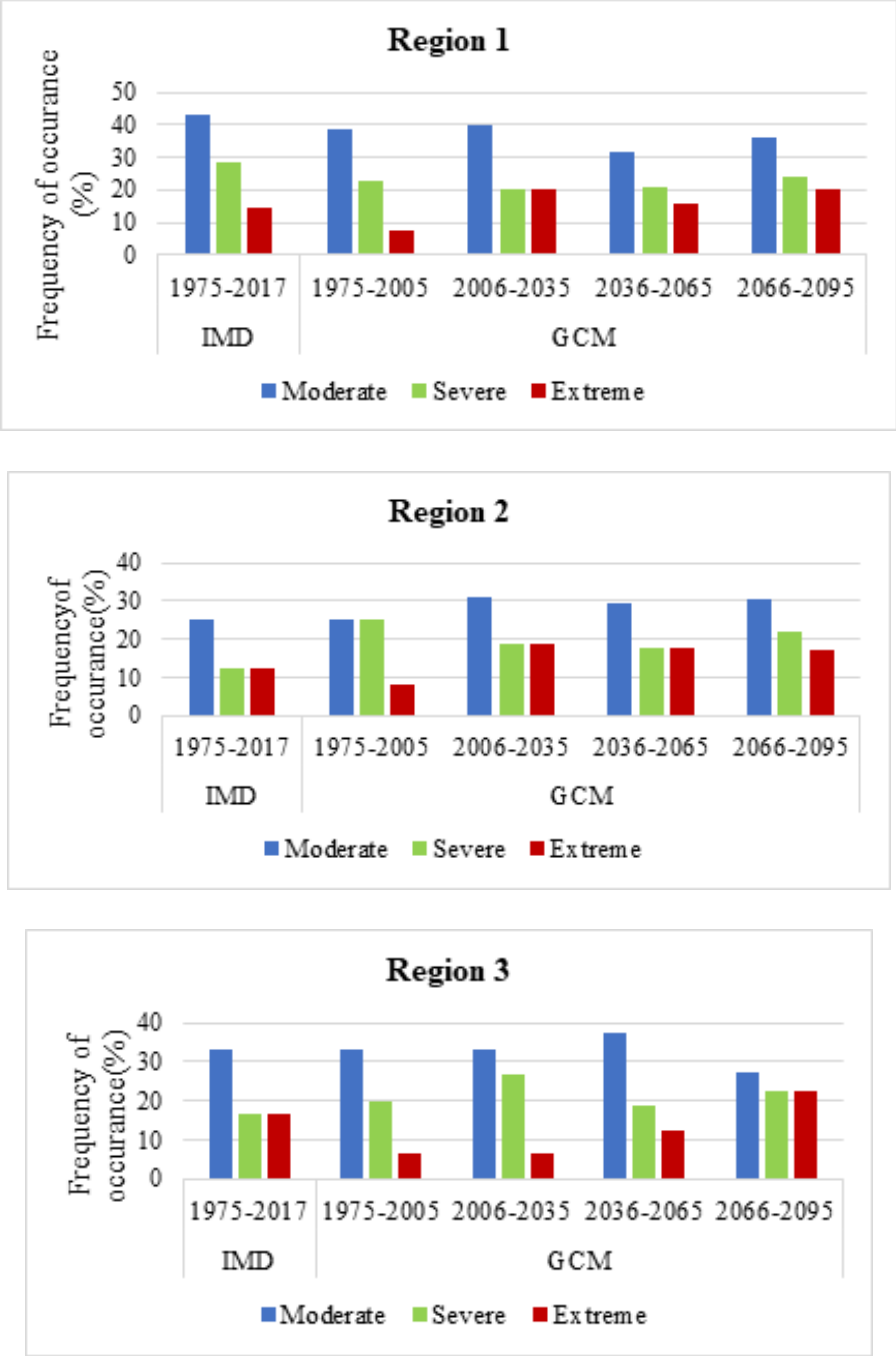

Figure 7.3 (b) SPEI12 - Frequency of occurrence

Furthermore, an analysis of optimal parameter values and the corresponding probabilities of duration is presented in Table 7.3(a) and (b) for SPI12 and SPEI12, respectively. The performance assessment involves the consideration of various probability distributions to model drought severity and duration, calibrated through the inverse cumulative distribution of distinct univariate distributions. Subsequently, the joint probability dependence across diverse return periods is computed using the inverse h-function of the best-fit copula.

For each homogenous region, SDF curves are formulated, as illustrated in Fig. 7.4 (a) for SPI and 7.4 (b) for SPEI. Notably, Regions 1 and 3 exhibit elevated severity levels across different return periods, indicative of a heightened frequency of drought occurrences in the regions under investigation. Furthermore, the SDF curves demonstrate an upward concavity for all regions in this analysis, signifying an augmentation in severity with an increase in duration.

Table 7.3 (a): SPI12 - Best probability distributions fit for characteristics of drought

Variable	Distribution	K-S	C-M	A-D	K-S	C-M	A-D	K-S	C-M	A-D
		Region 1			Region 2			Region 3		
Drought severity	Exponential	0.23	0.22	1.23	0.21	0.22	1.68	0.24	0.33	1.85
	Normal	**0.13**	**0.08**	**0.39**	0.31	0.28	1.57	0.25	0.31	1.76
	Log normal	0.22	0.26	1.47	**0.15**	**0.08**	**0.48**	0.22	0.25	1.34
	Gamma	0.19	0.18	1.11	0.17	0.17	0.74	0.23	0.31	1.43
	Weibull	0.21	0.17	0.71	0.16	0.29	0.67	**0.19**	**0.22**	**1.31**
	Gumbel	0.24	0.28	1.76	0.24	0.23	1.43	0.24	0.34	1.86
Drought duration	Exponential	0.23	0.23	0.97	**0.16**	**0.05**	**0.65**	0.26	0.31	1.95
	Normal	0.26	0.35	2.16	0.24	0.23	1.25	0.27	0.34	1.94
	Log normal	**0.15**	**0.17**	**0.73**	0.18	0.11	0.82	0.28	0.35	2.16
	Gamma	0.24	0.27	1.03	0.17	0.12	0.78	0.29	0.33	1.97
	Weibull	0.29	0.22	1.26	0.20	0.09	0.75	**0.23**	**0.24**	**1.83**
	Gumbel	0.26	0.26	1.52	0.21	0.16	1.13	0.26	0.38	2.04

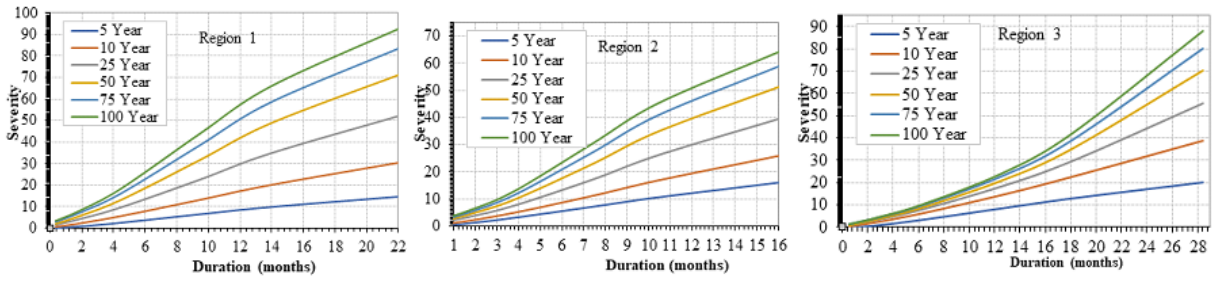

Figure 7.4 (a) SDF curves for various return periods of SPI12

Table 7.3 (b): SPEI12 - Best probability distributions fit for characteristics of drought

Variable	Distribution	K-S	C-M	A-D	K-S	C-M	A-D	K-S	C-M	A-D
		Region 1			Region 2			Region 3		
Drought severity	Exponential	**0.13**	**0.17**	**0.79**	0.29	0.23	1.45	0.24	0.32	1.88
	Normal	0.27	0.57	2.02	**0.15**	**0.07**	**0.46**	0.27	0.33	1.84
	Log normal	0.22	0.46	0.88	0.18	0.25	0.69	0.24	0.27	1.57
	Gamma	0.23	0.26	1.02	0.23	0.21	0.78	**0.18**	**0.22**	**1.21**
	Weibull	0.21	0.45	0.81	0.19	0.18	0.76	0.24	0.24	1.44
	Gumbel	0.25	0.3	1.76	0.22	0.25	1.44	0.26	0.31	1.96
Drought duration	Exponential	**0.14**	**0.13**	**0.77**	0.23	0.22	0.88	0.22	0.28	1.83
	Normal	0.25	0.31	1.76	0.25	0.21	1.18	0.27	0.32	1.88
	Log normal	0.23	0.25	0.87	0.21	0.19	0.73	0.25	0.34	2.12
	Gamma	0.23	0.19	1.12	0.19	0.24	0.83	**0.18**	**0.24**	**1.07**
	Weibull	0.19	0.15	0.88	**0.17**	**0.11**	**0.65**	0.26	0.31	1.86
	Gumbel	0.26	0.27	1.68	0.20	0.23	1.01	0.24	0.32	1.77

Table 7.4 (a): SPI12 - Best fit copula model

Copula	θ	L-L	AIC	θ	L-L	AIC	θ	L-L	AIC
	Region 1			Region 2			Region 3		
Clayton	**6.87**	**18.13**	**-54.44**	6.62	18.12	-46.54	6.66	16.74	-41.34
Frank	24.54	28.74	-64.43	17.75	21.04	-46.13	**3.15**	**14.57**	**-38.68**
Gumbel	8.75	23.48	-60.18	**5.33**	**15.52**	**-41.52**	5.76	15.67	-39.28
Galambos	7.58	23.08	-58.15	4.88	18.82	-43.08	5.98	18.54	-40.02
Plackett	26.53	29.42	-63.32	17.89	20.46	-44.54	7.36	21.22	-40.47

Table 7.4 (b): SPEI12 - Best fit copula model

Copula	θ	L-L	AIC	θ	L-L	AIC	θ	L-L	AIC
	Region 1			Region 2			Region 3		
Clayton	10.47	21.85	-56.47	7.84	18.47	-46.49	8.27	19.41	-41.47
Frank	23.87	28.75	-64.87	**4.91**	**15.28**	**-40.39**	**3.42**	**14.87**	**-36.41**
Gumbel	**4.63**	**20.94**	**-55.75**	6.42	17.31	-42.42	5.73	15.38	-38.65
Galambos	5.89	23.47	-58.74	5.39	16.01	-43.45	4.39	18.64	-40.44
Plackett	24.28	29.47	-65.34	13.17	19.42	-44.81	11.74	20.42	-42.19

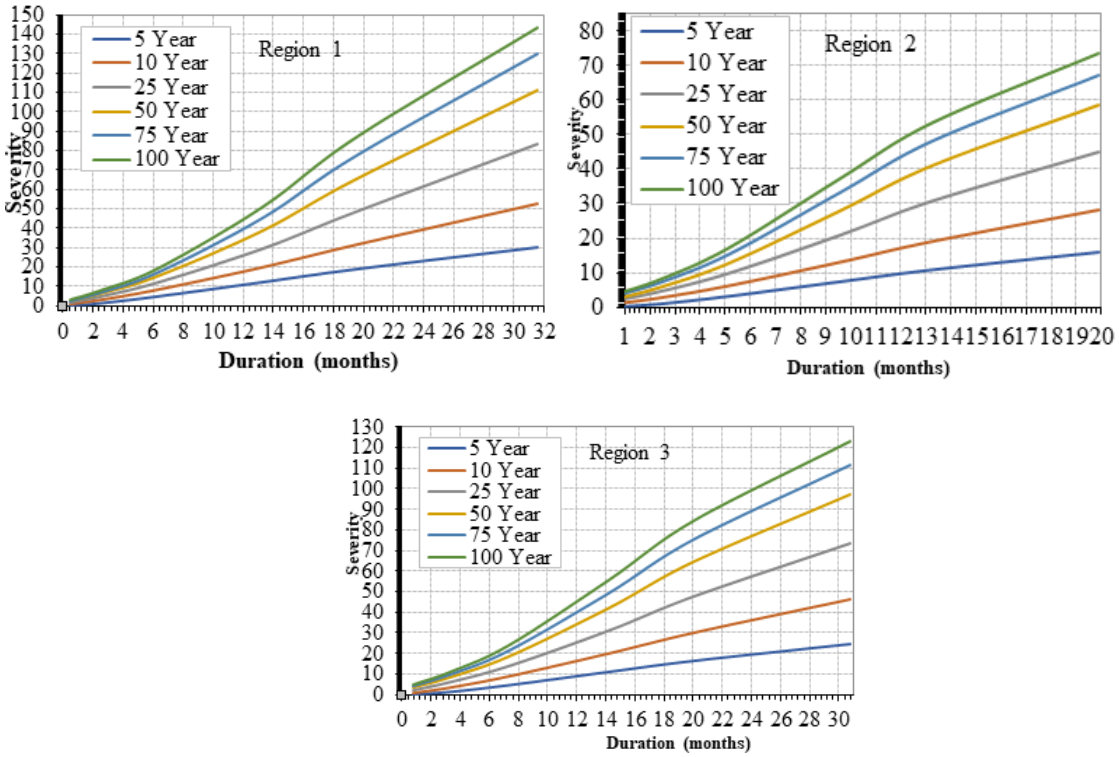

Figure 7.4 (b) SDF curves for various return periods of SPEI12

7.3.2.2 Severity-Area-Frequency analysis

For various spatial extents, gamma distribution is identified as the optimal fit. Parameters of the Distribution are determined with the L - moments method. The SAF curves corresponding to various return periods (5, 10, 25, 50, 75, 100) and Future scenarios (2021-2025, 2061-2065 and 2091-2095) are depicted in Fig. 7.5 (a) for SPI12 and Fig 7.5 (b) for SPEI12. For regions 1-3; 1971-1976, 1984-1989, 1995-2000 and 2000-2005 timespans are identified as the most severe drought periods as compared to the projected SAF curves. Analysis of Fig. 7.5(a) reveals that region 1 exhibited higher severity values for both IMD and GCMs datasets. Additionally, region 3 manifests a steeper slope in comparison to other two regions indicating a heightened risk of drought for small spatial extents.

Regarding SPEI12 from Fig 7.5 (b) region 3 experienced higher severity values for both IMD and GCMs datasets, with a steeper slope compared to regions 1 and 2. Notably, there is an inverse relationship observed between severity and spatial extent – an increase in the percentage of the area results in a decrease in severity and vice versa. The SAF curves elucidate that severity values

ranging between 10 to 25 are prominent for 50% of the area, diminishing with an expansion in areal extent for both SPI12 and SPEI12.

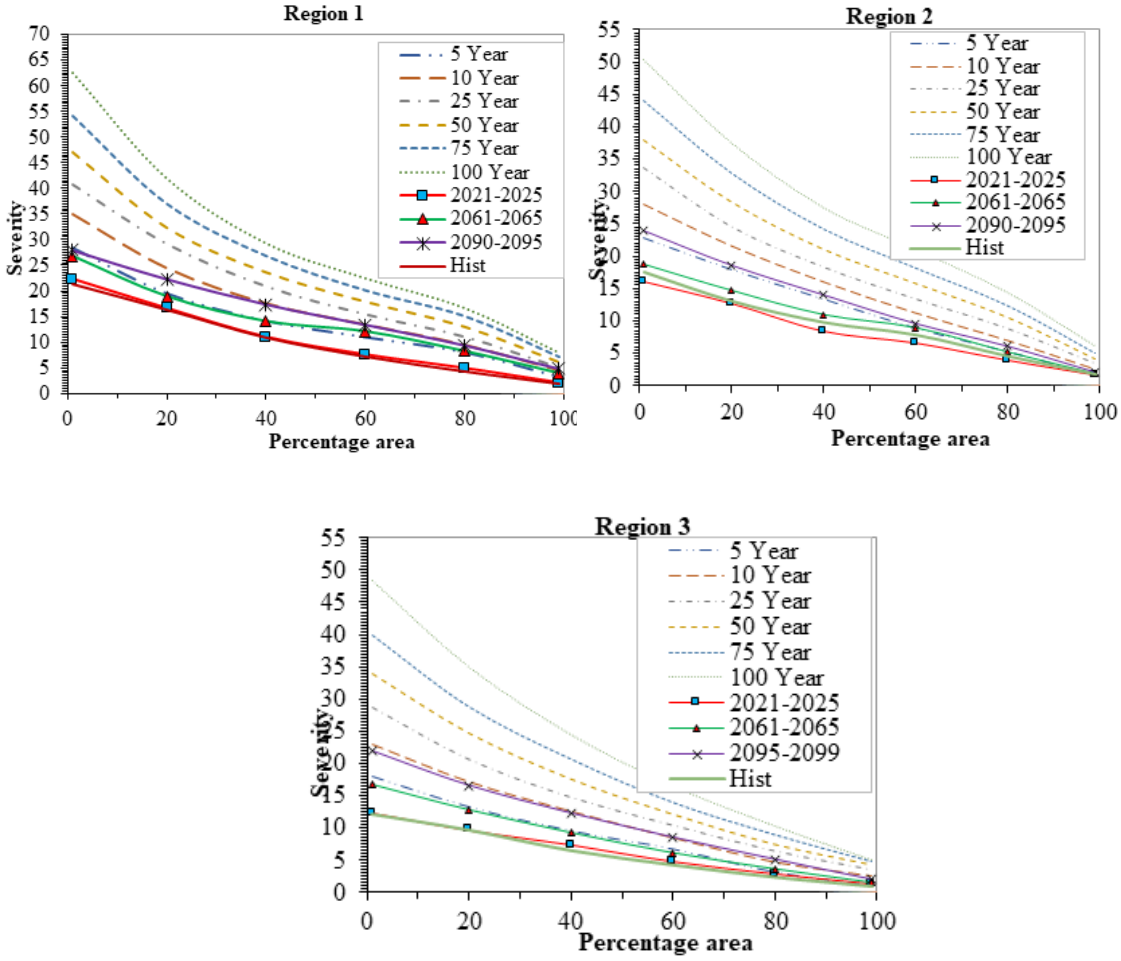

Figure 7.5 (a) SAF curves for various return periods of SPI12

7.4. Discussions

Upon closer examination of the findings, it becomes evident that an escalation in both the intensity and duration of drought is observed across virtually all regions and throughout the temporal progression. The investigation into the incidence of various drought categories (moderate, severe and extremely severe) indicates a probable uptick in the frequency of drought occurrences in most regions, barring region 3. Analysis of Severity-Duration-Frequency (SDF) curves indicates a consistent trend where the severity rate tends to rise with prolonged durations in most regions. Nevertheless, critical drought events are anticipated to manifest across diverse time scales in three

homogeneous regions. Furthermore, the derived Standardized Anomaly Frequency (SAF) curves imply that droughts are likely to encompass a larger spatial extent for lower severity values across all regions.

The SAF study previously examined highlights an anticipation of an increased areal extent of drought in the latter part of the century (Gupta and Jain, 2018). Notably, Indian regions exhibit steeper SAF curve slopes characterized by heightened variability in topographical and hydrological attributes. The SAF curves serve as valuable tools for comparing past and future drought scenarios. Consequently, the results indicate that India is currently grappling with severe droughts in the region 3 significantly impacting the local population. Prolonged droughts, attributed to insufficient soil moisture, underscore the importance of regulating turbulent heat flux and boundary layer distribution to mitigate surface energy loss (Alapaty et al., 1997).

Furthermore, a surge in population corresponds to an elevated demand for energy. Presently standing as the third-largest global consumer of energy, following China and the United States, India contends with an escalating need for electricity, exerting a direct influence on the prospective availability of water resources. Consequently, proactive measures such as enhanced preparedness, vigilant monitoring and accurate prediction of droughts emerge as pivotal adaptation strategies to mitigate the risks associated with impending droughts. Policymakers should formulate strategic frameworks tailored to address local and regional vulnerabilities, ensuring successful mitigation of drought risks induced by climate change.

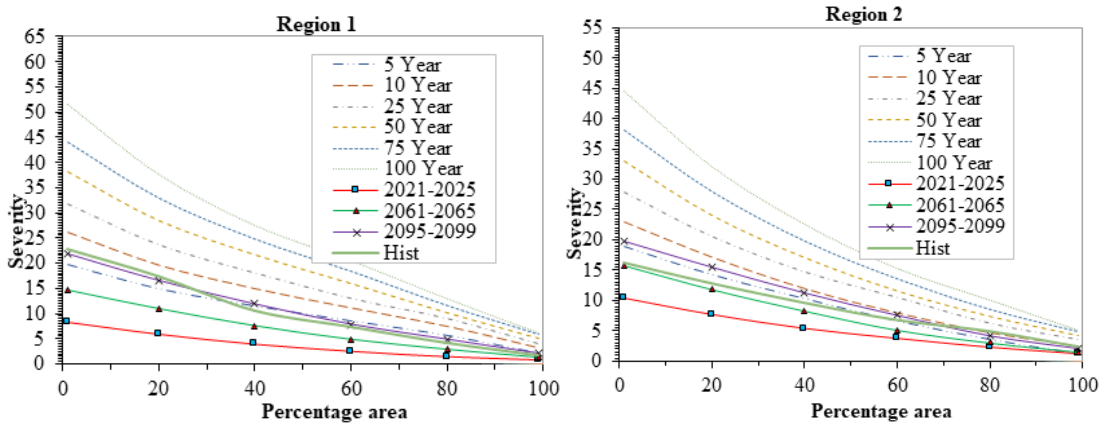

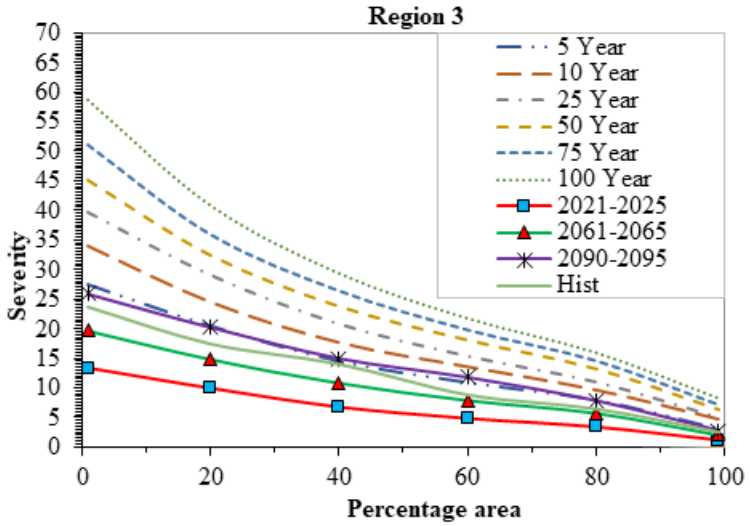

Figure 7.5 (b) SAF curves for various return periods of SPEI12

7.5. Conclusion

- In later part of twenty-first century mean interarrival time is reduced and number of droughts have increased for both SPI and SPEI.
- The mean inter-arrival time is maximum for region 3 followed by region 1 and these regions are also experiencing highest values of maximum severity and duration
- It is evident that moderate drought events exhibit a significant increase in both historical records and future projections across all studied regions. Specifically, these events constitute approximately 30% of all observed drought occurrences.
- The potential exists for an increased occurrence of droughts characterized by shorter mean interarrival times, elevated severity and extended duration in the future, with Region 1 anticipated to experience the highest frequency, followed by Region 3 and then Region 2.
- Over the temporal progression, a noteworthy rise in drought severity across varying durations, paralleling the increase in temporal extent.
- Regions 1 and 3 consistently show increased severity across various return periods, reflecting heightened drought frequency. Additionally, all regions exhibit upward-concave SDF curves, indicating severity escalation with prolonged durations.

- For regions 1-3; 1971-1976, 1984-1989, 1995-2000 and 2000-2005 timespans are identified as the most severe drought periods as compared to the projected SAF curves.
- Region 1 showed higher severity values in both IMD and GCMs datasets, while region 3 displayed a steeper slope, suggesting increased drought risk at smaller spatial extents compared to other regions.
- An inverse relationship was observed between severity and spatial extent, with severity values between 10 to 25 prominently affecting 50% of the area, diminishing as the areal extent increases for SPI12 and SPEI12 SAF curves.
- The high point of drought hazard is envisaged during the periods 2036-2065 and 2066-2095, demonstrating heightened susceptibility compared to other analyzed intervals.

CHAPTER 8

CONCLUSIONS

This chapter is organized as follows: Section 8.1 presents the summary of this study, Section 8.2. Conclusions, 8.3 Research contributions, 8.4 Limitations of the study and 8.5 Scope for the future study.

8.1 Summary of the Thesis

In this study, suitable Global Climate Models (GCMs) are identified through the comprehensive analysis of CMIP5 datasets at the first phase which include historical and future climate projections. A thorough evaluation of GCMs based on their performance metrics is conducted which involves assessing their ability to simulate historical climate conditions accurately.. Ensemble models are identified using a group decision-making analysis, ensuring a robust selection process. Following this, suitable models are downscaled and spatially projected to the study area.

In the second phase, delineation of homogeneous regions and drought characteristics analysis is performed. historical precipitation and temperature data is used for each homogeneous region to evaluate drought characteristics. Relevant drought indices SPI12,SPEI12 and SC_PDSI are computed for each homogenous region. The temporal trends namely severity and duration are assessed and drought events are distributed regionally to examine the historical drought patterns.

In the subsequent third section, a pivotal aspect of our study involves a detailed examination of the intricate relationship between climate indices and drought indices. This analysis provides valuable insights into the complex interplay between climate patterns and the occurrence and severity of drought events. The relationship between climate indices and drought indices (SPI, SPEI, SC_PDSI) helped in analyzing the variations in climate patterns impact drought occurrences and severity

Finally, SDF and SAF curves are employed to comprehensively depict the characteristics of drought events within each homogeneous region. It also helps to understand the severity of drought events with duration and its frequency of occurrence. These curves serve as invaluable tools for quantifying and visualizing the severity, spatial extent and frequency of drought occurrences, providing a holistic understanding of the drought landscape within the study area.

8.2 Conclusions

The conclusion of the entire work includes.

- The identified suitable ensemble models for P include FGOALS-g2, CMCC-CMS and INMCM4.0. BCC-CSM1.1(m), CanESM2, and MIROC5 are deemed suitable GCMs for T_{max}. For T_{min}, the recommended ensemble comprises CanESM2, BCC-CSM 1-1(m) and ACCESS1.0. For T_{avg}, MIROC5, CNRM-CM5 and BCC-CSM1.1 (m) emerge as the suitable models.
- The optimal number of clusters is determined to be three for the study region. South zone of region 1 comprises 14 districts of Telangana, North zone of region 2 comprises 7 districts; east zone of region 3 comprises 10 districts.
- For SPI, the most severe and protracted drought event occurs in region 2 from June 2001 to August 2005, exhibiting a severity of 44.43 and a duration spanning 51 months. Followed by region 3 and 1. SPEI exhibited a severity of 81.07 and a duration of 86 months for region 1 from August 2006 to September 2013. SC_PDSI major drought events occurred in region 3 from March 1979 to April 1988, exhibiting a severity of 227.75 and a duration of 108 months.
- In case of SPI, the period 1984-1987; 2001 to 2003; and 2011 to 2013 has experienced droughts for all regions; SPEI faced drought events during 1984-1986; 1992-1994; 2006-2017; SC_PDSI experienced drought for all regions during 1992 to 1994 and 2008- 2011.
- For SPI, A sustained coherence in interannual variability is discerned throughout the temporal spans of 1980-1995 and 2002-2017, primarily evident at time scales ranging from 16 to 40 months. Notably, intermittency is observed between 4 to 12 months during different years for MEI. The SOI, interannual coherence is evident between 1975-1990 and 1995-2017, spanning time scales from 16 to 40 months.
- A substantial correlation in overlap periods is observed in 1984-1987, 2010-2013 and 2016-2017 among all drought indices with climate factors.
- In later part of twenty-first century mean interarrival time is reduced and number of droughts have increased for both SPI and SPEI. A possibility to experience a high number of droughts with less mean arrival time, high severity and duration in the future for region 1 followed by region 3 and 2.

- The prognosticated drought SAF curves delineate the interplay between drought severity, spatial extent and recurrence in relation to the drought return period. Concurrently, SAF curves prove instrumental in scrutinizing the future outlook of annual drought severity, including its spatial occurrences represented as a percentage of the total area.
- SAF curves serve as a valuable tool for the comparative analysis of historical drought occurrences against those projected from future climate scenarios, leveraging GCMs outputs.
- Over the temporal progression, a noteworthy rise in drought severity across varying durations, paralleling the increase in temporal extent.
- The high point of drought hazard is envisaged during the periods 2036-2065 and 2066-2095, demonstrating heightened susceptibility compared to other analyzed intervals.

The results and findings based on the application of statistical techniques in this study gives insight to use suitable GCMs for drought related climate impact studies and this study offers a view on potential drought condition in Telangana state, India.

8.3 Research contributions

- GCM Selection advances spatially projecting GCM outputs to align with specific spatial resolution by improving precision of climate data in local analyses. This includes using a group decision-making approach to select a robust ensemble of models that provides accurate climate projections for the study area.
- Delineating homogenous regions based on climatic data allows for more nuanced analysis of drought impact at regional context in understanding drought patterns and spatial distribution.
- Intricate relationship between teleconnections and drought indices elucidate variations in climatic patterns influence over drought occurrences and severity which offers valuable insights in driving drought events
- Development of SDF and SAF curves contributes deeper understanding of the relationship between severity, duration , frequency and spatial extent. This novel application provides a comprehensive view of the impact of droughts on different spatial scales, enhancing the assessment of drought impacts on regional and local levels.

These contributions collectively advance the understanding of drought dynamics and their interplay with climate factors, providing valuable tools and insights for managing and mitigating drought impacts in the study region and potentially beyond.

8.4 Limitations of the study

- **GCM Limitations:** The study relies on a selection of Global Climate Models (GCMs) from the CMIP5 dataset. Despite rigorous selection processes, inherent uncertainties and biases in these models can affect the accuracy of climate projections. Variability in model performance and the choice of models included in the ensemble may influence results.
- **Resolution Mismatch:** Even after downscaling, the spatial resolution of climate data might not perfectly align with the heterogeneous nature of the study region. This can limit the granularity of the analysis and might affect the accuracy of drought characterization.
- **Index Limitations:** Each drought index has its own limitations and assumptions. For instance, SPI focuses solely on precipitation, while SPEI incorporates potential evapotranspiration, and SC_PDSI accounts for soil moisture. The differences in these indices may lead to variations in drought characterization and might not fully capture the complexity of drought conditions.

8.5 Future Scope

1. The identified suitable ensemble GCMs can be further used in climate impact assessment studies based on precipitation, temperature, drought, flood and temperature extremes and so on at regional scale.
2. The suitability of other popular drought indices can be investigated at a seasonal scale incorporating the CMIP5 models.
3. In this study, efforts have been made to identify meteorological droughts. However, hydrological, agricultural and socio-economic drought is the area where this work can be extended further in future.
4. A well-structured Drought Information System (DIS) and Decision Support System (DSS) can be designed to effectively manage drought mitigation and response efforts.
5. An attempt can be made to develop a common drought model for all types of agro-climatic regions which would serve as a tool for drought assessment, monitoring and management.

REFERENCES

Adarsh, S., Karthik, S., Shyma, M., Prem, G. Das, Shirin Parveen, A. T., & Sruthi, N. (2018). Developing Short Term Drought Severity-Duration-Frequency Curves for Kerala Meteorological Subdivision, India Using Bivariate Copulas. KSCE Journal of Civil Engineering, 22(3), 962–973. https://doi.org/10.1007/s12205-018-1404-9

Alamgir, M., Khan, N., Shahid, S., Yaseen, Z. M., Dewan, A., Hassan, Q., & Rasheed, B. (2020). Evaluating severity–area–frequency (SAF) of seasonal droughts in Bangladesh under climate change scenarios. Stochastic Environmental Research and Risk Assessment, 34(2), 447–464. https://doi.org/10.1007/s00477-020-01768-2

Allen, P. M., Harmel, R. D., Dunbar, J. A., & Arnold, J. G. (2011). Upland contribution of sediment and runoff during extreme drought: A study of the 1947-1956 drought in the Blackland Prairie, Texas. Journal of Hydrology, 407(1–4), 1–11. https://doi.org/10.1016/j.jhydrol.2011.04.039

Alexander, M. A., Blade, I., Newman, M., Lanzante, J. R., Lau, N. C., and Scott, J. D.′ The atmospheric bridge: The influence of enso teleconnections on air–sea interaction over the global oceans. Journal of climate, 15(16):2205–2231, 2002.

Amirataee, B., Montaseri, M., & Rezaie, H. (2018). Regional analysis and derivation of copula-based drought Severity-Area-Frequency curve in Lake Urmia basin, Iran. Journal of Environmental Management, 206, 134–144. https://doi.org/10.1016/j.jenvman.2017.10.027

Araghi, A., Martinez, C. J., Adamowski, J., & Olesen, J. E. (2018). Spatiotemporal variations of aridity in Iran using high-resolution gridded data. International Journal of Climatology, 38(6), 2701–2717. https://doi.org/10.1002/joc.5454

Araghi, A., Mousavi-Baygi, M., Adamowski, J., & Martinez, C. (2017). Association between three prominent climatic teleconnections and precipitation in Iran using wavelet coherence. International Journal of Climatology, 37(6). https://doi.org/10.1002/joc.4881

Ashok, K., Guan, Z., & Yamagata, T. (2003). Influence of the Indian Ocean Dipole on the Australian winter rainfall. Geophysical Research Letters, 30(15). https://doi.org/10.1029/2003GL017926

Asong, Z. E., Wheater, H. S., Bonsal, B., Razavi, S., & Kurkute, S. (2018). Historical drought patterns over Canada and their teleconnections with large-scale climate signals. Hydrology and Earth System Sciences, 22(6), 3105–3124. https://doi.org/10.5194/hess-22-3105-2018

Bezdek, J. C. (1974). Numerical taxonomy with fuzzy sets. Journal of Mathematical Biology, 1(1). https://doi.org/10.1007/BF02339490

Bezdek, James C. (1973). Cluster validity with fuzzy sets. Journal of Cybernetics, 3(3). https://doi.org/10.1080/01969727308546047

Bezdek, J. C. Objective function clustering. In Pattern recognition with fuzzy objective function algorithms, pages 43–93. Springer, 1981.

Bhuvaneswari, K., Geethalakshmi, V., Lakshmanan, A., Srinivasan, R., & Sekhar, N. U. (2013). The Impact of El Niño/Southern oscillation on hydrology and rice productivity in the cauvery basin, India: Application of the soil and water assessment tool. Weather and Climate Extremes, 2. https://doi.org/10.1016/j.wace.2013.10.003

Bisht, D. S., Chatterjee, C., Raghuwanshi, N. S., & Sridhar, V. (2018a). Spatio-temporal trends of rainfall across Indian river basins. Theoretical and Applied Climatology, 132(1–2), 419–436. https://doi.org/10.1007/s00704-017-2095-8

Bisht, D. S., Chatterjee, C., Raghuwanshi, N. S., & Sridhar, V. (2018b). An analysis of precipitation climatology over Indian urban agglomeration. Theoretical and Applied Climatology, 133(1–2), 421–436. https://doi.org/10.1007/s00704-017-2200-z

Bisht, D. S., Sridhar, V., Mishra, A., Chatterjee, C., & Raghuwanshi, N. S. (2019). Drought characterization over India under projected climate scenario. International Journal of Climatology, 39(4), 1889–1911. https://doi.org/10.1002/joc.5922

Bonaccorso, B., Peres, D. J., Castano, A., & Cancelliere, A. (2015). SPI-Based Probabilistic Analysis of Drought Areal Extent in Sicily. Water Resources Management, 29(2). https://doi.org/10.1007/s11269-014-0673-4

Bondarabadi, S. R., Saghafian, B., & Raziei, T. (2008). Severity-Area-Frequency curves of drought and wet periods. https://www.researchgate.net/publication/255596509

Burke, E. J., & Brown, S. J. (2010). Regional drought over the UK and changes in the future. Journal of Hydrology, 394(3–4). https://doi.org/10.1016/j.jhydrol.2010.10.003

Cancelliere, A., & Salas, J. D. (2004). Drought length properties for periodic-stochastic hydrologic data. Water Resources Research, 40(2). https://doi.org/10.1029/2002wr001750

Chaturvedi, R. K., Joshi, J., Jayaraman, M., Bala, G., & Ravindranath, N. H. (2012). Multi-model climate change projections for India under representative concentration pathways. In CURRENT SCIENCE (Vol. 103, Issue 7).

Chowdhury, M.R. (2022). Overview of Weather, ENSO, and Climate Scale. In: Seasonal Flood Forecasts and Warning Response Opportunities. Disaster Risk Reduction. Springer, Cham. https://doi.org/10.1007/978-3-031-17825-2_4

Clausen, B., & Pearson, C. P. (1995). Regional frequency analysis of annual maximum streamflow drought. Journal of Hydrology, 173(1–4). https://doi.org/10.1016/0022-1694(95)02713-Y

D.P. Lettenmaier, G. McCabe, & E. Stakhiv. (1996). Global Climate Change: Effect on Hydrologic Cycle. In: Water resources handbook / Larry W. Mays (Larry W. Mays (ed.)). McGraw-Hill.

Dai, A. (2011). Drought under global warming: A review. In Wiley Interdisciplinary Reviews: Climate Change (Vol. 2, Issue 1, pp. 45–65). Wiley-Blackwell. https://doi.org/10.1002/wcc.81

Dai, A. (2013). Increasing drought under global warming in observations and models. Nature Climate Change, 3(1), 52–58. https://doi.org/10.1038/nclimate1633

Dalezios, N. R., Loukas, A., Vasiliades, L., & Liakopoulos, E. (2000). Severity-duration-frequency analysis of droughts and wet periods in Greece. Hydrological Sciences Journal, 45(5), 751–769. https://doi.org/10.1080/02626660009492375

Das, P. K., Dutta, D., Sharma, J. R., & Dadhwal, V. K. (2016). Trends and behaviour of meteorological drought (1901-2008) over Indian region using standardized precipitation-evapotranspiration index. International Journal of Climatology, 36(2), 909–916. https://doi.org/10.1002/joc.4392

Dracup, J. A., Lee, K. S., & Paulson, E. G. (1980a). On the definition of droughts. Water Resources Research, 16(2). https://doi.org/10.1029/WR016i002p00297

Dracup, J. A., Lee, K. S., & Paulson, E. G. (1980b). On the statistical characteristics of drought events. Water Resources Research, 16(2). https://doi.org/10.1029/WR016i002p00289

Dunn, J. C. A fuzzy relative of the isodata process and its use in detecting compact well-separated clusters. 1973.

Errasti, I., Ezcurra, A., Sáenz, J., & Ibarra-Berastegi, G. (2011). Validation of IPCC AR4 models over the Iberian Peninsula. Theoretical and Applied Climatology, 103(1), 61–79. https://doi.org/10.1007/s00704-010-0282-y

Fan, K., Liu, Y., & Chen, H. (2012). Improving the prediction of the east asian summer monsoon: New approaches. Weather and Forecasting, 27(4), 1017–1030. https://doi.org/10.1175/WAF-D-11-00092.1

Farge, M. (1992). Wavelet transforms and their applications to turbulence. Annual Review of Fluid Mechanics, 24(1). https://doi.org/10.1146/annurev.fluid.24.1.395

Fordham, D. A., Wigley, T. M. L., & Brook, B. W. (2011). Multi-model climate projections for biodiversity risk assessments. Ecological Applications, 21(8). https://doi.org/10.1890/11-0314.1

Ganguli, P. (2014). Probabilistic analysis of extreme droughts in Southern Maharashtra using bivariate copulas. ISH Journal of Hydraulic Engineering, 20(1). https://doi.org/10.1080/09715010.2013.843279

Genest, C., Ghoudi, K., & Rivest, L. p. (1995). A semiparametric estimation procedure of dependence parameters in multivariate families of distributions. Biometrika, 82(3). https://doi.org/10.1093/biomet/82.3.543

Genest, Christian, & Favre, A.-C. (2007). Everything You Always Wanted to Know about Copula Modeling but Were Afraid to Ask. Journal of Hydrologic Engineering, 12(4). https://doi.org/10.1061/(asce)1084-0699(2007)12:4(347)

Genest, Christian, & Rivest, L. P. (1993). Statistical inference procedures for bivariate Archimedean copulas. Journal of the American Statistical Association, 88(423). https://doi.org/10.1080/01621459.1993.10476372

Gleckler, P. J., Taylor, K. E., & Doutriaux, C. (2008). Performance metrics for climate models. Journal of Geophysical Research Atmospheres, 113(6). https://doi.org/10.1029/2007JD008972

Goyal, M. K., Gupta, V., & Eslamian, S. (2017). Hydrological Drought: Water Surface and Duration Curve Indices. Handbook of Drought and Water Scarcity, 45–71. https://doi.org/10.1201/9781315404219-4

Goyal, M. K., & Ojha, C. S. P. (2012). Downscaling of precipitation on a lake basin: Evaluation of rule and decision tree induction algorithms. Hydrology Research, 43(3). https://doi.org/10.2166/nh.2012.040

Goyal, M. K., & Sharma, A. (2016). A fuzzy c-means approach regionalization for analysis of meteorological drought homogeneous regions in western India. Natural Hazards, 84(3), 1831–1847. https://doi.org/10.1007/s11069-016-2520-9

Grinsted, A., Moore, J. C., & Jevrejeva, S. (2004). Nonlinear Processes in Geophysics Application of the cross wavelet transform and wavelet coherence to geophysical time series (Vol. 11). http://www.pol.ac.uk/home/research/waveletcoherence/

Gupta, V., Asce, S. M., Manoj, ;, Jain, K., Singh, V. P., & Asce, F. (2020). Multivariate Modeling of Projected Drought Frequency and Hazard over India. https://doi.org/10.1061/(ASCE)HE.1943

Gupta, V., Kumar Jain, M., & Singh, V. P. (2020). Multivariate Modeling of Projected Drought Frequency and Hazard over India. Journal of Hydrologic Engineering, 25(4). https://doi.org/10.1061/(asce)he.1943-5584.0001893

Han, Z., Huang, S., Huang, Q., Leng, G., Wang, H., He, L., Fang, W., & Li, P. (2019). Assessing GRACE-based terrestrial water storage anomalies dynamics at multi-timescales and their correlations

with teleconnection factors in Yunnan Province, China. Journal of Hydrology, 574, 836–850. https://doi.org/10.1016/J.JHYDROL.2019.04.093

Hawkins, E., & Sutton, R. (2011). The potential to narrow uncertainty in projections of regional precipitation change. Climate Dynamics, 37(1), 407–418. https://doi.org/10.1007/s00382-010-0810-6

Hayes, M., Svoboda, M., Wall, N., & Widhalm, M. (2011). The lincoln declaration on drought indices: Universal meteorological drought index recommended. Bulletin of the American Meteorological Society, 92(4), 485–488. https://doi.org/10.1175/2010BAMS3103.1

Hisdal, H., & Tallaksen, L. M. (2003). Estimation of regional meteorological and hydrological drought characteristics: A case study for Denmark. Journal of Hydrology, 281(3). https://doi.org/10.1016/S0022-1694(03)00233-6

Hwang, C., and Yoon, K. (1981). Multiple attribute decision-making, methods and applications, a state-of the art survey, Springer-Verlag. doi: 10.1007/978-3-642-48318-9.

Intergovernmental Panel on Climate Change [IPCC]. (2013). Climate change: The physical science basis, contribution of working group I to the fifth assessment report of the intergovernmental panel on climate change. Cambridge UK and New York, USA: Cambridge University Press. Johnson,

Janga Reddy, M., & Ganguli, P. (2012). Application of copulas for derivation of drought severity-duration-frequency curves. Hydrological Processes, 26(11), 1672–1685. https://doi.org/10.1002/hyp.8287

Jiang, Z., Tai-Jen, G., And, C., & Wu, M.-C. (2003). Large-Scale Circulation Patterns Associated with Heavy Spring Rain Events over Taiwan in Strong ENSO and Non-ENSO Years. http://www.cpc.noaa.

Jiang, R., Xie, J., He, H., Luo, J., & Zhu, J. (2015). Use of four drought indices for evaluating drought characteristics under climate change in Shaanxi, China: 1951–2012. Natural Hazards, 75(3), 2885–2903. https://doi.org/10.1007/s11069-014-1468-x

Joe, H. (1997). Multivariate Models and Multivariate Dependence Concepts. In Multivariate Models and Multivariate Dependence Concepts. https://doi.org/10.1201/9780367803896

Johnson, F., & Sharma, A. (2009). Measurement of GCM skill in predicting variables relevant for hydroclimatological assessments. Journal of Climate, 22(16), 4373–4382. https://doi.org/10.1175/2009JCLI2681.1

Johnson, F., Westra, S., Sharma, A., & Pitman, A. J. (2011). An assessment of GCM skill in simulating persistence across multiple time scales. Journal of Climate, 24(14), 3609–3623. https://doi.org/10.1175/2011JCLI3732.1

Kang, H., & Sridhar, V. (2017). Combined statistical and spatially distributed hydrological model for evaluating future drought indices in Virginia. Journal of Hydrology: Regional Studies, 12, 253–272. https://doi.org/10.1016/j.ejrh.2017.06.003

Kang, H., & Sridhar, V. (2018). Assessment of Future Drought Conditions in the Chesapeake Bay Watershed. Journal of the American Water Resources Association, 54(1), 160–183. https://doi.org/10.1111/1752-1688.12600

Kang, H., & Sridhar, V. (2019). Drought assessment with a surface-groundwater coupled model in the Chesapeake Bay watershed. Environmental Modelling and Software, 119, 379–389. https://doi.org/10.1016/j.envsoft.2019.07.002

Kang, H., & Sridhar, V. (2021). A near-term drought assessment using hydrological and climate

forecasting in the Mekong River Basin. International Journal of Climatology, 41(S1), E2497–E2516. https://doi.org/10.1002/joc.6860

Karamouz, M., Nazif, S., & Falahi, M. (2012). Hydrology and hydroclimatology: Principles and applications. Hydrology and Hydroclimatology: Principles and Applications, 1–705. https://doi.org/10.1201/B13771/HYDROLOGY-HYDROCLIMATOLOGY-KARAMOUZ-NAZIF-FALAHI

Kim, T.-W., Valdés, J. B., & Yoo, C. (2006). Nonparametric Approach for Bivariate Drought Characterization Using Palmer Drought Index. Journal of Hydrologic Engineering, 11(2). https://doi.org/10.1061/(asce)1084-0699(2006)11:2(134)

Kim, T. W., Valdés, J. B., & Aparicio, J. (2002). Frequency and spatial characteristics of droughts in the Conchos River Basin, Mexico. Water International, 27(3), 420–430.

Kingston, D. G., Stagge, J. H., Tallaksen, L. M., & Hannah, D. M. (2015). European-scale drought: Understanding connections between atmospheric circulation and meteorological drought indices. Journal of Climate, 28(2), 505–516. https://doi.org/10.1175/JCLI-D-14-00001.1

Kripalani, R. H., & Kulkarni, A. (2001). Monsoon rainfall variations and teleconnections over South and East Asia. International Journal of Climatology, 21(5), 603–616. https://doi.org/10.1002/joc.625

Kripalani, R. H., & Singh, S. V. (1993). Large scale aspects of India-China summer monsoon rainfall. Advances in Atmospheric Sciences, 10(1), 71–84. https://doi.org/10.1007/BF02656955

Kug, J. S., Jin, F. F., & An, S. Il. (2009). Two types of El Niño events: Cold tongue El Niño and warm pool El Niño. Journal of Climate, 22(6), 1499–1515. https://doi.org/10.1175/2008JCLI2624.1

Kumar, P., Wiltshire, A., Mathison, C., Asharaf, S., Ahrens, B., Lucas-Picher, P., Christensen, J. H., Gobiet, A., Saeed, F., Hagemann, S., & Jacob, D. (2013). Downscaled climate change projections with uncertainty assessment over India using a high resolution multi-model approach. Science of the Total Environment, 468–469. https://doi.org/10.1016/j.scitotenv.2013.01.051

Liu, X., Wang, S., Zhou, Y., Wang, F., Li, W., & Liu, W. (2015). Regionalization and Spatiotemporal Variation of Drought in China Based on Standardized Precipitation Evapotranspiration Index (1961-2013). Advances in Meteorology, 2015. https://doi.org/10.1155/2015/950262

Lobell, D. B., Burke, M. B., Tebaldi, C., Mastrandrea, M. D., Falcon, W. P., & Naylor, R. L. (2008). Prioritizing climate change adaptation needs for food security in 2030. Science, 319(5863), 607–610. https://doi.org/10.1126/science.1152339

Loon, A. Van, Loon, A. F. Van, & Van Lanen, H. A. J. (2013). Article in Water Resources Research. Water Resources Research, 49, 1–20. https://doi.org/10.1029/wrcr.20147

Loukas, A., & Vasiliades, L. (2004). Probabilistic analysis of drought spatiotemporal characteristics inThessaly region, Greece. Natural Hazards and Earth System Sciences, 4(5/6), 719–731. https://doi.org/10.5194/NHESS-4-719-2004

M. P. Shewale, & Shravan Kumar. (2005). CLIMATOLOGICAL FEATURES OF DROUGHT INCIDENCES IN INDIA.

Maccioni, P., Kossida, M., Brocca, L., & Moramarco, T. (2015). Assessment of the Drought Hazard in the Tiber River Basin in Central Italy and a Comparison of New and Commonly Used Meteorological Indicators. Journal of Hydrologic Engineering, 20(8). https://doi.org/10.1061/(asce)he.1943-5584.0001094

Manatsa, D., Mushore, T., & Lenouo, A. (2017). Improved predictability of droughts over southern Africa using the standardized precipitation evapotranspiration index and ENSO. Theoretical and Applied Climatology, 127(1–2), 259–274. https://doi.org/10.1007/s00704-015-1632-6

Maxino, C. C., McAvaney, B. J., Pitman, A. J., & Perkins, S. E. (2008). Ranking the AR4 climate models over the Murray-Darling Basin using simulated maximum temperature, minimum temperature and precipitation. International Journal of Climatology, 28(8). https://doi.org/10.1002/joc.1612

Mckee, T. B., Doesken, N. J., & Kleist, J. (1993). THE RELATIONSHIP OF DROUGHT FREQUENCY AND DURATION TO TIME SCALES. In Eighth Conference on Applied Climatology.

McSweeney, C. F., Jones, R. G., Lee, R. W., & Rowell, D. P. (2015). Selecting CMIP5 GCMs for downscaling over multiple regions. Climate Dynamics, 44(11–12), 3237–3260. https://doi.org/10.1007/s00382-014-2418-8

Mirakbari, M., Ganji, A., & Fallah, S. R. (2010). Regional Bivariate Frequency Analysis of Meteorological Droughts. Journal of Hydrologic Engineering, 15(12). https://doi.org/10.1061/(asce)he.1943-5584.0000271

Mishra, A. K., & Desai, V. R. (2005). Spatial and temporal drought analysis in the kansabati river basin, india. International Journal of River Basin Management, 3(1), 43–52. https://doi.org/10.1080/15715124.2005.9635243

Mishra, A. K., & Singh, V. P. (2009). Analysis of drought severity-area-frequency curves using a general circulation model and scenario uncertainty. Journal of Geophysical Research Atmospheres, 114(6). https://doi.org/10.1029/2008JD010986

Mishra, A. K., Singh, V. P., & Desai, V. R. (2009). Drought characterization: A probabilistic approach. Stochastic Environmental Research and Risk Assessment, 23(1), 41–55. https://doi.org/10.1007/s00477-007-0194-2

Mishra, A. K., & Singh, V. P. (2010). A review of drought concepts. In Journal of Hydrology (Vol. 391, Issues 1–2, pp. 202–216). https://doi.org/10.1016/j.jhydrol.2010.07.012

Mujumdar, P., & Nagesh Kumar, D. (2012). Hydrologic modeling of floods enables more accurate assessment of climate Floods in a Changing Climate: Hydrologic Modeling International Hydrology Series Floods in a Changing Climate: Hydrologic Modeling Floods in a Changing Climate Hydrologic Modeling I. www.cambridge.org/mujumdar,

Nam, W. H., Hayes, M. J., Svoboda, M. D., Tadesse, T., & Wilhite, D. A. (2015). Drought hazard assessment in the context of climate change for South Korea. Agricultural Water Management, 160, 106–117. https://doi.org/10.1016/j.agwat.2015.06.029

Nelsen, R. B. (2007). An introduction to copulas. Springer Science & Business Media, 269.

Niu, J. (2013). Precipitation in the Pearl River basin, South China: Scaling, regional patterns, and influence of large-scale climate anomalies. Stochastic Environmental Research and Risk Assessment, 27(5), 1253–1268. https://doi.org/10.1007/s00477-012-0661-2

Panofsky, H. A., & Brier, G. W. (1968). Some Applications of Statistics to Meteorology. In Pennsylvania State University.

Perkins, S. E., Pitman, A. J., Holbrook, N. J., & McAneney, J. (2007). Evaluation of the AR4 climate models' simulated daily maximum temperature, minimum temperature, and precipitation over Australia using probability density functions. Journal of Climate, 20(17), 4356–4376. https://doi.org/10.1175/JCLI4253.1

Perkins, S. E., Pitman, A. J., & Sisson, S. A. (2009). Smaller projected increases in 20-year temperature returns over Australia in skill-selected climate models. Geophysical Research Letters, 36(6). https://doi.org/10.1029/2009GL037293

Pitman, A. J., Arneth, A., & Ganzeveld, L. (2012). Regionalizing global climate models. In International Journal of Climatology (Vol. 32, Issue 3). https://doi.org/10.1002/joc.2279

Pomerol, J.C., and Romero, S.B. (2000). Multicriterion decision in management: Principles and practice, Kluwer Academic, Netherlands

Rad, A. M., Ghahraman, B., Khalili, D., Ghahremani, Z., & Ardakani, S. A. (2017). Integrated meteorological and hydrological drought model: A management tool for proactive water resources planning of semi-arid regions. Advances in Water Resources, 107.

Rajsekhar, D. ;, Mishra, A. ;, & Singh, V. P. (2011). Drought Regionalization of Brazos River Basin using entropy approach http://docs.lib.purdue.edu/ddad2011http://docs.lib.purdue.edu/ddad2011/40

Rajsekhar, D., Singh, V. P., & Mishra, A. K. (2015a). Integrated drought causality, hazard, and vulnerability assessment for future socioeconomic scenarios: An information theory perspective. In Journal of Geophysical Research (Vol. 120, Issue 13, pp. 6346–6378). Wiley-Blackwell. https://doi.org/10.1002/2014JD022670

Rajsekhar, D., Singh, V. P., & Mishra, A. K. (2015b). Hydrologic Drought Atlas for Texas. Journal of Hydrologic Engineering, 20(7). https://doi.org/10.1061/(asce)he.1943-5584.0001074

Raju, K. S., & Kumar, D. N. (2014). Ranking of global climate models for India using multicriterion analysis. Climate Research, 60(2), 103–117. https://doi.org/10.3354/cr01222

Srinivasa Raju, K., Sonali, P., & Nagesh Kumar, D. (2016). Ranking of CMIP5-based global climate models for India using compromise programming. *Theoretical and Applied Climatology*, *128*(3–4), 563–574. https://doi.org/10.1007/s00704-015-1721-6

Rathinasamy, M., Agarwal, A., Parmar, V., Khosa, R., & Bairwa, A. (2017). Partial wavelet coherence analysis for understanding the standalone relationship between Indian Precipitation and Teleconnection patterns. http://arxiv.org/abs/1702.06568

Reddy, M. J., & Ganguli, P. (2013). Spatio-temporal analysis and derivation of copula-based intensity-area-frequency curves for droughts in western Rajasthan (India). Stochastic Environmental Research and Risk Assessment, 27(8), 1975–1989. https://doi.org/10.1007/s00477-013-0732-z

Reddy, M. J., & Singh, V. P. (2014). Multivariate modeling of droughts using copulas and meta-heuristic methods. Stochastic Environmental Research and Risk Assessment, 28(3), 475–489. https://doi.org/10.1007/s00477-013-0766-2

Reichler, T., & Kim, J. (2008). How well do coupled models simulate today's climate? Bulletin of the American Meteorological Society, 89(3), 303–311. https://doi.org/10.1175/BAMS-89-3-303

Riebsame, E., Changnon, A., & Karl, R. (1991). Drought and Natural Resources Management in the United States: Impacts and Implications of the 1987-89 Drought.

Saghafian, B., Shokoohi, A., & Raziei, T. (2003). Drought spatial analysis and development of severity-duration-frequency curves for an arid region. IAHS-AISH Publication, 278.

Salman, S. A., Shahid, S., Ismail, T., Ahmed, K., & Wang, X.-J. (2018). Selection of climate models for projection of spatiotemporal changes in temperature of Iraq with uncertainties. Atmospheric Research, 213, 509–522. https://doi.org/10.1016/j.atmosres.2018.07.008

Salman, S. A., Shahid, S., Ismail, T., Al-Abadi, A. M., Wang, X. jun, & Chung, E. S. (2019). Selection of gridded precipitation data for Iraq using compromise programming. Measurement: Journal of the International Measurementnfederation, 132, 87–98. hSanderson, B. M., Knutti, R., & Caldwell, P. (2015). A representative democracy to reduce interdependency in a multimodel ensemble. Journal of Climate, 28(13), 5171–5194. https://doi.org/10.1175/JCLI-D-14-00362.1

Sanderson, B.M., Knutti, R., and Caldwell, P. (2015a).“A representative democracy to reduce interdependency ina multimodel ensemble.” J. Clim., 28, 5171–5194. doi: 10.1175/ JCLI-D-14-00362.1.

Sanderson, B. M., Wehner, M., & Knutti, R. (2017). Skill and independence weighting for multi-model assessments. Geoscientific Model Development, 10(6), 2379–2395. https://doi.org/10.5194/gmd-10-2379-2017

Santos, M. A. (1983). Regional droughts: A stochastic characterization. Journal of Hydrology, 66(1–4). https://doi.org/10.1016/0022-1694(83)90185-3

Sehgal, V., Sridhar, V., & Tyagi, A. (2017). Stratified drought analysis using a stochastic ensemble of simulated and in-situ soil moisture observations. Journal of Hydrology, 545, 226–250. https://doi.org/10.1016/j.jhydrol.2016.12.033

Sen, Z. (1980). Statistical analysis of hydrologic critical droughts. In Journal of the Hydraulics Division, ASCE (Vol. 106, Issues HY1, Proc. Paper, 15134). https://doi.org/10.1061/jyceaj.0005362

Shiau, J.-T., & Shen, H. W. (2001). Recurrence Analysis of Hydrologic Droughts of Differing Severity. Journal of Water Resources Planning and Management, 127(1). https://doi.org/10.1061/(asce)0733-9496(2001)127:1(30)

Shiau, J. T. (2003). Return period of bivariate distributed extreme hydrological events. Stochastic Environmental Research and Risk Assessment, 17(1–2), 42–57. https://doi.org/10.1007/s00477-003-0125-9

Shiau, J. T. (2006). Fitting drought duration and severity with two-dimensional copulas. Water Resources Management, 20(5), 795–815. https://doi.org/10.1007/s11269-005-9008-9

Shiau, J. T., & Modarres, R. (2009). Copula-based drought severity-duration-frequency analysis in Iran. Meteorological Applications, 16(4), 481–489. https://doi.org/10.1002/met.145

Shiau, Jenq Tzong, Feng, S., & Nadarajah, S. (2007). Assessment of hydrological droughts for the Yellow River, China, using copulas. Hydrological Processes, 21(16), 2157–2163. https://doi.org/10.1002/hyp.6400

Sklar, A. (1959). Fonctions de r{é}partition {à} {n} dimensions et leurs marges (Distribution functions of {n} dimensions and their marginals). Publications de l’Institut Statistique de l’Universit{é} de Paris, 8.

Smith, I., and Chiew, F. (2010). “Document and assess methods for generating inputs to hydrological models and extend delivery of projections across Victoria.” Final report for Project 2.2.5P. South Eastern Australian Climate Initiative, CSIRO Land and Water, Acton

Sperber, K. R., Annamalai, H., Kang, I. S., Kitoh, A., Moise, A., Turner, A., Wang, B., & Zhou, T. (2013). The Asian summer monsoon: An intercomparison of CMIP5 vs. CMIP3 simulations of the late

20th century. Climate Dynamics, 41(9–10), 2711–2744. https://doi.org/10.1007/s00382-012-1607-6

Srinivasa Raju, K., Sonali, P., & Nagesh Kumar, D. (2017). Ranking of CMIP5-based global climate models for India using compromise programming. Theoretical and Applied Climatology, 128(3–4). https://doi.org/10.1007/s00704-015-1721-6

Tallaksen, L.M. and Van Lanen, H.A. (2004) Hydrological Drought: Processes and Estimation Methods for Streamflow and Groundwater. Vol. 48, Elsevier, Amsterdam.

TALLAKSEN, L. M., MADSEN, H., & CLAUSEN, B. (1997). On the definition and modelling of streamflow drought duration and deficit volume. Hydrological Sciences Journal, 42(1). https://doi.org/10.1080/02626669709492003

Tan, X., Gan, T. Y., & Shao, D. (2016). Wavelet analysis of precipitation extremes over Canadian ecoregions and teleconnections to large-scale climate anomalies. Journal of Geophysical Research, 121(24), 14469–14486. https://doi.org/10.1002/2016JD025533

Tase, N. (1976). AREA-DEFICIT-INTENSITY CHARACTERISTICS OF DROUGHTS. Colo State Univ (Fort Collins) Hydrol Pap, 87.

Tebaldi, C., & Knutti, R. (2007). The use of the multi-model ensemble in probabilistic climate projections. In Philosophical Transactions of the Royal Society A: Mathematical, Physical and Engineering Sciences (Vol. 365, Issue 1857, pp. 2053–2075). Royal Society. https://doi.org/10.1098/rsta.2007.2076

Thilakarathne, M., & Sridhar, V. (2017). Characterization of future drought conditions in the Lower Mekong River Basin. Weather and Climate Extremes, 17. https://doi.org/10.1016/j.wace.2017.07.004

Torrence, C., & Compo, G. P. (n.d.). A Practical Guide to Wavelet Analysis.

Torrence, C., & Webster, P. J. (1999). Interdecadal changes in the ENSO-monsoon system. Journal of Climate, 12(8 PART 2). https://doi.org/10.1175/1520-0442(1999)

Urcid, G and Ritter, G. X. C-means clustering of lattice auto-associative memories for endmember approximation. In Advances in Knowledge-Based and Intelligent Information and Engineering Systems, pages 2140–2149. IOS Press, 2012.

Vasiliades, L., Loukas, A., & Patsonas, G. (2009). Evaluation of a statistical downscaling procedure for the estimation of climate change impacts on droughts. Natural Hazards and Earth System Science, 9(3). https://doi.org/10.5194/nhess-9-879-2009

Vicente-Serrano, S. M., Beguería, S., & López-Moreno, J. I. (2010). A multiscalar drought index sensitive to global warming: The standardized precipitation evapotranspiration index. Journal of Climate, 23(7), 1696–1718. https://doi.org/10.1175/2009JCLI2909.

Vicente-Serrano, S. M., Beguer´ıa, S., and Lopez-Moreno, J. I.´ Comment on “characteristics and trends in various forms of the palmer drought severity index (pdsi) during 1900–2008” by aiguo dai. Journal of Geophysical Research: Atmospheres, 116(D19), 2011.

Wallace, J. M., & Gutzler, D. S. (1981). Teleconnections in the geopotential height field during the Northern Hemisphere winter. Monthly Weather Review, 109(4). https://doi.org/10.1175/1520-0493(1981)

Wayne C Palmer. (1965). USWB_Meteorological_Drought_1965. Meteorological Drought , 30.

Wells, N., Goddard, S., & Hayes, M. J. (2004). A Self-Calibrating Palmer Drought Severity Index. Journal of Climate, 17, 2335–2351.

Wilhite, D. A. (2000). Drought as a natural hazard: Concepts and definitions. Drought: A Global Assessment.

Wilhite, D. A., Sivakumar, M. V. K., & Pulwarty, R. (2014). Managing drought risk in a changing climate: The role of national drought policy. Weather and Climate Extremes, 3, 4–13. https://doi.org/10.1016/j.wace.2014.01.002

Xie, X. L., & Beni, G. (1991). A validity measure for fuzzy clustering. IEEE Transactions on Pattern Analysis and Machine Intelligence, 13(8). https://doi.org/10.1109/34.85677

Xu, C.-Y. (1999). Climate Change and Hydrologic Models: A Review of Existing Gaps and Recent Research Developments. In Water Resources Management (Vol. 13).

Xu, L., Chen, N., Zhang, X., Chen, Z., Hu, C., & Wang, C. (2019). Improving the North American multi-model ensemble (NMME) precipitation forecasts at local areas using wavelet and machine learning. Climate Dynamics, 53(1–2). https://doi.org/10.1007/s00382-018-04605-z

Yevjevich, V., & Ica Yevjevich, V. (1967a). An objecti ve approach to definitions and investigations of continental hydrolog ic drought s an objective approach to definitions and investigations of continental hydrologic droughts.

Yevjevich, v., & ica yevjevich, v. (1967b). An objecti ve approach to definitions and investigations of continental hydrolog ic drought s an objective approach to definitions and investigations of continental hydrologic droughts.

Zargar, A., Sadiq, R., Naser, B., & Khan, F. I. (2011). A review of drought indices. In Environmental Reviews (Vol. 19, Issue 1). https://doi.org/10.1139/a11-013

Zeleney, M. (1973). Compromise programming, University of South Carolina Press, Columbia, SC, 262–301.

Zhang, B., Zhao, X., Jin, J., & Wu, P. (2015a). Development and evaluation of a physically based multiscalar drought index: The standardized moisture anomaly index. Journal of Geophysical Research, 120(22), 11,575-11,588. https://doi.org/10.1002/2015JD023772

Zhang, Y., Li, Y., Ge, J., Li, G., Yu, Z., & Niu, H. (2018). Correlation analysis between drought indices and terrestrial water storage from 2002 to 2015 in China. Environmental Earth Sciences, 77(12). https://doi.org/10.1007/s12665-018-7651-8

Zhu, Z., Piao, S., Xu, Y., Bastos, A., Ciais, P., & Peng, S. (2017). The effects of teleconnections on carbon fluxes of global terrestrial ecosystems. Geophysical Research Letters, 44(7). https://doi.org/10.1002/2016GL071743

Publications

1. **K Sreelatha** & P Anand Raj (**2019**): Ranking of CMIP5-based global climate models using standard performance metrics for Telangana region in the southern part of India, ISH Journal of Hydraulic Engineering, DOI: 10.1080/09715010.2019.1634648

2. **K Sreelatha** & P AnandRaj (**2020**): Regional evaluation of global climate models for precipitation, maximum and minimum temperature over southern-part of India, ISH Journal of Hydraulic Engineering, DOI: 10.1080/09715010.2020.1779137

3. Satish Kumar, K; AnandRaj, P; **Sreelatha, K**; Bisht, D.S.; Sridhar, V. Monthly and Seasonal Drought Characterization Using GRACE-Based Groundwater Drought Index and Its Link to Teleconnections Across South Indian River Basins. Climate **2021**, 9, 56.

4. Satish Kumar K, AnandRaj P, **Sreelatha K**, Sridhar V. Regional analysis of drought severity-duration-frequency and severity-area-frequency curves in the Godavari River Basin, India. Int J Climatol. **2021**; 41, 5481-5501.

5. Kumar, K.S.; AnandRaj, P.; **Sreelatha, K.;** Sridhar, V. Reconstruction of GRACE terrestrial water storage anomalies using Multi-Layer Perceptrons for South Indian River basins. *Sci. Total Environ.* **2023**, *857*.

Conference

Regional Optimization of Global Climate Models for Maximum and Minimum Temperature (NOEIAS- 2019)

BRIEF CURRICULUM VITAE

Ms. KOPPALA SREELATHA is a full-time Research scholar in the Department of Civil Engineering, National Institute of Technology, Warangal-506004, India. She has received her undergraduate degree in Civil Engineering from Yogi Vemana University, Kadapa and postgraduate degree in Water Resources Engineering from Visveswaraya National Institute of Technology, Nagpur, Maharashtra, India. Her research interests are in the areas of drought and climate change impact assessment, groundwater storage assessments, remote sensing and GIS applications in hydrology. During her doctoral research, she has published 6 papers in international peer-reviewed and reputed journals and conferences.

DOCTORAL COMMITTEE

The Doctoral Committee of Ms. KOPPALA SREELATHA, full time Ph.D., Research Scholar (Enrolment Number: 716002) is as follows:

Doctoral Committee Chairman	Dr. T D Gunneswara Rao Professor, Department of Civil Engineering, National Institute of Technology, Warangal-506004.
Research Supervisor	Dr. P Anand Raj Professor, Department of Civil Engineering, National Institute of Technology, Warangal-506004.
Internal Member	Dr. K Venkata Reddy Professor, Department of Civil Engineering, National Institute of Technology, Warangal-506004.
Internal Member	Dr. P Hari Prasad Reddy Associate Professor, Department of Civil Engineering, National Institute of Technology, Warangal-506004.
External Member	Dr. K N S Kasi Viswanadham Professor, Department of Mathematics, National Institute of Technology, Warangal-506004.